University of California
Los Angeles

Coordinated Actuation for Sensing Uncertainty Reduction

A dissertation submitted in partial satisfaction
of the requirements for the degree
Doctor of Philosophy in Electrical Engineering

by

Aman Kansal

2006

The dissertation of Aman Kansal is approved.

Gaurav S. Sukhatme

Deborah Estrin

William J. Kaiser

Gregory J. Pottie, Committee Co-chair

Mani B. Srivastava, Committee Co-chair

University of California, Los Angeles

2006

Table of Contents

List of Figures

List of Tables

Acknowledgments

The work in this dissertation was facilitated by the efforts of several people, beginning first and foremost with my co-advisers Prof Mani B Srivastava and Prof Gregory J Pottie. I am grateful to Prof Srivastava for not only providing starting directions in the basic problem space explored in this dissertation but significant help in shaping the specifics of the problem addressed. His constant encouragement and flexibility in exploring risky off-shoots of the primary hypothesis provided for a very exciting and enjoyable research environment for my thesis research. I am also thankful to Prof Pottie for his constant feedback and the wider perspective on modeling the relevant factors in the problems studied. The extensive collaborative opportunities provided by him for exploring fundamental problems in sensing with collaboration among multiple sensors and information theoretic considerations were also very beneficial in pursuing my research objectives. The significant advice received from both my advisers in the domains of technical writing and accurate expression of the research findings are also worthy of acknowledgment.

I am also grateful to my thesis committee members Prof Deborah Estrin, Prof William Kaiser, and Prof Gaurav Sukhatme. Their continued feedback has gone beyond an external evaluation of the work and has provided me with valuable suggestions and a deeper understanding of the issues explored.

I have been fortunate that this work was also supported by the Networked Infomechanical Systems (NIMS) project at Center for Embedded Networked Sensing (CENS) at UCLA. The efforts by NIMS team members on various related aspects of the problems addressed in this thesis provided a richer understanding and wider applicability for the work.

I am also indebted to my student collaborator James Carwana for the several lengthy experiments designed, developed, and executed with me for one of the modules of the system developed as part of this dissertation. I also wish to thank Eric Yuen and Michael Stealey for their efforts on some of the initial experimental studies for this dissertation. I further acknowledge the efforts of other students who worked with me on several problems in controllably mobile sensor networks that are related to, though not covered in, this dissertation, including Arun Somasundara, Jonathan Friedman, David Lee, Parixit Aghera, and Advait Dixit. I am also grateful to several others who collaborated on multiple complimentary problems in sensor networks, including Jason Hsu, Sadaf Zahedi, Ameesh Pandya, Mohammad Rahimi, Aditya Ramamoorthy, Richard Pon, Maxim Batalin, Duo Liu, Vijay Raghunathan, Dunny Potter, Saurabh Ganeriwal, and David Jea.

A special note of thanks is also due to my undergraduate advisers Prof Uday Desai, Prof Abhay Karandikar, and Prof Rakesh Lal who introduced me to advanced research in networking, wireless communication, and embedded networks for the first time. Gratitude is also due to Rick Baer at Agilent Technologies for the valuable exposure to practical system development issues and in-depth insights into the behavior of cameras and other technology components used in this dissertation.

I would also like to thank the faculty at University of California Los Angeles who have contributed greatly to my education including Prof Michael Fitz, Prof Adnan Darwiche, Prof Mario Gerla, Prof Izhak Rubin, and Prof Kung Yao.

The work for this dissertation was carried out at the Networked and Embedded Systems Laboratory (NESL) at the Electrical Engineering Department, UCLA and I am grateful to the several members of NESL, including but not limited to Vlasios Tsiatsis, Andreas Savvides, Ramkumar Rengaswamy, Roy Shea,

Heemin Park, Laura Balzano, and Simon Han, for helping in various forms including the numerous discussions held at NESL, assistance with equipment issues, sharing opinions and philosophical insights on issues in my research area, and last but not the least for fueling excitement about sensor networks.

I express my deepest gratitude to my parents, Vandana and Devinder Kansal, for their constant support and love. Their extremely valuable contributions to my initial education and an early exposure to the scientific process were instrumental in my research pursuits. I am also grateful to my wife, Vasudha Kaushik, for her support and tolerance.

This research was supported in part by the National Science Foundation (NSF) under Grant Nos. ANI-00331481 and 0306408, the Center for Embedded Networked Sensing (CENS) at University of California Los Angeles, the Office of Naval Research (ONR) under the AINS program, and the DARPA PAC/C program.

Vita

1979	Born, Patiala, Punjab, India.
2001	B. Tech., Electrical Engineering Indian Institute of Technology Bombay Mumbai, India.
2001-2002	Teaching Assistant, Department of Electrical Engineering, IIT Bombay. Courses: EE 421 Communication System Theory, and EE 764 Wireless and Mobile Communications.
2002	M. Tech., Communications and Signal Processing Indian Institute of Technology Bombay Mumbai, India.
2002	University of California Regents Fellowship, Department of Electrical Engineering, University of California Los Angeles.
2003-2005	Graduate Student Researcher, Networked and Embedded Systems Laboratory, Department of Electrical Engineering, University of California Los Angeles.
2005	Summer Intern, Agilent Labs, Palo Alto, California.
2005-2006	Graduate Student Researcher, Networked and Embedded Systems Laboratory, Department of Electrical Engineering, University of California Los Angeles.
2006 –	Researcher, Microsoft Research.

Publications

MA Batalin, M Rahimi, Y Yu, D Liu, A Kansal, G Sukhatme, W Kaiser, M Hansen, G Pottie, MB Srivastava, and D Estrin. Call and Response: Experiments in Sampling the Environment. In Proceedings of ACM Sensys, November 3-5, 2004, Baltimore, MD.

S Ganeriwal, A Kansal and MB Srivastava. Self-aware Actuation for Fault Repair in Sensor Networks. In Proceedings of IEEE International Conference on Robotics and Automation (ICRA) April 26 - May 1, 2004, New Orleans, LA.

J Hsu, S Zahedi, A Kansal, MB Srivastava. Adaptive Duty Cycling for Energy Harvesting Systems. ACM-IEEE International Symposium on Low Power Electronics and Design (ISLPED), October 4-6, 2006, Tegernsee, Germany.

J Hsu, S Zahedi, D Lee, J Friedman, A Kansal, V Raghunathan, and MB Srivastava. Demo Abstract: Heliomote: Enabling Long-Lived Sensor Networks Through Solar Energy Harvesting. In Proceedings of ACM Sensys, November 2-4, 2005, San Diego, CA.

A Kansal, J Carwana, WJ Kaiser, and MB Srivastava. Demo Abstract: Coordinating Camera Motion for Sensing Uncertainty Reduction. In Proceedings of ACM Sensys, November 2-4, 2005, San Diego, CA.

A Kansal, J Carwana, WJ Kaiser, and MB Srivastava. Acquiring Medium Models

for Sensing Performance Estimation. In Proceedings of IEEE SECON, September 26-29, 2005, Santa Clara, CA.

A Kansal and UB Desai. Motion Constraint Based Handoff Protocol for Mobile Internet. In Proceedings of IEEE Wireless Communications and Networking Conference (WCNC), March 16-20, 2003, New Orleans, LA.

A Kansal and UB Desai. Handoff Protocol for Bluetooth Public Access. In Proceedings of IEEE International Conference on Personal Wireless Communications (ICPWC), December 15-17, 2002, New Delhi, India.

A Kansal and UB Desai. A rapid handoff protocol for mobility in Bluetooth public access networks. In Proceedings of the Fifteenth International Conference on Computer Communication, August 2002, Mumbai, India.

A Kansal and UB Desai. Mobility support for Bluetooth public access. In Proceedings of IEEE International Symposium on Circuits and Systems (ISCAS), May 26-29, 2002, Phoenix, AZ.

A Kansal, J Hsu, MB Srivastava, V Raghunathan. Harvesting Aware Power Management for Sensor Networks. In Proceedings of the 43rd Design Automation Conference (DAC), July 24-28, 2006, San Fransisco, CA.

A Kansal, W Kaiser, G Pottie, MB Srivastava, and G Sukhatme. Virtual High Resolution for Sensor Networks. In Proceedings of ACM SenSys, November 1-3, 2006, Boulder, CO.

A Kansal and A Karandikar. An Overview of Delay Jitter Control for Packet Audio in IP-Telephony. In IETE Technical Review, Vol. 20, No. 4, July-August 2003.

A Kansal and A Karandikar. Adaptive delay adjustment for low jitter audio over Internet. In Proceedings of IEEE Globecom, November 25-29, 2001, San Antonio, TX.

A Kansal and A Karandikar. Jitter free Audio Playout over Best Effort Packet Networks. In Proceedings of ATM Forum International Symposium on Broadband Communication in the New Millennium, August 2001, New Delhi, India.

A Kansal, D Potter and MB Srivastava. Performance Aware Tasking for Environmentally Powered Sensor Networks. In Proceedings of ACM Joint International Conference on Measurement and Modeling of Computer Systems (SIGMETRICS) June 12-16, 2004, New York, NY.

A Kansal, M Rahimi, WJ Kaiser, MB Srivastava, GJ Pottie, and D Estrin. Controlled Mobility for Sustainable Wireless Networks. In Proceedings of IEEE Sensor and Ad Hoc Communications and Networks (SECON) October 4-7, 2004, Santa Clara, CA.

A Kansal, A Ramamoorthy, GJ Pottie, MB Srivastava. On sensor Network Lifetime and Data Distortion. In Proceedings of IEEE International Symposium on Information Theory (ISIT), September 4-9, 2005, Adelaide, Australia.

A Kansal and MB Srivastava. Distributed Energy Harvesting for Energy Neutral Sensor Networks. In IEEE Pervasive Computing, Vol 4, No. 1, January-March 2005.

A Kansal and MB Srivastava. Energy Harvesting Aware Power Management. Book Chapter, in Wireless Sensor Networks: A Systems Perspective,Eds. N Bulusu and S Jha, Artech House, 2005.

A Kansal, A Somasundara, D Jea, MB Srivastava, and D Estrin. Intelligent Fluid Infrastructure for Embedded Networks. In Proceedings of ACM International Conference on Mobile Systems, Applications and Services (MobiSys), June 6-9, 2004, Boston, MA.

A Kansal and MB Srivastava. An Environmental Energy Harvesting Framework for Sensor Networks. In Proceedings of ACM/IEEE Int'l Symposium on Low Power Electronics and Design (ISLPED), August 25-27, 2003, Seoul Korea.

A Kansal, L Xiao, and F Zhao. Relevance Metrics for Coverage Extension Using Community Collected Cell-phone Camera Imagery. In Proceedings of ACM SenSys Workshop on World-Sensor-Web: Mobile Device Centric Sensor Networks and Applications, October 31, 2006, Boulder, CO.

A Kansal, E Yuen, WJ Kaiser, G Pottie and MB Srivastava. Sensing Uncertainty Reduction Using Low Complexity Actuation. In Proceedings of ACM Third International Symposium on Information Processing in Sensor Networks (IPSN) April 26-27, 2004, Palo Alto, CA.

A Pandya, A Kansal, GJ Pottie, and MB Srivastava. Lossy Source Coding of Multiple Gaussian Sources: m-helper problem. In Proceedings of IEEE Information Theory Workshop (ITW) October 24-29, 2004, San Antonio, TX.

A Pandya, A Kansal, GJ Pottie, and MB Srivastava. Fidelity and Resource Sensitive Data Gathering. In Proceedings of the 42nd Allerton Conference, September 8-12, 2004, Allerton, IL.

Abstract of the Dissertation

Coordinated Actuation for Sensing Uncertainty Reduction

by

Aman Kansal

Doctor of Philosophy in Electrical Engineering

University of California, Los Angeles, 2006

Professor Mani B. Srivastava, Co-chair

Professor Gregory J. Pottie, Co-chair

The quality of data returned by a senor network is a crucial parameter of performance since it governs the range of applications that are feasible to be developed using that network. Higher resolution data, in most situations, enables more applications and improves the reliability of existing ones. In this thesis we discuss methods that use controlled motion to increase the image resolution in a network of cameras. In our prototype system, our methods can provide up to 15000x advantage in resolution, depending on tolerable trade-offs in sensing delay.

Mobility itself may have a high resource overhead, and hence a constrained form of mobility is exploited, which has low overheads but provides significant reconfiguration potential. Specifically, we concentrate on pan, tilt, and zoom motion for cameras. Other forms of constrained motion are also mentioned.

An architecture that allows each node in the network to learn the medium and phenomenon characteristics is presented. A quantitative metric for sensing performance is defined based on real sensor and medium characteristics. The

problem of determining the desirable network configuration is expressed as an optimization of this metric. A distributed optimization algorithm is developed to compute a desirable network configuration and adapt it to environmental changes.

A key property of our algorithm is that convergence to a desirable configuration can be proved even though no global coordination is involved. Other desirable properties of the algorithm, such as convergence accuracy and convergence time are also studied. Its relationship to previously known optimization heuristics is also discussed.

A network protocol to implement this algorithm is discussed for execution in a totally distributed manner. The protocol involves exchanging messages only in a well-defined neighborhood.

We evaluate our methods using simulations and experiments on our prototype system. Real world data is used for testing the algorithm.

CHAPTER 1

Introduction

Several research efforts [SS02, PK00, EGH00b, RAS00, SS03, SMP01a, SMP01b] have established the feasibility of compact, wireless and low energy devices for sensor networks. A wide range of applications have been prototyped using such systems in education [SMP01a, SS03], science [CEE01, MPS02], arts and entertainment [BMK02] and defense [MSL04]. In this work we consider the fundamental functionality used by all the above applications – sensing the application specific phenomenon in the deployment environment. Unlike traditional computing systems, sensor networks must deal with complex and inherently noisy inputs from the physical world. A given application needs a certain sensing performance, which must be guaranteed in the face of unpredictable phenomenon distributions and the presence of static and mobile environmental obstacles. The system designer is challenged to not only provide the required performance within the resource constraints of embedded sensor nodes and a limited power budget but also ensure autonomous operation of the system in unknown environments. Environment specific customization is not desirable, as it hinders rapid deployment. Our objective is to develop methods for understanding and controlling the uncertainty in the sensed data.

For instance, in the case of image data, the data uncertainty may be related to the resolution at which the desired space is covered. This spatial resolution may determine if a desired application can be realized or not using the network.

Higher resolution may enable newer applications. Higher resolution also helps reduce the effect of transducer noise since more pixels may be allocated to the same spatial region. Suppose the density at which the cameras are deployed and the image resolution of each camera is such that a unit length in real space, placed at any point in the area covered by the network, maps to P pixels in the image. Then, we define the coverage resolution[1] as $Ppixels/m$. Different points in the covered area may be at different distances from the respective nearest camera and coverage resolution may be defined to be that provided at the worst case point covered by the network. Figure 1.1(a) shows an example scene desired to be covered by a camera network. Suppose the image data is to be used by a sensor network application interested in photographing the vehicles in the scene. A small portion of the scene where a vehicle is present is shown at $15pixels/m$ resolution in Fig. 1.1(b). This resolution may be sufficient for applications interested in detecting vehicles, such as using motion detection, in the scene but not for applications interested in recognizing the vehicles. Figure 1.1(c) shows[2] a small section of the same field of view with the coverage resolution increased to $200pixels/m$. Such a resolution may enable an application that is interested in recognizing the vehicles present in the scene. The simple example clearly shows that increasing the resolution may enable newer applications. Given a finite set of sensing resources, it is thus important to provide the highest coverage resolution feasible with those resources.

There are many ways in which the resolution may be improved. Given the feasible maximum sensor density, signal processing may be used to combine images

[1]Pixels on some sensing devices may be rectangular rather than square making a unit length in space map to different number of pixels depending on whether the length is considered aligned horizontally or vertically. For such devices, we arbitrarily choose to align the unit length horizontally for defining coverage resolution.

[2]The image resolution in the printed paper may vary from the resolution of image data used in the figure.

(a) Scene (b) 15 pix/m (c) 200 pix/m

Figure 1.1: Resolution determines feasible data processing.

from multiple cameras to obtain a higher resolution image, sometimes referred to as a super-resolution image [SCI05]. Another method to increase resolution with a given set of sensing resources is to use motion, and we discuss this latter approach in this thesis.

Motion helps improve sensing in at least three ways:

Phenomenon Adaptivity: Motion may be used to adaptively focus sensing resources on regions of interest. For instance, suppose the camera used to capture the image shown in Figure 1.1(a) has pan, tilt, and zoom motion capabilities. Then the total sensing resources used to obtain the image shown in Fig. 1.1(a) may be allocated, using those limited motion capabilities, to the small region shown in Fig. 1.1(c). The application using the image data is interested only in regions where phenomena of interest, such as the vehicles in this example, are present and to that application, motion makes it appear that the sensor network is providing a $200 pixel/m$ equivalent spatial resolution even though significantly fewer sensing resources are being used.

Medium Adaptivity: Practical deployment environments rarely ever provide an isotropic sensing medium without obstacles. Clearly, a sensor can use

motion to reduce the occlusions to its view due to obstacles in the medium. Such use of motion assumes that the sensor can obtain information about the obstacles, either from its own data or through external means. Further, when multiple sensors are present they may use motion to minimize overlap areas among their coverage, and hence potentially focus on smaller regions, providing a high resolution coverage within those smaller regions.

Increased Sensor Range: Mobile sensors can patrol a larger volume, depending on the acceptable motion delay.

Motion itself may have a high resource overhead but the sensing advantages often outweigh the cost of motion for appropriate system design choices. To this end, we focus our discussion on a specific type of motion capability in the cameras, namely the ability to pan, tilt, and zoom. Such cameras are sometimes referred to as *active cameras* in computer vision or *motile* sensors[3] in robotics. There are several reasons which motivate us to restrict to this type of motion:

1. The navigational overheads of such constrained motion and very low compared to navigating an unconstrained mobile robot, which requires significant hardware and software resource overheads.

2. The energy requirements for constrained motion are lower than unconstrained mobility since the bulkier components such as the battery, motors and processing platform can stay stationary while only the transducer has to move.

3. Such motion is feasible in tethered nodes such as high bandwidth video sensors where wireless communication may limit data quality.

[3]The terms motility and mobility are used differently in biology literature and we will not consider that usage here.

4. If the tolerable delay in sensing is small, then only a limited range of motion may be feasible within the actuation time allowed and small motion capabilities are sufficient to exploit the delay available.

5. In certain applications the intrusion into user space due to unconstrained mobile nodes may not be acceptable while small motion such as pan, tilt, and zoom can be incorporated with negligible intrusion.

We also discuss some other forms of constrained, low-overhead motion modalities.

An interesting analogy of using motion to leverage limited sensing resources occurs in human eyes. The resolution is highest in the center of the retina and gradually degrades toward the periphery [PG02]. This is an attempt to minimize sensing resources (in this case, neurons) and at the same time maximize spatial resolution and field of view. Rapid eye movements are used to shift the focus of attention toward a peripheral region when some event, such as motion, is detected by the low resolution peripheral view [BRD05].

1.1 Key Contributions

The goal of this work is to explore the issues in system design when motion is used for reducing sensing uncertainty in a sensor network. A review of the prior work reveals that the approach proposed in this paper has not been considered before for providing high-resolution coverage.

First, we discuss if and when it helps to use motion as opposed to alternative methods, such as, using a higher density of static sensors to improve the resolution at which the area of interest is covered. We focus specifically on constrained motion with low resource overheads and discuss why and when this particular form of motion is preferred over other alternatives. We discuss the trade-offs

involved, such as the time it takes for the motion actuators to provide the virtual high-resolution coverage. We systematically characterize this time as the actuation delay, which is a crucial design parameter, and we discuss it in depth. Some of the work that lead to the findings in this regard was performed in collaboration and is available in [KYK04] and [KKP04].

Second, we discuss a system architecture which modularizes the various functions of the motion coordination task. A constrained form of mobility is used, to minimize the resource cost of motion itself. The system architecture describes the various components required to effectively use motion capabilities.

Third, we develop a motion coordination algorithm that helps use motion capabilities with low delay. For this objective, we design a realistic sensing performance metric that models the actual coverage characteristics of the sensors, rather than relying on abstract disk based models. The motion coordination problem is expressed as an optimization of this metric over various possible node poses and orientations. Our distributed algorithm optimizes this global metric using only local communication in a well defined neighborhood. This allows scalability in the number of nodes and reduces the computational complexity of the optimization.

Fourth, we discuss some desirable properties of our proposed algorithm. We prove that our distributed algorithm converges to a desirable network configuration. Convergence is proved without assumptions on the differentiability or smoothness of the performance metric, but the nature of its dependence on sensors is exploited. This is important because the realistic camera coverage model, along with the presence of obstacles in the medium, does not yield a closed form expression for the objective function, and it is not immediately obvious if typical optimization procedures will converge when used with this function.

Fifth, we present a network protocol that implements our distributed motion control algorithm, and addresses practical details such as the message passing required for local coordination, and the termination of the motion without global coordination. The effect of environment dynamics on the motion strategy is considered. The performance of the protocol is studied through simulations that model multiple sensor network deployments with obstacles.

Sixth, we develop practical methods to provide information about the deployment environment that may further enhance the operation of our motion coordination algorithm, such as the distribution of the sensed phenomenon over space in the region being covered and the presence of obstacles that affect sensor range. The methods to collect information about obstacles use laser ranging from multiple nodes and aggregate the laser data to produce accurate medium maps that are useful not only for our motion coordination algorithm but may be applied to other sensor networks for characterizing the quality of coverage. The laser ranging and mapping methods result from collaborative work described in [KCK05a].

Finally, we design and implement a network of cameras with limited mobility, and supporting resources used to learn the presence of obstacles in the medium. We present an implementation of our proposed methods on this sensor network, and evaluate the performance of our proposed methods using real world data from our prototype system. Evaluations are performed in the context of practical applications which may be realized using our system. Our results indicate that the proposals in this work can help attain sensing at a previously unachievable resolution using available sensing resources.

1.2 Related Contributions

In addition to the above, some additional issues were explored involving the use of controlled motion in sensor networks and the reduction of uncertainty using collaboration among multiple sensors.

Apart from the benefits in sensing performance, controlled motion can also be used to enhance the communication performance in certain situations. Large amounts of delay tolerant data can be transferred using a mobile robot rather than wireless transmission. This is advantageous in terms of energy since it reduces the number of hops required and saves the energy spent by embedded energy constrained nodes for forwarding traffic along multi-hop routes. Additional advantages occur because the energy spent by the mobile node can even be replenished at a charging dock while the energy reserves of the sensor nodes embedded in the sensed environment may be hard to replenish. The analysis of the exact energy advantage was carried out in the collaborative work, available in [SKJ06]. The related system design issues such as the appropriate sleep management and routing protocols, along with a prototype implementation were also described in [SKJ06].

As mentioned before, the use of controlled motion is only one of the methods for improving sensing performance and other methods may be applied for the same objective as well. We also explored the benefits in sensing achievable though a fusion of data generated at multiple sensor nodes observing a distributed phenomenon. The results indicate that a lower distortion can be achieved with a given network throughput if the same throughput is shared among multiple sensors rather than used by a single sensor. The precise analysis along with the phenomenon model used and the quantitative analysis of the feasible distortion advantage is available in [PKP04].

1.3 Prototype system

The algorithms and methods discussed in this paper are developed in the context of a network of cameras with limited motion capabilities, or motility.

The sensed data consists of video streams from these cameras, which are processed frame by frame to detect events of interest. Detected events are then sensed at high resolution to provide higher fidelity data for more sophisticated data processing algorithms, such as those for recognition or classification of the events. The medium contains physical obstacles that cause occlusions in the covered region.

The lab scale test-bed is shown in Figure 1.2. Apart from the cameras, it also has other supporting resources such as medium mapping sensors and processing platforms.

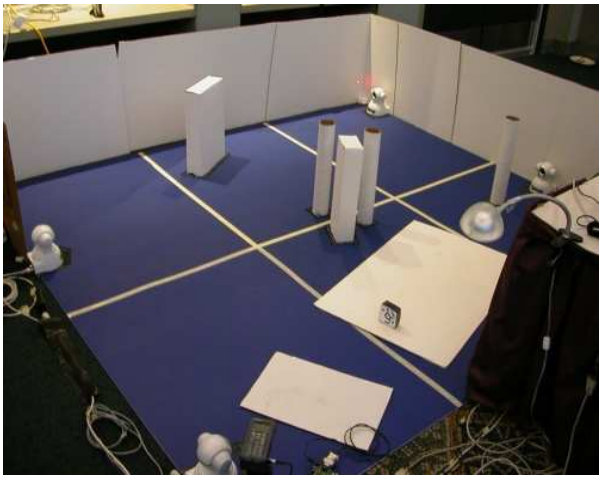

Figure 1.2: Protypte system with motile cameras and supporting resources.

We also used our prototype system to collect data outside the laboratory

setting, in an outdoor environment in the context of a more realistic application as discussed in a chapter 7.

1.4 Outline

This dissertation is organized as follows. The next chapter summarizes the prior work that is related to the considerations in our thesis. Chapter 3 discusses the potential sensing advantage from various types of constrained motion. Chapter 4 describes the design of the overall system architecture and various components used in realizing the advantages due to motion. Chapters 5 and 6 discuss the key components of the system architecture in greater detail, including the motion coordination algorithm developed. Chapter 7 describes the simulations, our system prototype, and the experiments performed to evaluate our proposals. Chapter 8 concludes the dissertation.

CHAPTER 2

Related Work

While there is little work on the problem of using motile sensors for improving the sensing uncertainty and coverage performance of sensor networks, several related problems have been explored. In this chapter, we summarize prior efforts from a variety of fields including computer vision, robotics and sensor networks in the general area of motion coordination for improving coverage related performance metrics.

The use of motion to enhance coverage in sensor networks has been considered in other works such as [WR05]; however, random motion was considered instead of controlled motion. Several motion coordination and configuration strategies have been explored using controlled motion for coverage and sensing uncertainty related performance. We study several of these here, and classify them by the type of algorithm used. This helps us clearly identify the commonalities and differences in the various approaches, and to exploit their salient features in designing the algorithms proposed for the specific reconfiguration problem of interest to us.

2.1 Estimation Theoretic Optimization

Some of the motion control methods utilize estimation performance or information theory based metrics to model the desired objective functions which are then optimized for, using analytical or numerical optimization methods.

An information theoretic measure of sensing uncertainty was used in [Gro02, GMK03]. A utility function was defined using an information measure of the sensor reading and was maximized with respect to the possible set of sensor motion choices. Numerical methods were used for optimization because the cost function lead to non-linear constraints. For deriving a distributed method the utility function was defined as a sum of the individual utilities at each node and a coupling term. One such coupling was through computing a global feature state information metric at all nodes, which depends on receiving all the other nodes' information metrics. The computational cost of such an approach must be carefully considered, since it can be a limiting factor for large scale embedded implementations with constrained processing capabilities. Also, while sharing a global state may be required for optimal coordination, this may not be feasible in large scale networks.

Another information measure was defined in [ZSR02] for quantifying the tracking performance. Rather than motion control, the utility metric was used for selecting the next best sensor based on the observations collected up to the current time. The information gain was measured using the Mahanalobis distance between the sensor location and estimated target location, which requires the covariance in target estimate from each potential sensor for evaluation. An alternative was also suggested for non-Gaussian cases when the probability distribution cannot be represented in parametric form, similar to the particle filter approach: the distribution of the next sensor reading was simulated using the sensor model and the current belief about target state. The simulated distribution was used for computing the entropy or other information measures for all possible sensor choices. Since the selection was limited to neighboring sensors, the method became inherently distributed; a single sensor was assumed to be tracking the target at any time and hence collaboration was limited. Other information or

estimation variance based cost functions have also been considered for tracking purposes, such as in [GJ96].

An alternative information measure is the Fischer Information Matrix, and has also been used, such as, in [AMB05]. A distributed solution was derived when sensors move on the boundary of the target region for a distance dependent sensor model. The algorithm resulted in each sensor moving toward the mid-point of its Voronoi segment. Conditions for convergence of this algorithm were also presented.

2.2 Geometric Optimization

These methods exploit geometric optimization and computational geometry tools to model the sensor properties and performance criteria. The optimization criterion is typically a geometric property such as area covered by a sensor or a specific geometric model for camera visibility.

Several camera placement strategies, also modeled as variants of the Art Gallery Problem [Chv75, OR87, Fis78], have been studied using these techniques. The problem is essentially to place omni-directional sensors with infinite range such that all points in the required region are covered by at least some sensor. The case where sensors are allowed to move is known as the Watchmen Tours problem and has also been explored [CNN93, EGH00a, GLL99, LLG97]. Several results on polygon covering for different classes of polygons and algorithms to centrally compute the best coverings are presented in [Nil94]. Further, the abstract polygon models are extended to more realistic camera coverage models in [ES04]. A model for camera coverage is taken in terms of its depth of field and angular field of view. The pan motion is modeled by considering the angular

positions that may be reached from any initial pan-angle within a time constraint T. An optimization problem is then formulated to determine the minimum number of cameras required to satisfy the coverage constraints and a computationally tractable procedure to solve the optimization problem in 2D is proposed. However, the procedure is centralized and works only for simple polygons, i.e., polygons without holes, since linear time algorithms are available to find the visible subregion of a simple polygon [GA81] (coverage regions with obstacles are thus not addressed). A variant which does consider occlusions appears in [CD00]. The coverage at a point due to a single camera is characterized in terms of the target density at that point, the resolution at which the point is covered and the probability of the point being occluded due to obstacles. The optimization problem is centralized and since the exact solution is computationally intractable, an existing evolutionary algorithm based heuristic is used. In [Suj02], a heuristic cost function is assigned which accounts for probabilistic information about occlusions, and camera visibility of known target locations. This cost function is optimized over all possible camera positions. This method is not distributed and the position is computed at each camera individually.

Some distributed geometric methods were surveyed in [CMB05]. Briefly, the coverage at a point was modeled as a function of the distance from the sensor which best covered this point (typically the nearest sensor, but may vary based on coverage function used), and the total coverage was defined as a weighted integral of the coverage at all points, the weights being based on a density function supported over the region of interest. Alternate cost functions for visibility based coverage (independent of distance within region of visibility) and some other coordination tasks were also discussed. The network configuration was then computed to optimize the chosen cost function. The interesting step in this optimization was that for certain cost functions, the gradient turned out to be spatially distrib-

uted over a well-chosen proximity graph. Some relevant proximity graphs from computational geometry were considered, such as the Voronoi and Delaunay relations. This allowed finding local optima using methods distributed over that proximity graph. The cost functions chosen lead to analytically tractable gradient computation and hence numerical optimization was not required. Specific examples of this approach may be found in [CMB04, OM04] among others.

2.3 Control Theoretic Methods

These methods draw from the analytical tools of control theory to ensure the stability and convergence properties, detecting reachability of certain states and detecting deadlock states of such algorithms. Simple control laws are typically used based on intuitive heuristics for achieving the desired goal.

A representation of the system state and control equations for a distributed system was presented as a summation of two functions, one dependent only on a node's local variables and the other dependent on state variables at other nodes, in [FLS02]. An interconnection matrix was written based on these and a reachability matrix was computed from it. The reachability matrix could be expressed as a directed graph and reachability analysis reduced to a graph search problem. Reachability is known to be useful for establishing controllability and observability. Stability was analyzed using the vector Lyapunov function, and a test matrix based on it. The analysis was demonstrated for a system with a linear control law where the position of each robot was commanded to be proportional to the sum of the positions of the other robots: a limit could be derived on the range of the proportionality constant within which the group of robots was stable. Outside this range, the amplitude of the control input could increase to unstable limits.

A stability and convergence analysis for local interaction based control laws was also presented in [JLM03]. The matrices representing the linear control law for varying neighborhood sets were written, and for the neighborhood relationships of interest, they were shown to satisfy the conditions of the Wolfowitz theorem, which states that an infinite product of such matrices approaches a constant. Thus, the system controlled by such matrices approached a steady state. Some other local interaction models were analyzed for stability in [GP04].

It will be interesting to analyze the stability and convergence of control laws proposed for motion coordination in our work. It may be noted however, that the methods above were described for linear control laws, while the control laws used in our work deviate from linearity.

2.4 Other Optimization Methods

Optimization functions other than those derived using geometric or information centric formulations have also been explored. While some of them use central optimization heuristics, others use highly distributed ones where an approximate global optimum is an emergent behavior of the algorithm.

A large class of distributed motion control methods for coverage maximization may be classified as potential field based algorithms. As an example consider [HMS02a]. The algorithm defines virtual forces which push nodes away from each other and from obstacles. The highly distributed actions of the robots lead to minimization of the potential energy of the system of forces and tends to maximize the coverage of the robots. The network does not spread infinitely due to opposing frictional forces which stop the nodes in a low energy state. Other such methods include [HMS02b, PS04].

The methods we propose are complimentary to those and may be used after an optimal deployment has been found using those methods. Unlike deployment methods which typically need not be concerned with motion delay, our methods address the actuation delay trade-off in providing high-resolution sensing.

Another such approach is found in [BR03], where the occurrence of events determined the motion steps for the sensor nodes, without any explicit coordination among nodes. Each sensor moved toward a detected event, and the distance moved was a function of the distance from the event. This function was so defined such that very far off events did not affect a sensor and this caused a natural clustering of sensors around events to emerge.

An interesting aspect of the method described in [BR03] is that it allowed the sensors to learn the event distributions and adapted the spatial sensor distribution to approach the event distribution. Each sensor learned the event distribution as events occurred and then updated its position based on the inverse of the event cumulative density function (CDF). This caused the sensor locations to acquire the same distribution as the events. While the motion step does not require communication with other sensors, the motion control law requires central coordination: each sensor needs to be aware of the location of all events to learn the event CDF meaningfully, and a large number of events may be required for the estimated CDF to match the true one. Here, an explicit metric was not optimized but the emergent behavior was to improve the match between sensor distribution and event distribution. It remains to be seen if the event distribution may be learned locally[1].

A multi-robot coordination mechanism based on virtual forces which are com-

[1]In our system, since the motion of each sensor is constrained to a local area, each sensor could learn the event distribution within its range of motion- this CDF will not be normalized with respect to the number of total events and any coordination among sensors must account for this fact.

puted from the target locations and positions of neighboring robots was presented in [PT02]. A weighted sum of these forces governed the robot motion. Coverage maintenance with mobile sensors was also considered in [MGE02] and [GKS04].

Another set of coordination algorithms for multiple mobile nodes for controlling their coverage are known as the pursuit-evasion algorithms. One example is the work presented in [AKS03] which assigns probabilities to different possible locations of the evaders based on past measurements and proposed heuristic reward functions for pursuers to cover those locations. Several heuristics are proposed and compared. The optimization itself is centralized.

In [OM02], the authors optimize camera position for improving the performance of 3D reconstruction. This was achieved by placing cameras such that the error variance in the position estimated was minimized. The error variance was computed by relating the error in the point in space to the error in the point in image plane over multiple images. The optimization was performed using a genetic algorithm as the search space is discontinuous and not much was known about its structure. Other variations which account for illumination effects and other limitations have been looked at as well. Note that the performance criterion being optimized for is the scene reconstruction capability rather than detection and recognition. The optimization was centralized. Controlled motion of a camera was also used for 3D scene reconstruction in [MC96]. The optimization function was defined as a weighted sum of the new scene information added due to the motion step, energy cost of distance moved and additional constraints to avoid unreachable locations. A heuristic optimization was employed which searches the parameter space at low granularity and a small region around the approximate optima at high granularity (it may thus not discover the global optimum). Only a single camera which could move anywhere in the scene was considered. Cam-

era position control has also been considered in visual servoing literature, where the goal is to optimize the position of a camera to maintain multiple features of interest in view [MC00]. The methods are typically designed for a single camera.

If the locations of all targets are known, methods from vehicle dispatching problems may be applied to allocate sensors to these known target locations [BP98]. A utility function was assigned to model the performance and a genetic algorithm applied for optimizing it.

Motion control methods have also been developed for coordinating the motion of multi-robot systems for solving other problems such as path planning, formation generation, formation keeping, traffic control, and multi-robot docking [APP02].

2.5 Active Cameras

Aside from controlling motion for mobile sensors or robots, the problem of improving sensing performance in networks of cameras with limited motion capabilities has been considered before in several works. Cameras with motility capabilities, such as pan, tilt, or zoom, are sometimes referred to as *active* cameras.

In [CRZ04], the authors used a set of motile cameras to detect and track multiple targets. Simultaneous detection and tracking was achieved by introducing simulated targets randomly over the area of interest and then having these simulated targets compete with real targets for sensing resources - this ensured that some sensing resources were also spent on searching the entire area while other resources are being used for tracking. A cost function called 'interest' was defined including both simulated and real targets and the camera positions were controlled to optimize this function. The interest in a target was non zero only

for cameras which could see it (from any of their pan-tilt positions) and the total network interest was modeled as a summation of the interest in each target. A factor graph [KFL01] was drawn to represent the dependence of the interest function on different sensors and the max-sum optimization algorithm for optimization over such graphs was used. This method can be implemented in a distributed manner with limited message passing among nodes. The optimum computed is a global optimum when the factor graph is a tree. These methods are complimentary to ours and may be used reactively when an event is detected from the configuration provided by our methods.

Multiple cameras were assigned to multiple tasks using a greedy cost function based approach in [CLF01]. A cost function was assigned to each sensor for each target based on a weighted sum of metrics assigned to visibility of the target, distance from the sensor, and the priority of the target. The cost was optimized using a central and greedy strategy- for each target, the sensor with the minimum cost was assigned to it, and the remaining sensors were assigned to targets for which they had the minimum cost. Another similar cost function based on target visibility, distance and possible camera poses was used in [AB03]. Future target positions were predicted from observed target trajectories and a central optimizer allotted sensors to different targets by minimizing the cost function.

Another multi-camera system combining a variety of motion capabilities including airborne and van mounted cameras was discussed in [KCL98] along with a discussion of the communication, target tracking and target classification algorithms among various other issues. The problem of camera orientation was addressed from the perspective of maintaining targets in field of view as either the mobile sensor platform or the target or both moved. A multi-camera system to track multiple targets was also described in [MU02] where cameras were

grouped as per the target being tracked by them, and a communication method using a shared memory was presented.

A multi-camera multi-target tracking system was also described in [MHT00] where the camera motion is controlled for the specific objective of tracking faces in a meeting-room application. A centralized algorithm is used and the cameras are oriented and zoomed to capture the speaker's face at high resolution. Other systems using motile cameras have been considered in [CDB04, THM00, STE98] among several other works for related coverage and tracking objectives.

However, these works are distinct from ours. They use motion to allocate the available sensing resource successively to different locations. The motion objectives are distinct from our objective of providing high-resolution, and the motion is typically used reactively to track certain events detected by the camera. Also, the actuation delay considerations are very different for our approach. None of the above discuss the use of multiple-resolutions. They attempt to maximize coverage at a given resolution. Our goal is to maximize resolution while balancing the opposing demand of maximizing coverage. One of our system design assumptions is that the phenomenon of interest can be detected at lower resolution but high resolution coverage is required for the specific sensing application using the data (such as recognizing if the phenomenon is important). We can use this assumption to provide higher resolution sensing in regions with detected events, by reducing resolution in uninteresting regions. In a fixed resolution system on the other hand, when a camera orients toward one region, coverage in another region may be totally lost.

2.6 Other Related Work

Apart from motion coordination, some other work is also of relevance to this research, in view of the coverage performance and the specific nature of system constraints relevant to us.

System reconfiguration may occur using methods other than mobility - for instance nodes may be toggled between active and sleep states depending on where the targets of interest are. This may be viewed as a special case of motion coordination where the motion is effected by turning a node to sleep at one location and activating another node at a different location. Some work has been performed in this direction, though with a different objective, for topology management in sensor networks. An example may be seen in [WXZ03a] among other work on topology management in sensor networks. A uniform coverage is desired and redundant nodes are deactivated to save energy. A distributed algorithm that activates sufficient sensors for maintaining coverage was presented. A related example is also the work on node selection for target tracking, presented in [ZSR02].

Designing a mobile sensor system which simultaneously addresses the tasks of detection, classification and tracking also raises interesting issues in the integration of various algorithmic components. Some work has looked into organizational strategies for combining the multiple components in an efficient and robust manner. In [TH], the authors proposed a layered approach where the lowest layers acted on larger amounts of data and filtered it out so that higher layers which need to do more complicated data processing received only potentially useful data. An interesting multi-camera prototype system, using static cameras and central algorithms, was described in [PMT01] and addressed several practical system design issues and integration of multiple vision algorithms.

In our work we assume that camera locations are known. Several localization strategies have been proposed for sensor networks [SHS01, MLR04] in general and for networks of cameras in particular [DR04, FGP06, MCB04]. For the type of motion being considered in our work, even a deployment time record of node installation locations suffices.

CHAPTER 3

Sensing Advantages of Small Motion

In this chapter we discuss the potential advantages in sensing due to small and constrained motion. As mentioned in chapter 1, the use of such motion is more practical due to its reduced resource and navigational overheads. We discuss two types of small motion - first, supported by an infrastructure such as a track or a cable, and second, consisting of pose change using pan, tilt, and zoom.

3.1 Small Motion On Infrastructure

Motion of this form may be achieved by mounting the sensor node on a small track or cable which guides the sensor node movement, such as used in [KPS03]. The motion may in fact be achieved by moving the cable itself, with the advantage that the bulkier components such as motors and batteries may stay static [HAG06].

Such motion yields advantage in sensing through allowing the sensors to minimize the effect of obstacles and also sense over a larger volume by moving to different points allowed along the infrastructure. The resolution of sampling may also be increased using such motion. Several of the findings presented in this section result from the collaborative work described in [KYK04].

3.1.1 Single Obstacle Model

We first analyze the effect of an obstacle on coverage. For the purpose of analysis we make several abstractions which will be removed gradually in simulations, laboratory tests and real world experiments presented subsequently. We carry out our analysis for a sensor with line of sight coverage model, such as a camera, for ease of exposition; the analysis can be extended to sensors in anisotropic media, acoustic sensors in a multi-path environment and other sensor specific coverage models.

Assume that sensors are deployed at uniform density d which yields an inter-sensor spacing a in a regular grid deployment. The analysis is performed for a two dimensional deployment, though similar calculations may be performed in 3D. Consider one sensor which is responsible for covering one tile of this grid, shown in Figure 3.1. Let the area for which one sensor is responsible be denoted by A. For the regular grid deployment $A = a^2$.

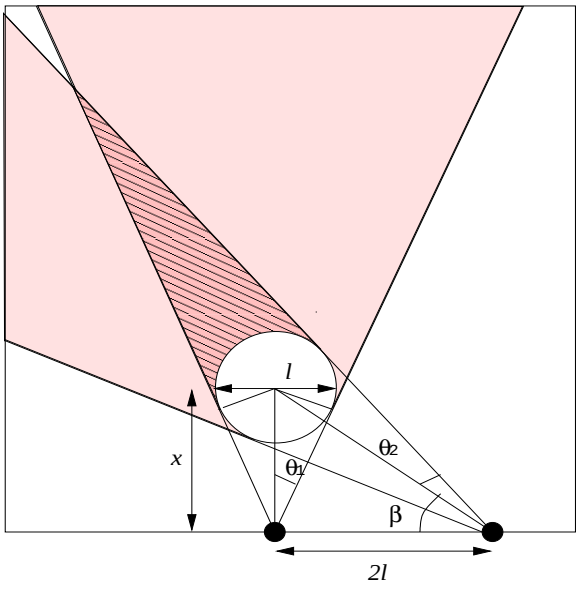

Figure 3.1: Abstract obstacle model for analytical calculation of coverage.

Consider a circular obstacle of diameter l present in this tile which blocks the coverage of the sensor. We will assume that the sensor is capable of limited mobility over a range which is a small multiple of l.

Suppose the area occluded by the obstacle is $A_{occluded}$ (shown shaded in Figure 3.1). To quantify the coverage, we define the probability of mis-detection, PoM, as

$$PoM = \frac{1}{A} \int_{A_{occluded}} f_{target}(x, y) dx dy \tag{3.1}$$

where $f_{target}(.,.)$ is the probability density of the target location within A.

When there is no design time knowledge of the target location, $f_{target}(.,.)$ becomes a uniform probability density. For this case, $PoM = A_{occluded}/A$.

When no obstacle is present, A is completely covered by the sensor and hence $PoM = 0$. Now consider the case when one obstacle is present. Consider the position of the obstacle shown in Fig. 3.1 such that both the tangents from the sensor to the obstacle circle meet the top edge of the tile. Let θ_1 be the angle made by the tangent to the obstacle edge with the vertical line joining the sensor and the center of the obstacle. Let the distance of the obstacle center from the sensor be x. Then,

$$A = a^2 - \pi \left(\frac{l}{2}\right)^2 \tag{3.2}$$

$$A^{static}_{occluded} = a^2 tan\theta_1 - \frac{l^2}{4tan\theta_1} - (\pi + \theta_1)\frac{l^2}{8} \tag{3.3}$$

where $\theta = sin^{-1}(l/2x)$. Next consider the case where the sensor is capable of moving a small multiple of l, say $2l$, on a track along the edge of the tile. The occluded area when the camera may use any location along its track to cover the

tile is shown hashed in the figure. This area is

$$A_{occluded}^{mobile} = \frac{l^2}{4} tan(\omega) - \frac{\omega l^2}{4} \tag{3.4}$$

where

$$\omega = \frac{\pi/2 + \theta_1 + \theta_2 + \beta}{2} \tag{3.5}$$

$$\theta_2 = sin^{-1}\left(\frac{l/2}{\sqrt{4l^2 + x^2}}\right) \tag{3.6}$$

$$\beta = tan^{-1}\frac{x}{2l} \tag{3.7}$$

To determine the magnitude of improvement for specific values of the model parameters, let us evaluate the gain due to mobility as the factor, G, by which the occluded area is reduced due to mobility:

$$G = \frac{A_{occluded}^{static}}{A_{occluded}^{mobile}} \tag{3.8}$$

where the expressions for the numerator and denominator were derived in equations 3.3 and 3.4.

We evaluate the above equation for a range of parameter values. Fig 3.2 shows G for $a = 100, l \in (5, 20)$ and the distance of obstacle, $x \in (20, 35)$. These values are such that the geometrical calculations above hold; the relative values of x, l and a are such that the figure drawn above represents the situation correctly, the calculations will change if the shapes of occluded areas differ.

Figure 3.2 shows clearly that limited range mobility reduces the occluded area significantly. Constrained mobility offers a dramatic impact, therefore, on detection probability for distributed sensors.

Analytical calculation may be continued for varying positions of the obstacle and may be extended for more than one obstacle. However, analysis becomes

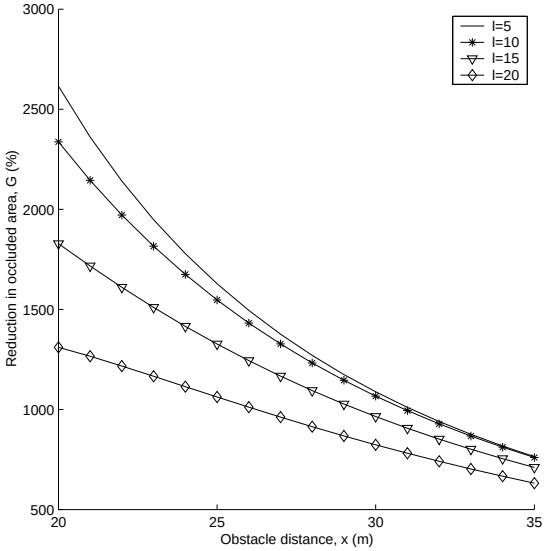

Figure 3.2: Calculating the advantage due to mobility for a simplified obstacle model.

intractable as the number of obstacles grows and we resort to simulations for evaluating more complex and representative environments.

3.1.2 Multiple Obstacles

The simulations consider several scenarios with multiple obstacles. The simulations model a 2D deployment; the effect of height is not accounted for in the obstacle model. Three dimensional calculations would be needed when sensors are observing the environment from a UAV or very high altitude.

Again, we consider sensors placed along edges of a square region, which as before models one tile of a large deployment. The mobile sensor is assumed to be able to move a short distance along the edge.

To model realistic obstacles, we first note than most everyday objects have a small aspect ratio. Also, for the line of sight sensor, it is not the exact shape

of the obstacle but the angle subtended by it at the sensor which determines the occlusion. With this reasoning, we simulate the obstacles as circular. A notable exception to small aspect ratio objects are walls and other forms of boundaries which will severely limit the coverage of a sensor and we do not expect small motion to overcome the effect of walls.

The obstacle diameter is assumed to be a random variable with uniform distribution, between 0 and $2l_{av}$. The density of obstacles is represented as number of obstacles per unit area. The obstacles are placed uniformly randomly over a square area of size 100×100. The random coordinates may lead to overlapping obstacles causing the formation of complex obstacle shapes. As discussed before, we are not concerned with the exact shape of an obstacle but rather with the occlusion caused by it. The sensor is again assumed to be capable of moving a distance d_{move} which is a small multiple of l_{av}.

Coverage is measured by evaluating the area which is visible to the sensor compared to the free area left in the square after the area occupied by the obstacles themselves is subtracted. The line of sight from the sensor to every point in the free area is tested and if there is an obstacle blocking it that point is assumed occluded. Coverage can be calculated by counting the occluded points and the visible points.

To suppress the effect of peculiar chance placements, for each choice of parameter values we average our measurements over 20 runs of the simulation. One of the sample obstacle placements is shown in Figure 3.3, with one sensor placed along the lower edge.

For the first simulation, there is one sensor placed at the center of the lower edge. The value of l_{av} is 5m. The obstacle density is varied from 1 obstacles in the square region to 15 obstacles. Coverage is evaluated for three cases: when there

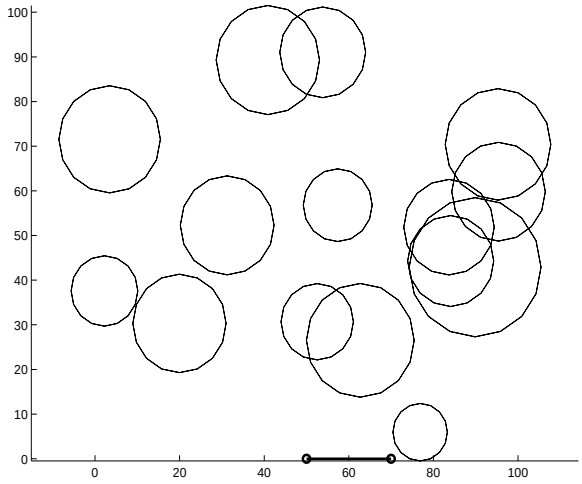

Figure 3.3: Sample obstacles in deployment terrain (The small line along the lower edge shows the track on which the sensor moves).

is no mobility, when the sensor can move l_{av} to one side of the center position and when the sensor can move $2l_{av}$, equally divided on both sides of the center position. Figure 3.4 shows the fraction of free area covered in each case. For each obstacle density, coverage is obtained by averaging over 20 obstacle placements, in each of the three sensor mobility cases.

The gains due to mobility in varying obstacle density, compared to a static sensor are shown in Figure 3.5. The gain is defined as:

$$G = \frac{PoM_{static}}{PoM_{mobile}} \tag{3.9}$$

The figure shows 200% to 700% gain for sensors with small mobility compared to static sensors.

The next simulation studies the advantage due to mobility in varying obstacle size. The value of l_{av} varies between 5 and 20m in a 100×100 area. The number of obstacles is kept fixed at 10. Figure 3.6 shows the multiplicative reduction in mis-detection probability, G. The labels 1 and 2 along the x-axis refer to cases

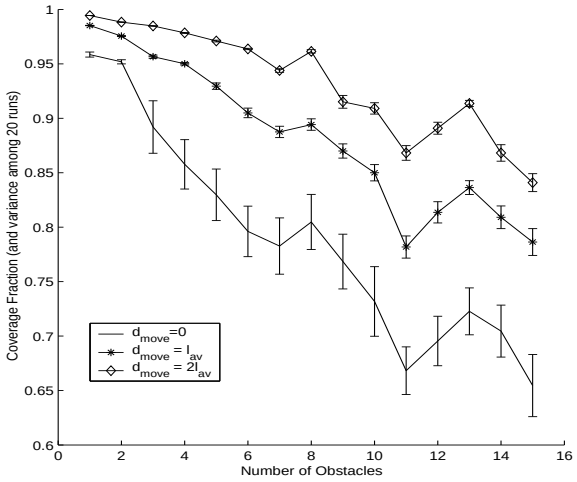

Figure 3.4: Coverage with varying obstacle density, with and without mobility. The error bars show the variance among 20 runs with different random obstacle placements.

when the sensor is allowed to move l_{av} and $2l_{av}$ respectively. Again, actuation shows significant advantage, giving more than a factor of 2 improvement. The variance in the results from the 20 random topologies, not plotted for brevity, is less than 0.05 in all cases. The simulation results are very encouraging and verify that the performance gains expected in simplified analysis with a single obstacle are also expected with realistic scenarios having multiple obstacles and varying camera mobility range. These results motivate us to implement experimental systems which utilize small motion capability.

3.1.3 Experiments

The experimental system studies the improvement in coverage in the presence of realistic effects such as the actual detection algorithms operating on real sensor data, in the presence of transducer noise. The sensor angle of view may be constrained and illumination conditions may affect detection. Previous work on

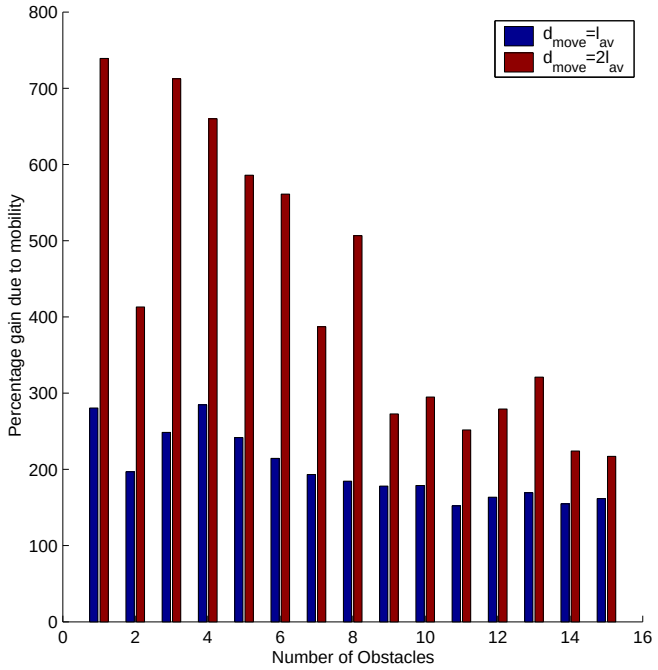

Figure 3.5: Actuation advantage (multiplicative reduction in probability of mis--detection) in varying obstacle density.

coverage in sensor networks [WXZ03b, MKP01, LWF03] has been based only on abstract sensor models, such as a circular disc coverage model, and not on measurements with real sensors; our experiment is one of the first attempts to corroborate the proposed coverage enhancement methods with real-world measurements.

This section describes the camera test-bed built for this purpose and our experiments on it in two different scenarios - a controlled laboratory environment and an outdoor environment with trees and foliage.

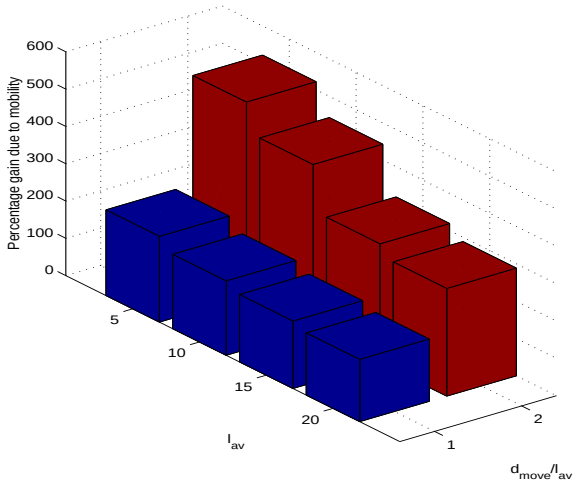

Figure 3.6: Actuation advantage (multiplicative reduction in probability of mis--detection) with varying obstacle size.

3.1.3.1 Laboratory Test-bed with Cameras and Obstacles

Figure 3.7 shows a picture of obstacles in our laboratory test-bed, seen from the camera location.

The sensor used on the test-bed is an Axis 2100 camera system [AXI]. The camera system is equipped with rotational articulation to enable imaging in the entire plane of rotation. The object being detected was large enough to cover a detectable area in the captured image, even when placed at the maximum distance from the camera in the region being covered.

The coordinates for obstacle placement are obtained from the actual location of trees in the Wind River forest [Win03]. The size of tree stems is assumed equal for simplicity of construction. Actual tree coordinates do not follow a uniformly random distribution due to physiological phenomena and using actual forest tree coordinates is expected to provide a realistic obstacle scenario. The obstacles used here are cylinders with diameter of 1 foot. They are placed in a 12 foot by

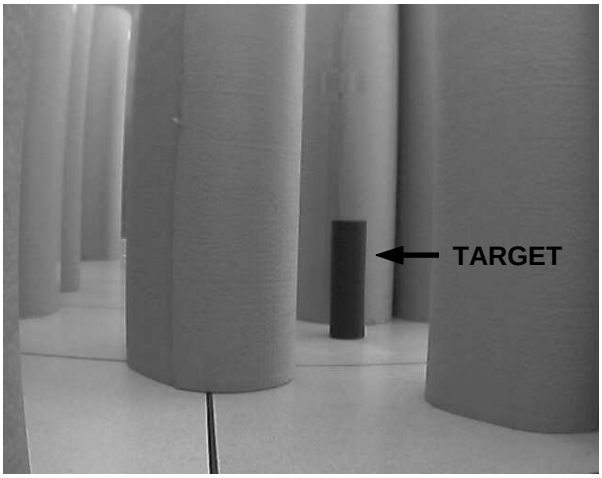

Figure 3.7: The laboratory test-bed for testing coverage advantage due to mobility.

12 foot grid. The tree coordinates are shown in Figure 3.8.

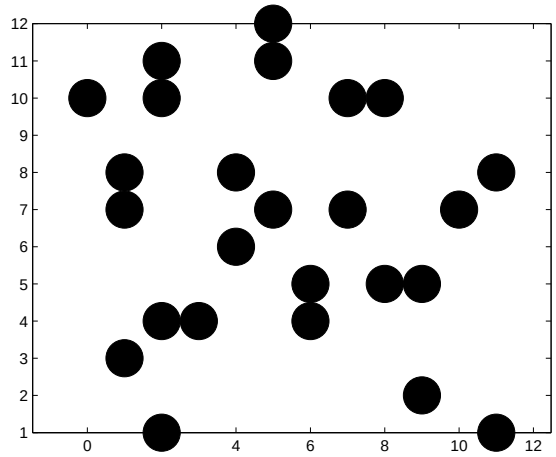

Figure 3.8: The coordinates of trees from Wind River forest [Win03] used to place the obstacles in laboratory test-bed.

The target being detected is a small cylinder of a different color than the obstacles. A simple image processing technique is used to detect the target in

the captured image. As the lighting in the laboratory is controlled, we can take an image of the background with no target present and detect the target by subtracting an image taken when the target is present from the background image. If the target is completely occluded, it is will not be detected. If it is partially occluded, we assume it as detected if the number of pixels visible is above a certain threshold. This threshold procedure reduces the contribution of noise associated with the camera system by ensuring that a minimum portion of the target is observed in order to declare a positive detection.

The experiment is performed as follows. First the camera is placed at the midpoint of one edge of the square area. With the camera stationary, the target is moved to uniformly spaced locations on the $12' \times 12'$ grid. The number of locations at which the camera is able to detect the target divided by the total number of locations at which the target was placed gives the coverage achieved by the static sensor.

Next the camera is assumed to be able to move a distance of two feet. Coverage is again computed using the previous target placement procedure but now if the target can be detected by the camera by moving along its track, the target is assumed detected.

Further, we vary the number of cameras available. One additional camera is successively added on each of the other edges. The mis-detection probabilities are plotted in Figure 3.9 for varying number of cameras, both for the stationary case and the mobile case. The mis-detection with mobility is significantly lower than the static case, reaching an order of magnitude improvement in some cases.

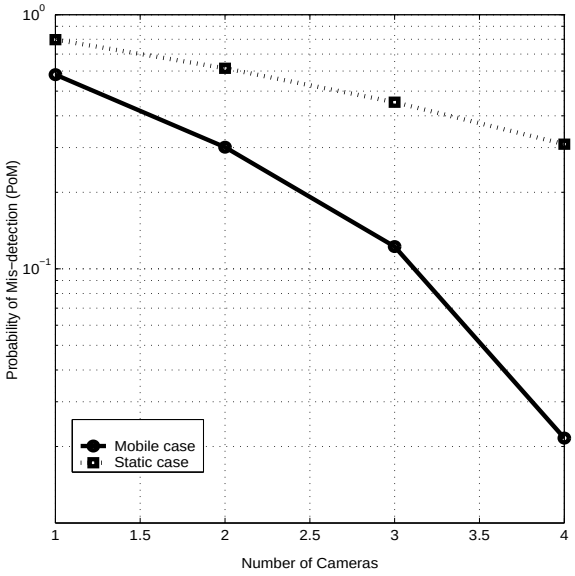

Figure 3.9: Probability of Mis-detection in laboratory test-bed experiments: varying number of cameras. PoM is lower with mobility.

3.1.3.2 Experiment in Trees and Foliage

We also test our findings outside the laboratory, using a more realistic setting. An environment with trees and foliage is selected, near our campus, shown in Figure 3.10.

The obstacles are no longer ideal cylinders and cameras do not operate in controlled lighting conditions. The cameras being used are not designed for outdoor usage and the image quality is affected by exposure to sunshine for the long duration required for collecting data in our experiments. This leads to some errors in our simple image processing techniques for detecting the target. It may be noted that the foliage causes rather large occlusions and our mobility here is much less than the mean obstacle diameter, instead of being an integral multiple of it.

The experiment performed consists of one camera placed along one edge.

Figure 3.10: Image of real world scene showing obstacles consisting of trees and foliage, among which the target is to be detected.

Coverage is measured over a $12' \times 12'$ grid in the forest. Detection probability is first measured when the camera is fixed at the midpoint of the edge. Then the camera is allowed to move two feet in one direction. Third the camera is allowed to move 2 feet in both directions. The mis-detection probabilities and gains are tabulated in Table 3.1. The measurements show that mobility even when lower than average obstacle length is able to provide significant advantage in reducing the uncertainty of sensing.

Table 3.1: Mis-detection probabilities with and without motion for real-world experiment

$CameraMode$	**PoM**	**G (%)(relative to static case)**
STATIC	0.3885	-
MOVE, 1 direction	0.2374	163.65
MOVE, 2 directions	0.1942	200.05

3.1.4 Two-dimensional Motion on Infrastructure

We mention an example where constrained motion helps increase the resolution of sensing, using a system that allows infrastructure supported motion in a two-dimensional plane. We proposed a system that allows the motors and power connections to be present at only one corner of the two dimensional plane being covered. The cables themselves are used to move the node across the plane and supply power to it. This reduces the payload moved by the motors since the motors and power supplies do not have to be moved. The system is rapidly deployable since it only requires the two supporting end poles to be installed at the location of interest. A schematic of the system is shown in Figure 3.11.

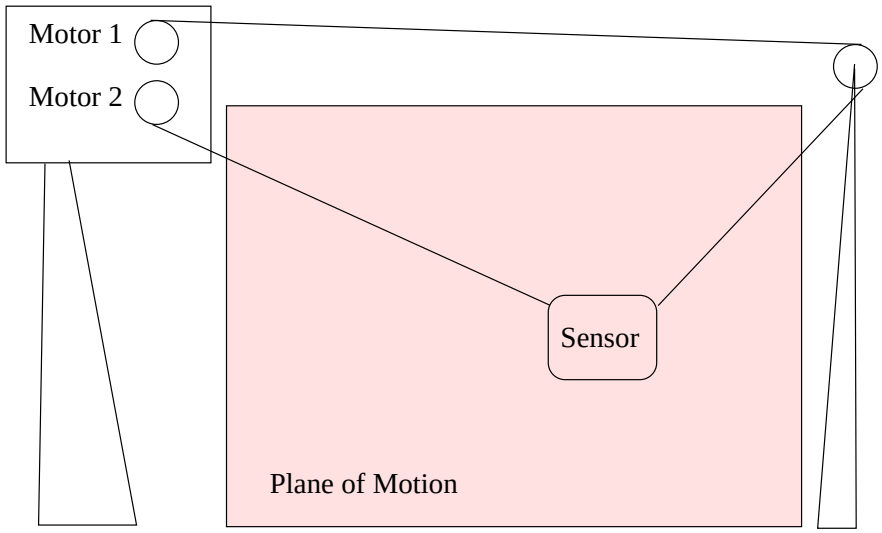

Figure 3.11: NIMS-LS: a system to provide infrastructure supported 2D motion.

Another system to provide 2D infrastructure supported motion was designed in [HAG06]. The infrastructure consists of a cable suspended horizontally between two supports at opposite ends of the plane of motion. The horizontal cable supports motion along the horizontal axis. A second cable in the vertical direction is used for motion along the vertical axis.

Consider an application where the concentration of nitrate radical (NO_3^-) is to be mapped across the cross-section of a river, such as shown in Figure 3.12. The

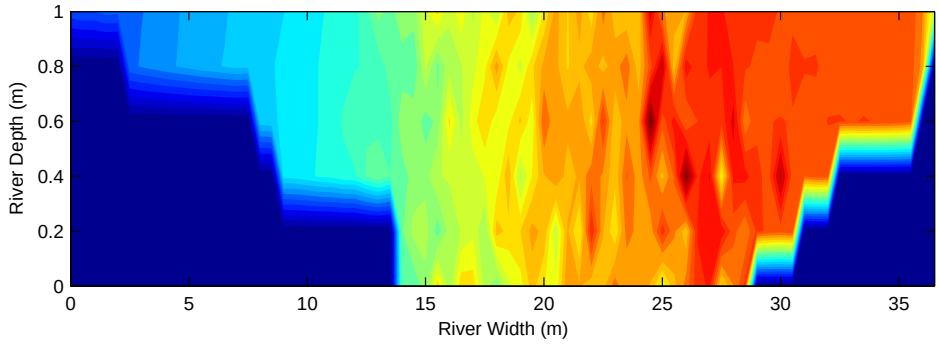

Figure 3.12: Nitrate concentration (mg/l) across the cross-section of a river.

available nitrate sensor node has a transducer surface $0.1m \times 0.1m$ that is used for sensing. Suppose nitrate concentration is to be mapped at 0.5m resolution. Then, installing the available sensor at every 0.5m across the river cross-section along with the deployment infrastructure such as metal trusses to support the sensors in the river is likely to interfere with the nitrate concentration map. On the other hand, a sensor with constrained motion in a 2D plane across the river cross-section, such as described above, can map the nitrate concentration at the required resolution without interfering significantly with the phenomenon. Assuming the concentration map does not change within the time it takes for the sensor movement to be completed, the nitrate concentration can be mapped at the required resolution.

3.2 Pan, Tilt, and Zoom Motion for Cameras

Pan, tilt and zoom can significantly extend the sensing coverage, despite its simplicity and ease of practical realization. For instance, the area covered by a camera can be increased by panning and tilting the camera head. As a represen-

tative example, we analyze the increase in coverage for a commercially available pan-zoom-tilt camera [Son04].Its actuation capabilities are summarized in Table 3.2.

Actuation	**Range**	**Speed**
Pan	+170 to -170 degrees	170°/second
Tilt	+90 to -25 degrees	76°/second
Zoom	25X (Horizontal field of view angle changes from 45° to 2°)	3 seconds/(1X to 25X)

Table 3.2: Example actuation specifications, for camera used in prototype, Sony SNC RZ30N.

Figure 3.13-(a) shows a simple model for the volume covered by the camera at its widest zoom, and without any pan and tilt. This volume, V_{static}, is approximated as a pyramid with a rectangular base of area $Ll \times Hl$ and height R_s. A small region near the vertex of the pyramid is not actually covered as the camera has a minimum focal distance and objects closer than this distance cannot be captured. For the above camera, at the widest zoom, this distance is 0.03m, which turns out to be negligible compared to the height of the pyramid, R, calculated below and this effect is thus ignored. Based on the minimum resolution desired for imaging, we can determine the range R_s which is satisfactorily covered by the camera. Let the image size be $L \times H$ pixels, taking L to be the horizontal dimension. Suppose the minimum spatial resolution needed for the application is such that a length l in space must cover at least one pixel. The image area of $L \times H$ pixels will then represent LHl^2 area in space. The horizontal field of view for the camera, $\theta_{fov,h}$, can then be used to calculate R for the required l value:

$$tan(\theta_{fov}/2) = \frac{lL/2}{R_s} \tag{3.10}$$

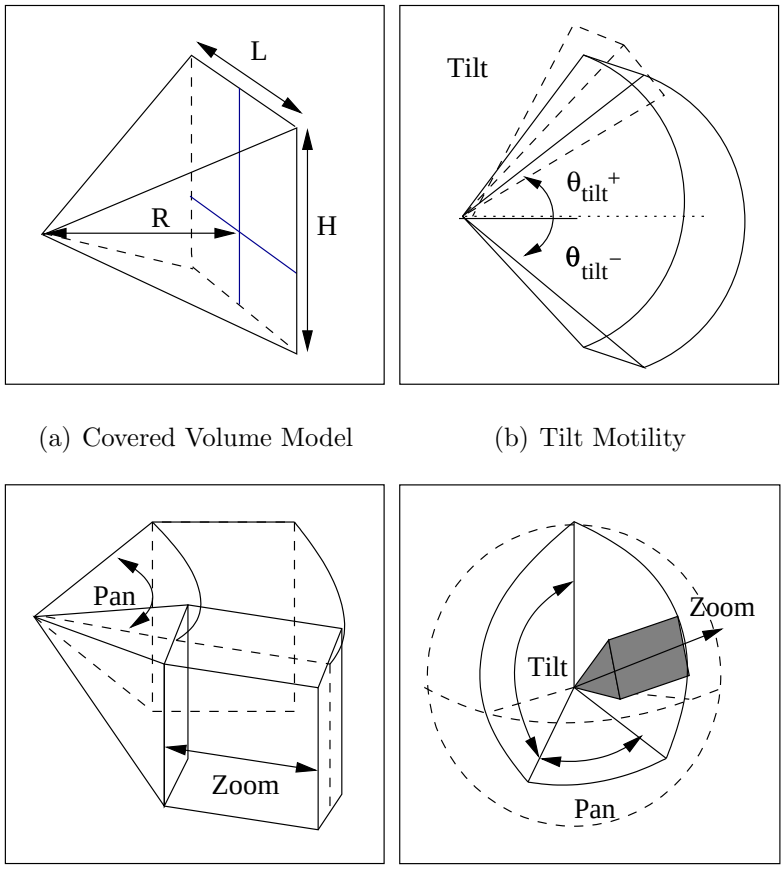

(a) Covered Volume Model (b) Tilt Motility

(c) Pan and Zoom Motility (d) PZT Motility

Figure 3.13: Actuation in a PZT camera (a) volume covered without actuation can be modeled as pyramid, (b) tilt capability increases the effective volume covered, (c) combined pan and zoom capabilities further increase the volume covered, and (d) volume covered when pan, tilt, and zoom are combined: this can be viewed as a portion of a sphere swept out using pan and tilt, where the thickness of the sphere depends on the zoom range.

The value of l depends on phenomenon size and the minimum image resolution needed by detection algorithms. Suppose $l = 1$cm is used. For the sample camera, $\theta_{fov,h} = 45°$, $L = 640$ pixels and $H = 480$ pixels, which yields $R_s = 7.27$m. This

value is within the focal range of the camera. The focal range may limit R and hence the usable range of l. We also assume that the illumination is sufficient for the zoom range available on the camera. Thus, V_{static} is given by:

$$V_{static} = \frac{LHR_s l^2}{3} \tag{3.11}$$

Now consider the volume covered with motility. When motorized zoom with a zoom factor of z is used, the range covered becomes zR_s. The additional volume covered is a cuboid of depth $(z-1)R_s$ and area $Ll \times Hl$. The total volume covered with zoom, V_z, becomes:

$$V_z = V_{static} + LH(z-1)R_s l^2 \tag{3.12}$$

and corresponding gain factor due to zoom motility, g_z, is $g_z = V_z/V_{static} = 3z-2$.

Let the tilt angles with respect to the plane of pan rotation be denoted θ^-_{tilt} in the downward direction and θ^+_{tilt} upwards, with their total being θ_{tilt}. The volume covered when the tilt capability is used, V_t, can be viewed as the volume of a sector of a disk of radius R_s, thickness Ll, and sector angle θ_{tilt} minus the volume of two cone sectors of radius R_s, height $Ll/2$ and sector angle θ_{tilt}. This volume is shown in Figure 3.13-(b). A half of the pyramid extends beyond the tilt range on each side, and these additional edge volume segments extending beyond the sector total up to V_s. The total volume covered with tilt motility, V_t, is thus:

$$V_t = V_{static} + \frac{\theta_{tilt}}{2\pi}\left[\pi R_s^2 Ll - 2\left(\frac{1}{3}\pi R_s^2 \frac{Ll}{2}\right)\right] \tag{3.13}$$

The calculation of the volume covered using pan motility is very similar, and is omitted for brevity. Figure 3.13-(c),(d) show the volumes covered when two or more actuation modes are combined. Evaluating these volumes yields the overall gain due to pan, zoom and tilt combined, g_{pzt}, to be:

$$g_{pzt} = (3z-2) + \frac{\theta_{tilt} R_s}{2Hl}(3z^2+1) +$$

$$\frac{\theta_{pan} z^3 R_s^2 (1 - \cos\theta_{tilt})}{LHl^2} + \left[\frac{cos\theta_{tilt}^{-} + cos\theta_{tilt}^{+}}{2L}\right] \frac{\theta_{pan} R_s}{2l} (3z^2 + 1) \quad (3.14)$$

This formula can also be used to calculate the gain due to motility primitives separately; for instance, substituting $z = 1$ and $\theta_{pan} = 0$ yields the formula for gain due to tilt alone. Note that g_{pzt} is independent of l as the quantity R_s/l in each term can substituted from equation (3.10) in terms of camera parameters $\theta_{fov,h}$ and L.

Substituting the values of L, H and other parameters from Table 3.2 in (3.14), we get the coverage improvements listed in Table 3.3.

Actuation	**Gain**
Pan only	7.74
Tilt only	4.04
Zoom only	73
Pan and Tilt	27.71
Pan and Zoom	6361
Tilt and Zoom	2908
Pan, Tilt, and Zoom	226940

Table 3.3: Coverage Improvement with PZT actuation

Clearly, actuation yields a significant advantage in coverage, especially when two or more simple forms of actuation are combined together. For example, the last row in the table shows that the pan, zoom and tilt actuation can reduce the number of cameras required by over five orders of magnitude, in unobstructed environments.

3.2.1 Usable Range of PZT Motion

The above calculations assumed the entire range of motion capabilities is usable. However, in a practical setting, only a part of it may be used, such as due to the tolerable delay available for motion, or the motion triggering mechanism. Suppose the motion triggering mechanism is such that the camera uses its pan, tilt, and zoom motion to zoom in to a location where an event is detected from its wide angle view. Then clearly, the entire pan range may not be utilized but only the pan range equal to the field of view angle in the horizontal direction may be used. Also, the useful zoom range is limited to the difference in resolutions required for detection and the final sensing task. We analyze the coverage gain with these effects next. Suppose the resolution required for the final sensing objective is such that the camera can image up to the maximum distances R_s. The volume covered by the camera can be modeled as a pyramid of height R_s with the base area $Ll_s \times Hl_s$, and its vertex at the camera[1]. This yields the volume over which the desired sensing resolution is provided, say, V_s. Suppose detection can occur when a distance l_d is mapped to a single pixel-length, which similarly leads to a volume V_d over which detection is feasible.

Figure 3.14-(a) shows the volumes V_s and V_d. The camera can provide the resolution l_s at points outside V_s, but within V_d, by using its pan, tilt and zoom motion. The maximum advantage that may occur in coverage due to motion is $G = V_d/V_s$, if the camera has motion capabilities to reach any point in V_d at the resolution l_s and sufficient time is available for that motion to occur. Figure 3.14-(a) also shows the pan, tilt and zoom ranges required to cover the entire V_d. Suppose the time taken for that motion, referred to as the actuation delay, is τ. The advantage G may be reduced if the tolerable actuation delay

[1]A small region near the vertex may be too close for focus limitations but its volume is assumed insignificant compared to the entire pyramid

does not permit reaching some fraction of V_d. The tolerable delay τ depends on the event dynamics. Consider again the example camera: it has a field of view $\theta_{fov,h} = 45°$ in the horizontal direction and $\theta_{fov,v} = 30°$ in the vertical direction, which determine the horizontal and vertical vertex angles respectively for V_d. It has pan and tilt ranges of 340° and 115° respectively, which are more than sufficient to cover the entire V_d. The zoom range is 25, which means that the maximum ratio R_d/R_s supported is 25. The pan and tilt speeds are $170°s^{-1}$ and $57.5°s^{-1}$ respectively. The time taken for zoom is non-linear and was measured experimentally for the entire zoom range (Figure 3.14-(b)).

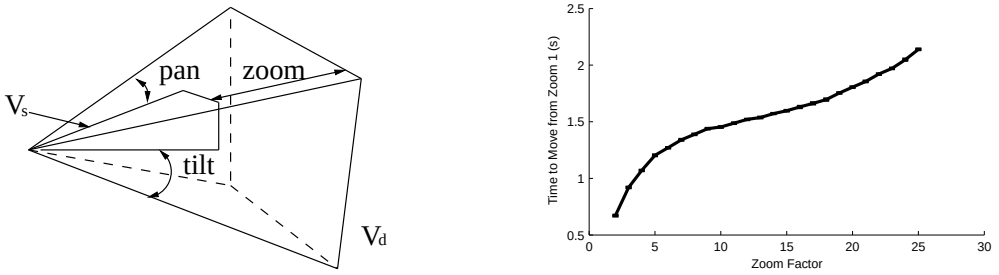

(a) Covered Volumes

(b) Zoom Delay

Figure 3.14: (a) Covered volumes for detection and sensing phases, with the pan, tilt, and zoom required to provide sensing resolution within the detection volume. (b) The time to change zoom measured as a function of the zoom step. The communication delay in sending the zoom command was separately characterized and has been subtracted from the motion time.

The detailed calculation of the advantage in covered volume due to motion, G, for these capabilities is skipped for brevity. The derived value of G is plotted in Figure 3.15 for various values of τ ranging from zero to the maximum time required to exploit the entire motion range and various values of R_d/R_s within the zoom range of the camera. Note that G is quite large and hence plotted

on a log scale. The region in the figure corresponding to actuation delay above $1s$ and the ratio $R_s/R_d > 2$ shows more than an order of magnitude advantage in coverage. Applications with sensing requirements that lie in this region will benefit significantly from the algorithms discussed in this thesis.

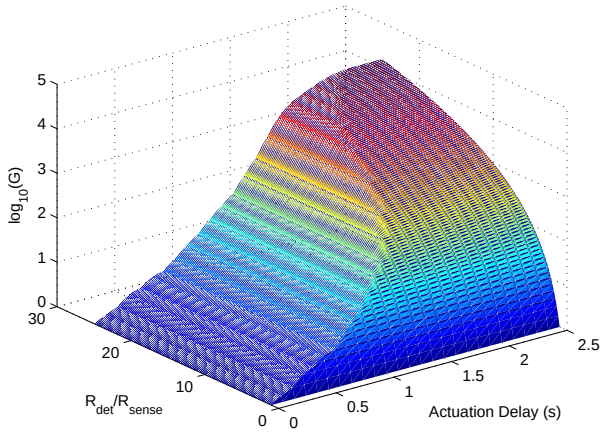

Figure 3.15: Evaluating coverage gain due to motion with varying actuation delay and difference in detection and identification resolution.

3.2.2 Advantage with Multiple Nodes

The preceding analysis showed how motion can help improve sensing when it is used for providing high resolution coverage on demand from a given pose. There are additional ways in which motion may improve coverage, specifically by optimizing the initial configuration itself. These additional advantages becomes relevant when the sensor nodes with pan, tilt, and zoom capabilities are used in a network, rather than at a single node.

First, a random deployment may cause two sensors to be covering overlapping areas while other areas remain uncovered. Motion allows efficient orientation of

the sensors to cover non-overlapping areas.

Second, regions blocked by obstacles for one sensor may be viewable by another sensor, if that sensor chooses the appropriate position or orientation. Among the multiple possible network configurations, the positions of the nodes can be collaboratively adjusted to minimize occlusions. Just as with infrastructure supported motion, pan, tilt, and zoom motion may also be used to achieve this.

As an illustration, figure 3.16-(a) shows a random placement of 20 sensors in a $25m \times 25m$ area, each oriented randomly, and in the presence of obstacles. The circles represent obstacles in the sensing medium and the sensor locations are marked with small diamonds. The sectors of circles indicate covered regions,

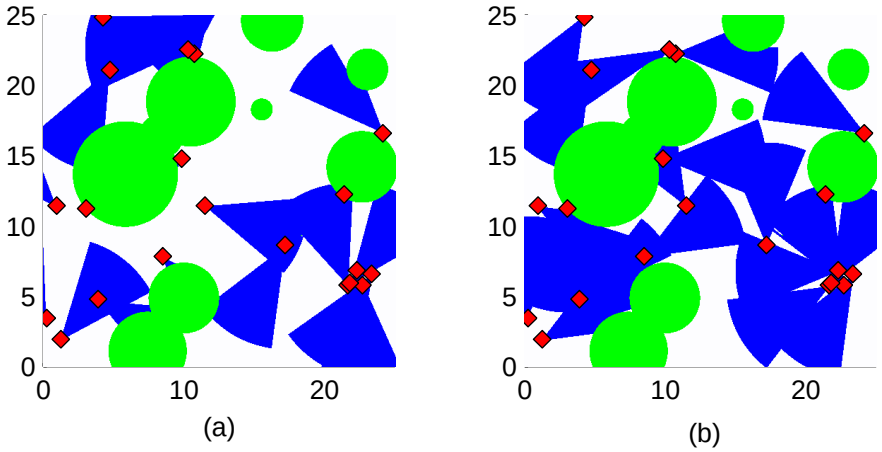

Figure 3.16: Instantaneous coverage increase: (a) a sample topology showing randomly oriented sensors, and (b) sensor orientations changed using pan capability.

modeling a 45° field of view and a range, $R_s = 7.3m$, as calculated earlier for the sample sensor. If these sensors have pan capability, their orientations can be changed. Figure 3.16-(b) shows a changed network, where the number and loca-

tion of nodes has remained the same, only the orientations have been updated using pan motility. Figure 3.17 shows this gain with varying node density. A distributed algorithm to update the sensor orientations, and achieve a configuration such as shown in Figure 3.17 is considered in chapter 5.

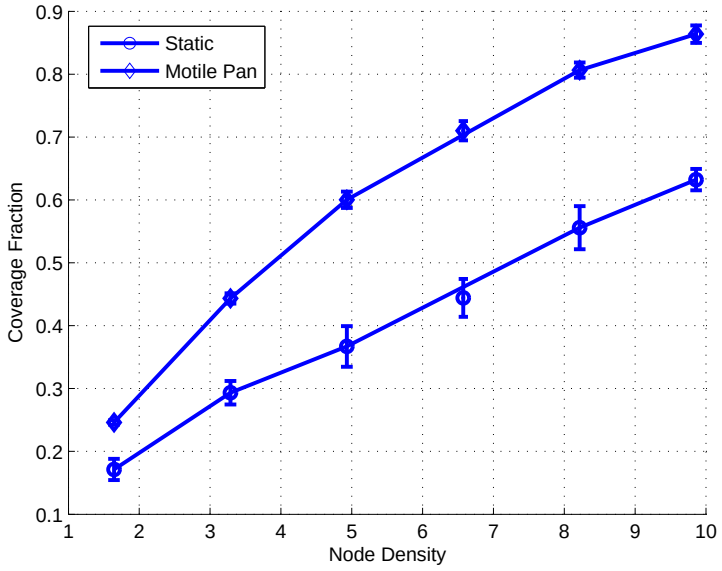

Figure 3.17: Coverage advantage when pan actuation is used for initial reconfiguration only, at multiple densities. Error bars show standard deviation across 10 random topologies. (Node density is measured as the number of sensors in the area covered by a single sensor.)

3.3 Trade-offs in Using Small Motion

The preceding analysis and simulations for various types of constrained motion show that this practical form of motion which is easy to integrate in an embedded sensor network, has a significant potential to impact sensing performance. However, it is of interest to compare this approach against other alternatives that

may be used to improve sensing performance, and explore the trade-offs related to various choices. There are two obvious alternatives to the use of motility. One is to use a much higher density of static nodes and the other is to use an even lower density of mobile nodes with long range motion capabilities. We will discuss how small mobility compares to these.

3.3.1 Feasible Resolution

The deployment environment may limit the density of static sensors that may be deployed. This limit may arise from various reasons. The ability to provide mounting supports may be restricted to a limited number of locations within the environment being monitored. The size of the sensor node limits the density of deployment. A very high density of sensors may interfere with the phenomenon itself. Additionally network capacity, such as the channel bandwidth in a wireless system, may limit the density of nodes. The provision for energy may impose another limitation. If a wired energy infrastructure is provided, the density at which the cabling can be installed will limit the node density. For systems using environmentally harvested energy, the amount of energy available in the environment may limit the number of nodes.

Consider for instance the resolution feasible using a finite set of sensing resources with and without motion. The image shown in Fig. 1.1(a) is obtained using a 1 Megapixel (1MP) camera. The resolution of coverage over the region of interest is: $40 pixels/m$ at the near end of the road and $7 pixels/m$ at the far end of the road in the scene. In the image shown in Figure 1.1(c), the same 1MP sensing resource is allocated to a small region achieving $200 pixels/m$ resolution over that region. Providing such high resolution coverage over the entire scene using only static cameras, mounted at the same location, requires sensing resources of

784MP[2].

Let us compare what motion may achieve. Suppose the 1MP camera used to obtain the image is equipped with pan, tilt, and zoom motion capabilities. Then, a zoom of 13X along with a small pan and tilt motion is sufficient for this 1MP camera to capture the image shown in Fig. 1.1(c) by focusing its sensing resources selectively on a small region. These motion capabilities may be used to get high resolution at any subregion of the scene shown in Fig. 1.1(a) and thus motion has provided a virtual 784MP resolution using only 1MP sensing resource. There are several issues in using the latter alternative such as the delay in carrying out the pan, tilt, and zoom steps and the issue of finding out the regions of interest. These issues will be discussed at length in the subsequent sections. For situations when those issues can be satisfactorily addressed, using motion is a significantly better alternative.

Thus, for the application scenario of interest, if the required resolution cannot be achieved with a static system (such as if 784 1MP cameras are impractical to be deployed in the above example), but can be achieved with a mobile network, clearly, the use of motion is to be preferred.

There may be other applications where the resolution achieved by a static network of low power cameras such as developed in [RBI05] may suffice. In some instances, the area to be covered may be so small, such as a known choke point in the field of view, that high resolution can be provided using a static cameras. Again, motion may not be required to increase resolution in that scenario.

[2]Deploying cameras closer to the road could enable the use of much lower resolution cameras such as used in red-light violation monitoring systems, but we assume that we are not allowed to install our equipment on the city road infrastructure.

3.3.2 System Deployment and Operation Cost

A second concern in choosing to use motion may be the system cost. Suppose the number of nodes required in a static network is N_s and the number of mobile nodes to get comparable coverage is N_m. Excluding certain applications such as those where the sensor nodes are scattered from an airplane over an open field, most applications, particularly those in indoor and urban environments, require each sensor node to be individually deployed at a specific location, often manually. For instance, deploying a camera requires mounting it on a wall or ceiling, installing a dome or cover, and connecting it to a wired or wireless communication network. For the current generation of cameras, deployment also involves providing a power connection, although batteries or environmentally harvested energy may power future generations of low power cameras. Suppose the deployment cost per node is c_{dep}. Suppose the cost of data processing at the back-end for data received from a node is c_p. These two costs are likely to be same for both static and mobile nodes. Suppose also that the cost of a static node including maintenance for the duration of deployment is c_s. Denote the corresponding number for a mobile node as c_m. This number depends on the type of motion capabilities included in the mobile node. The total system cost for the static case becomes $N_s(c_s + c_{dep} + c_p)$ and that for the mobile case becomes $N_m(c_m + c_{dep} + c_p)$. Noting that the node costs c_s and c_m are likely to diminish with advances in camera sensors and MEMS based motion technology, in addition to the fact that c_{dep} and c_p are same for both types of nodes, leads to the conclusion that the trade-off will be determined primarily by values of N_s and N_m. For the current generation cameras, since the difference between c_s and c_m is within an order of magnitude while the difference between N_s and N_m is greater than an order of magnitude, typically several orders of magnitude for examples considered in this thesis, again the trade-off is

dominated by N_s and N_m.

3.3.2.1 Example

We now consider an example coverage scenario and compare the N_s and N_m for it. To decouple the trade-off arising due to motion delay for this example, let us first assume that the persistence time or the Nyquist interval of the sensed phenomenon is $T = 3s$, which allows the pan and linear motion motility to be used fully. For nodes with unconstrained mobility, while the range of motion is potentially infinite, only a finite motion is possible within the tolerable delay. We assume a velocity $v = 100cm/s$ for such mobile nodes, as navigation and traction support for such speeds has already been demonstrated in experimental platforms. We also allow the mobile nodes to be able to turn with maximum agility at the same speed, which implies that an unconstrained mobile node may move and orient to any position within the distance vT.

The exact relation between the numbers of static and mobile sensors required is dependent on the medium and the nature of deployment, and hence we generate random topologies with multiple obstacle and sensor configurations. The obstacles are again cylindrical and the sensors are arranged in a 2D deployment interspersed with the obstacles, over a $20m \times 20m$ area. Ten random topologies of obstacles and sensor placement are evaluated. The number of sensors is varied to compare the coverage at different node densities. We evaluate the coverage for four alternatives: static nodes, nodes with pan only motility, nodes with one dimensional limited linear motility, and nodes with full unconstrained mobility. Note that only a single calculation is performed for the fully mobile nodes, as the initial random configuration is not relevant for this case; these nodes may re-position themselves to the best initial configuration from which the allowable

mobility range of vT then allows them to cover the maximum area.

Figure 3.18 shows these results. Clearly, lower densities are required with actuation for the same coverage quality. For instance, at 90% coverage, the static density is 7 times higher than that with pan actuation. This suggests small actuation can significantly lower the system cost. Unconstrained motion has an even lower N_m but the cost and complexity of the mobile nodes may be unacceptable for the system.

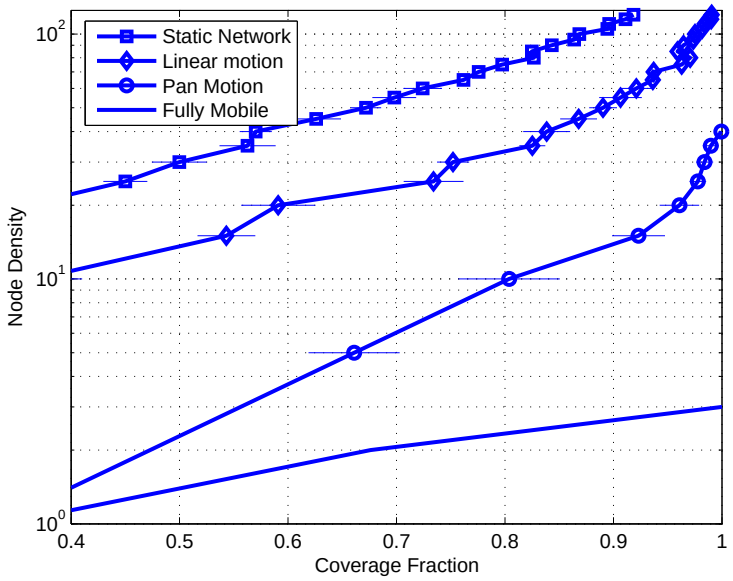

Figure 3.18: Alternative deployments: Coverage fraction with and without actuation at different deployment densities. Node density is the number of nodes in a $20m \times 20m$ square region, where each sensor covers a sector of 45° with radius $R_s = 7.3m$. The error bars show the standard deviation across 10 random topologies simulated.

Such numbers for N_s and N_m provide an approximate insight into the appropriate system design choice, since the operational and deployment costs are

determined largely by these two quantities. One may however, for a specific system, compute the node costs as well and compare the system cost in terms of the node costs.

The cost needs be evaluated for the particular sensors of interest for a system, and the costs may change over time. Here we compare the system cost for known values of c_s and c_m for various motion alternatives. First, we do not account for $(c_{dep} + c_p)$, which makes the comparison harsher on the alternatives with motion. Installation costs as high as 75% of the system cost have been reported [Far01]. Here, the savings in $(c_{dep} + c_p)$ due to a lower N_m compared to a static system are not being considered. Second, the off-the-shelf fully mobile nodes do not have built-in reliable navigation and localization subsystems, rather they have a traction platform with appropriate interfaces for adding deployment specific navigational support. We ignore the costs of these additions, thus losing the significant advantage that motile nodes have in that they do not need such extra support. Third, the cost of the motile node considered is with three motile capabilities- pan, tilt, and zoom even though only the pan capability is considered in the above density evaluation. Obviously, the cost of a pan-only camera will be lower than one with all three motility primitives. Figure 3.19 shows the cost trade-off, and even with the harsher comparison, the motile nodes offer a significant advantage. The costs considered are USD 800 for a static network camera [SNC04], 1300 for a pan-tilt-zoom network camera from the same manufacturer and having similar optical capabilities [Son04], and 35000 for a fully mobile node [Pac04]. For linear actuation, we assumed the cost to be 1200, assuming the static node cost plus an additional track, motor and motor controller.

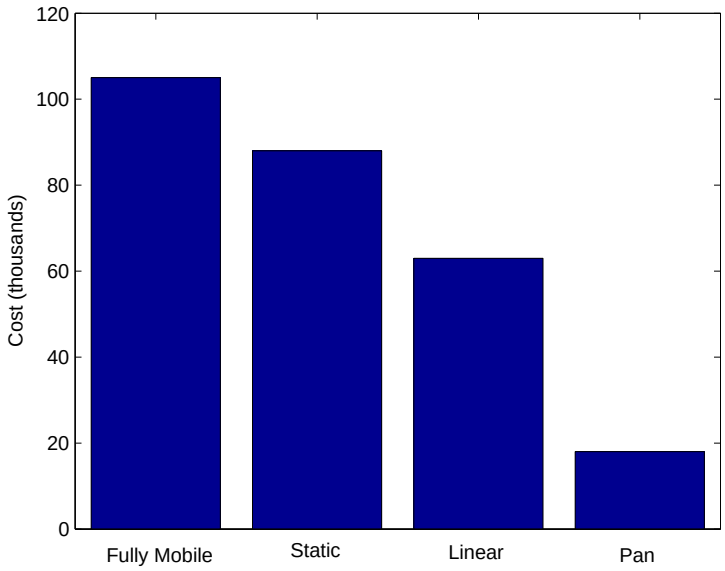

Figure 3.19: Converting the node density to total network cost, at 90% coverage point.

3.3.3 Actuation Delay

Another difference between a static and mobile network is that while in a static network, the sensing is instantaneous, it is not so in a mobile one. Since the mobile camera takes a finite non-zero time for the actuating to the region of interest, there is a delay before the application receives the desired high-resolution data. We call this delay the actuation delay. The advantage in resolution depends on the tolerable actuation delay; the motion advantage disappears if the tolerable delay is zero. Hence, this is a crucial issue in deciding whether motion may be used.

The actuation delay scales better than linearly with the number of cameras saved. Recall the earlier example where 784 static 1MP cameras were required

to obtain the desired resolution. A naïve approach can achieve a linear scaling in delay. For instance, a single camera may be actuated to perform a raster scan visiting the appropriate pan, tilt, and zoom poses to successively cover the small regions covered by the 784 cameras. However, a better strategy such as using the single 1MP camera to cover the entire scene at low resolution, applying a low resolution algorithm to detect regions of interest in the field of view and actuating only to cover those regions, reduces the delay significantly. In this case, the camera does not visit all 784 poses but only a few of those, depending on the number of detected events.

We will consider the delay trade-off in greater depth in designing the motion coordination methods to exploit small motion capabilities for improving sensing performance.

CHAPTER 4

System Architecture

The preceding discussion motivated the choice of small motion for improving sensing performance in certain scenarios as opposed to other alternatives. In scenarios where such motion is indeed the preferred choice, a key design issue is to provide a system architecture that exploits motion capabilities effectively to provide the best possible sensing performance. As mentioned before, we design our methods for a system of cameras with pan, tilt, and zoom capabilities and some of our design choices are thus specific to image sensors.

A naïve method to use motion for reducing the sensing uncertainty is to successively allocate the available sensing resources to small regions such that high quality coverage is provided at each region, in a time shared manner. However, this method has a high delay penalty. An alternative method, that promises significant advantages in delay, is feasible in several applications. This method is as follows: allocate available sensing resources sparsely to cover the region of interest at a low resolution that is sufficient to detect the phenomenon of interest, and then selectively concentrate more sensing resources on regions where the phenomenon is detected, providing an equivalent high-resolution coverage to the overlying application using the sensor network. This approach is feasible in all applications where a low resolution coverage is sufficient to detect the phenomenon, such that high resolution coverage may then be provided only at the locations where the phenomenon of interest is detected. There are several

applications where detection of an event of interest may be carried out at low resolution. For instance faces can be detected using color detection [BSP04], which requires a lower resolution than required for recognizing the faces. Humans or vehicles in a scene may be detected using motion detection, whereas high resolution coverage may be required for the actual surveillance application logging a high resolution image of the visitors. In other applications, an alternate sensor modality may be used for detection. For instance, magnetic sensors may be used to detect vehicles and then image sensing resources may be allocated to the required region. An acoustic beam forming technique may be used to detect where an animal call originates [WEG03] for an ecology application, or where a shooter is present for an urban security application [MSL04], and then high resolution imaging may be directed toward that location.

Obviously, one of the system components required in realizing this approach is a motion control method to carry out the motion required each time a phenomenon detection occurs. A simple example of this motion occurs in a camera with pan, tilt and zoom capabilities: the camera may zoom in to the pixel location in its field of view where a phenomenon of interest is detected. More sophisticated motion strategies may be used for other objectives such as providing coverage by multiple cameras when a phenomenon of interest is detected by one of them. The exact requirements are application specific, and some methods have been explored for such motion control [CDB04, CLF01, THM00, STE98].

Somewhat less obvious perhaps, and not previously studied to the best of our knowledge, is the need for methods that allows the system to use the motion capabilities effectively, such as with low delay, for the above mentioned motion control component. We focus our attention on this latter aspect. Before the movement of nodes to provide high resolution coverage takes place, the phenomenon must be

detected and the system is thus required to provide a good detection performance. Further, when the movement occurs, the actuation delay is a key consideration, particularly when the mobile network approach is compared to the alternative of using a higher density of static sensors to achieve the same resolution. Clearly, this delay should be characterized. The system should use motion capabilities in such a way that the actuation delay is small for phenomena occurring at any point in the area covered by the network. The limits on tolerable delay will also limit the range of motion that may be used.

Our objective is to develop a system architecture that provides the required detection performance and helps minimize the actuation delay.

Additionally, the system architecture should also attempt to exploit any information available about the deployment environment. Specifically, the following two types of information may be useful in controlling motion: a map of obstacles in the sensing medium and the expected spatial distribution of the phenomenon being sensed. It is desirable that the system architecture include components in the system to learn such information and that it allows the network to gather and use such information in a distributed manner.

We now discuss our system design in view of the design objectives mentioned above and also describe additional design choices made in our system. We are not concerned with the actual application level image processing algorithms but only with providing the high resolution image for such processing.

The various system components required to support the above mentioned objectives have been modularized into the blocks shown in Figure 4.1.

Block I, labeled medium characteristics, represents any means available to the network for learning the locations of the obstacles. If available, this knowledge helps the motion strategy to minimize occlusions. Such methods may be based

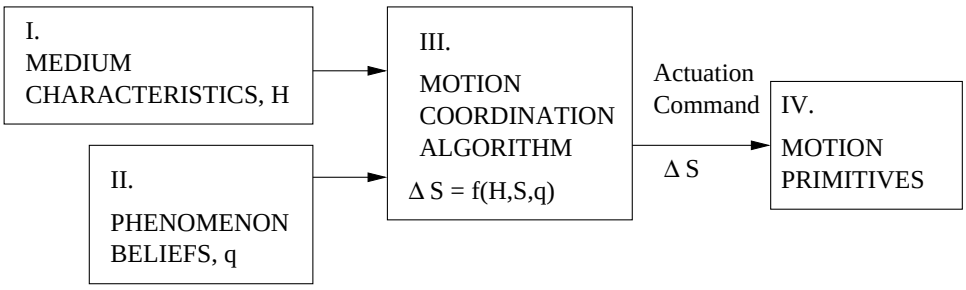

Figure 4.1: System software architecture.

on the use of range sensors [HH03] or in the case of cameras, the use of stereo-vision. If this block is not available, known sensor coverage models assuming an obstacle-free space may be employed, albeit with a performance penalty. In our testbed, we use laser ranging to map the obstacles, as discussed in chapter 6.

Block II, labeled event distribution, denotes any methods available in the system to learn the spatial distribution of interesting events. As an example, consider a network of cameras deployed to capture all the faces of people present in a shopping mall. Motile cameras can adapt their poses to provide lower actuation delay in specific regions where more people are present, such as a food court at meal times or a box office before show times. The functionality of this block may be realized using various means. For instance, the block may use a high density deployment of low power sensors (Eg. Passive Infra-Red sensors) for detecting human motion, or using the cameras themselves at low resolution to detect an event, for learning the distribution of the phenomenon over space. The specific methods used in our work are discussed in chapter 6.

Block III, labeled motion coordination algorithm, represents the algorithm used to choose the appropriate pan, tilt, and zoom setting at each camera such that actuation delay, when some event is detected, is minimized. We refer to these reconfiguration methods are proactive motion control methods to keep them dis-

tinct from the motion control methods used reactively after an event is detected, for zooming in to that particular event and sensing it at high resolution. This block also includes the network protocol required to implement the motion coordination algorithm in a distributed manner. We discuss this block in greater detail in chapter 5.

Block IV, labeled motion actuators, represents the motion capabilities available in the system. These motion capabilities are used both by the proactive method to choose a good configuration for the network and by the reactive methods for providing the high resolution sensing when an interesting event is detected. In our system these actuators are the pan, tilt, and zoom motors in the camera. The camera used allows controlling its motion capabilities via sending it command packets in HTTP format with hardware specific values for various motion settings. We developed a driver, in Java, with a programmer friendly interface that accepts the required pan, tilt, and zoom motion steps in decimal values. Our driver takes care of converting these to hardware specific format and packetizing them as per the protocol required by the hardware.

This architecture is distinct from previously designed active camera networks that used motion to patrol larger areas [CRZ04, CLF01, STE98, CDB04] that required constant motion for the patrol. On the other hand, the low resolution detection phase that we use does not require constant motion. Further those methods are mostly designed for the reactive phase of tracking events after being detected. That is distinct from the high-resolution objective we present. Also, the previous works do not proactively configure the system to reduce the actuation delay.

Assumption: In designing our system architecture in view of the above design issues, we have made the following general assumption. We assume that each sen-

sor knows its location. This assumption is required only for improving the sensing performance through coordination among multiple nodes. A local rudimentary strategy to use motion without any coordination among sensors is also mentioned, and while it does not require the use of location information, such a strategy performs significantly worse than one with coordination. The assumption about the availability of location information is reasonable in many applications since the location information is required to geostamp the sensor data itself. Several localization strategies have been proposed for sensor networks [SHS01, MLR04] in general and for networks of cameras in particular [DR04, FGP06]. For the type of motion being considered in our work, even a deployment time record of node installation locations suffices.

4.1 Technology Context

While our prototype is implemented using the current technology generation of cameras, we believe that our system architecture is designed to support the anticipated technology trends in this domain. More compact and lower power cameras are becoming available for use in wireless sensor networks. MEMS based motion technology will enable significantly more compact and lower power pan and tilt mechanisms for such devices. Electrically controlled lens focus for changing the zoom, such as being developed for zoom-capable cellphone cameras, will enable the zoom capability to be accessible in compact low power wireless camera nodes likely to be used in future sensor networks. As more and more applications that use image data emerge given the increasing accessibility of the underlying technology, our methods for increasing the resolution will be increasingly relevant for newer generations of camera networks. Further the potential for significantly larger numbers of cameras made feasible through these emerging technologies will

directly benefit from the distributed and scalable nature of our methods.

Also, as technology evolves, the image resolution in terms of number of pixels at a camera and the processing capabilities may increase, such as with Moore's Law. This may enable a given number of static cameras in a network to achieve a higher resolution than possible with the current generation hardware. For certain applications, this increased resolution may mean that the required resolution becomes feasible with static cameras alone. The architecture we presented may be used to obtain still higher resolution when it helps enable newer applications or improve the performance of existing ones further.

CHAPTER 5

Motion Coordination Methods

We now consider block III of Figure 4.1 in detail: motion coordination algorithms to achieve a desirable network configuration, and adapt it to the spatio-temporal dynamics of the environment. Our focus is on distributed methods, due to scalability concerns.

We express the problem of motion coordination algorithm design as an optimization of a specific sensing performance objective. This performance objective models the two key considerations in using motion - the actuation delay and the detection activity required to guide the actuation. We begin with the discussion of a quantitative metric to characterize this performance objective.

5.1 Sensing Performance

The first important consideration in motion coordination is the choice of the sensing performance metric to quantify the value of a given network configuration. Our camera coverage model depends on three parameters. The camera can view any point not closer than its minimum focal distance R_{min}, and not farther than R_{max} beyond which distance the spatial resolution is too poor to be of interest. The camera has an angular field of view θ_{fov}. The three parameters R_{max}, R_{min}, and θ_{fov}, change with the zoom setting of the camera. Given this model, the sensing performance is characterized as follows.

5.1.1 Actuation Delay

The first quantity of interest is the actuation delay achieved by the network configuration. As mentioned before, complete coverage is only provided at a resolution lower than required for the final sensing application, and the cameras are zoomed in to the relevant location when an event of interest is detected. The actuation delay depends on the time taken by the camera to actuate (using its pan, tilt, and zoom motion) for providing the required high resolution coverage after an event is detected. It is defined concretely below.

Let the region to be covered by the network be denoted by $\mathcal{A}$ and let p be a point in $\mathcal{A}$. Suppose an event is detected at a point p. Suppose the time taken by the camera to pan, tilt and zoom for focusing at the point p is denoted by $\tau(p)$. It can be measured in terms of the motor capabilities of the node. Since the pan and zoom are driven by separate motors and can occur in parallel, the time required is:

$$\tau(p) = max\{\delta\theta_p * \omega_p, t_p(\delta_z)\} \tag{5.1}$$

where $\delta\theta_p$ is the pan angle to be moved to direct the sensor at p, ω_p is the angular pan speed, δ_z is the change in zoom required for achieving the required classification resolution at p, and $t_p(\delta_z)$ is the time required for changing the zoom. Note that $t_p(\delta_z)$ is a non-linear function of δ_z and a closed form expression is not available for it. We have experimentally measured it for integral values of δ_z for our sensor, and we use a linear interpolation in between the measured values (Figure 3.14-(b)). The tilt time can be considered similarly as the pan time, but our system deployment is two-dimensional and hence tilt is ignored.

This quantity $\tau(p)$ is defined to be the actuation delay for that particular point p, for the given camera. In a network, multiple cameras may be able to actuate to point p. We define $\tau(p)$ to be the one required by the specific camera

chosen for detection, as described below.

5.1.2 Detection Performance

Second, the coverage metric must also characterize the detection performance. Several possible metrics exist for this, beginning with a purely geometric coverage metric which quantifies the area in line of sight of the sensors, to more sophisticated estimation theoretic metrics which quantify the probability of detection based on the noise models and collaboration among sensors. Let $c(p)$ denote the detection performance at point p. Since detection depends on resolution, we model $c(p)$ as proportional to the resolution at which a sensor s views p, measured in the number of pixels per unit area. This is a more accurate model than a purely distance based one, since the resolution depends not only on the distance but also the zoom setting of the camera and obstacles in the medium. For simplicity we assume no coordination among sensors for detection. Since multiple cameras may have $c(p)$ in their field of view, we define $c(p)$ to be the highest value provided by any one of sensors observing p.

5.1.3 Performance Objective

To aggregate the above factors into a single metric, we consider a linear combination of the two metrics to determine the sensing performance, $f(p)$, at a point:

$$f(p) = w * c(p) + (1 - w)\{1/\tau(p)\} \tag{5.2}$$

The choice of the weighting parameter w, where $0 \leq w \leq 1$, determines the proportion of the contribution of actuation delay and detection terms to the performance. The value $1/\tau(p)$ is capped to a maximum when $\tau(p) = 0$.

Apart from maximizing the probability of detection, and minimizing the actuation delay, it may also be of interest to maximize the area covered. Let $1(p)$ be a binary function which takes the value 1 at covered points and 0 at others.

The network may have to be geared toward regions where more events are expected. Suppose that the event distribution function is known at all points $p \in \mathcal{A}$ and is denoted $q(p)$. Considering the above factors, we define the coverage utility at a point as:

$$u(p) = (1 - \alpha) f(p) * q(p) + \alpha * 1(p) \tag{5.3}$$

where α is a constant weight, $0 \leq \alpha \leq 1$, determining the significance of coverage alone. Note that the second term in the above equation is not multiplied by $q(p)$. This allows maximizing the area covered, even when events are concentrated in a small region, by setting the value of α to be high. Methods to learn $q(p)$ are discussed in chapter 6.

Suppose the state, or pose, of a sensor node i is denoted by $\mathbf{s}_i = \{\theta_p, z\}$, where θ_p and z represent the pan and zoom settings respectively. The network configuration, for a network of N nodes is then denoted by $\mathbf{S} = \{\mathbf{s}_1, \mathbf{s}_2, ..., \mathbf{s}_N\}$. Given the pan and zoom ranges of a node, the node state $\mathbf{s}_i$ lies in a set $\mathcal{S}_i = \{[\theta_p^{min}, \theta_p^{max}], [1, z^{max}]\}$, where the superscripts min and max represent the minimum and maximum possible values respectively for the superscripted parameters. Let $\mathcal{S}$ represent the resultant set of possible network configurations. It is given by:

$$\mathcal{S} = \mathcal{S}_1 \times \mathcal{S}_2 \times \ldots \times \mathcal{S}_N \tag{5.4}$$

Using the metric defined above for each point, we now express the overall utility of a network configuration, $\mathbf{S}$, as:

$$U(\mathbf{S}) = \sum_{p \in \mathcal{A}} u(p) \tag{5.5}$$

The network reconfiguration problem can now be expressed as an optimization problem, where the goal is to determine the network configuration which maximizes the coverage utility:

$$\mathbf{S}_{opt} = \max_{\mathbf{S} \in \mathcal{S}} U(\mathbf{S}) \tag{5.6}$$

5.2 Distributed Motion Coordination

We now discuss a distributed algorithm to solve the above problem. A distributed approach is advantageous due to the reasons discussed below.

5.2.1 Complexity Considerations

It is not immediately obvious how the optimization problem can be solved efficiently because the optimization problem in (5.6) is NP-hard. Consider a special case of the problem: $\alpha = 1$. In this case the utility function is reduced to maximizing the coverage due to N sensors over a polygonal region with obstacles. So, if the problem in (5.6) can be solved in polynomial time, then a polynomial time solution exists to maximize coverage in a polygonal region with obstacles. However, that problem is known to be NP hard [CN88]. Thus, the problem in (5.6) is clearly NP-hard.

Further, the nature of $c(p)$ and $\tau(p)$ implies that $U(\mathbf{S})$ is not only non-linear but also not known in a closed form – it can only be evaluated numerically for each $\mathbf{S}$. As seen from equation (5.4), the search space is exponential in N and a brute force search over $\mathcal{S}$ is clearly out of the question.

The performance metric being used for optimization is a global metric for the entire network and depends on the state of multiple sensors. The phenomenon distribution and medium characteristics are learned locally. Thus, the perfor-

mance metric is not known at individual sensors given their local views and only partial knowledge about $q(p)$.

5.2.2 A Distributed Approach

A distributed solution will thus help ameliorate both communication overheads and computational complexity. Here, we define an algorithm to be distributed, if under its execution, each node exchanges messages only within a local neighborhood rather than with a central coordination entity or the entire network. The desirable local neighborhood for a node should minimize the number of communication hops required for coordination, and its size should not increase with the network size N.

Consider the utility function $U(\mathbf{S})$ defined in equation (5.5). This function is inherently distributed in that the utility value at a point p can only be influenced by a subset of the sensors: the ones which have p in their line of sight and within the maximum range of view from one or more of their possible poses. Denote the set of sensors which influence the utility value at p by $\beta(p)$. Collect together into a sub-region $\mathcal{B}_j$, all those points which share the common influencing sensor set $\beta(p)$, and denote this sensor subset by β_j. Suppose the entire region $\mathcal{A}$ can be divided into K such sub-regions. By definition the $\{\mathcal{B}_j\}_{j=1}^{K}$ are disjoint (the corresponding β_j are not). There may be points in region $\mathcal{A}$ that are not covered by any of the sensors; as a matter of notation, these may be denoted by $\mathcal{B}_K$ corresponding to $\beta_K = \Phi$, the null set. The utility function can now be decomposed into a summation over these disjoint sub-regions:

$$U(\mathbf{S}) = \sum_{j=1}^{K} \sum_{p \in \mathcal{B}_j} u(p) \tag{5.7}$$

Since each $\mathcal{B}_j$ corresponds to a sensor subset β_j and a set of N sensors may

have 2^N subsets, the number of terms in the above summation is potentially exponential. We can however map the above decomposition to one where the number of terms is linear in N. Let γ_i denote the subset of sensors which is the union of all subsets β_j to which sensor i belongs:

$$\gamma_i = \{j | \exists \beta_k \text{ such that } (i,j) \in \beta_k\} \tag{5.8}$$

The utility in the region within range of sensor i can only be affected by the sensors in γ_i. Given the state of each sensor in γ_i, sensor i can compute the set of points Γ_i at which i gives the highest $f(p)$ value. The sub-regions Γ_i are disjoint (though the sensor subsets γ_i are not) and $\{\Gamma_i\}_{i=1}^{N} \cup \mathcal{B}_K = \mathcal{A}$. Hence the utility function can be decomposed as:

$$U(\mathbf{S}) = \sum_{i=1}^{N} \sum_{p \in \Gamma_i} u(p) \tag{5.9}$$

The interesting property of this decomposition is that each each sensor only needs to communicate with sensors in γ_i to determine $U(\mathbf{S})$ over Γ_i. We call γ_i the neighborhood of sensor i. The set γ_i includes all sensors which may affect the computation of Γ_i from any pose selected at those sensors.

Suppose the region influenced by sensor i from all its poses is $\mathcal{V}_i$. Then, the set γ_i includes potentially all sensors influencing any point in $\mathcal{V}_i$. The expected cardinality of this set depends on the deployment density and the maximum distance up to which a sensor may influence coverage. For most practical sensors, the distance up to which they may sense is bounded, which implies that the cardinality of γ_i stays constant even as the network size, N, increases, at a given deployment density.

5.2.3 Coordination Algorithm

We now describe a distributed algorithm which requires each sensor to coordinate only with sensors within γ_i and yet improve the global utility function. Suppose a mechanism is available at sensor i to ensure that when it is changing its pose, all other sensors in γ_i will remain static. The communication protocol to realize this mechanism, and other implementation details will be discussed in the next section. The algorithm then proceeds as follows.

Sensor i searches over all its possible pan settings, and chooses the one for which the utility evaluated over $\mathcal{V}_i$ is maximum:

$$\theta_p(i) = \max_{\theta_p \in [\theta_p^{min}, \theta_p^{max}]} \sum_{p \in \mathcal{V}_i} u(p) \tag{5.10}$$

This is a one dimensional search and thus computationally tractable. After selecting its best pan setting, the sensor similarly selects its best zoom setting. After this pose update, sensor i stops and some other sensor j waiting on i may update its pose, again making sure that sensors in γ_j stay static during its update step.

This change in pose at i affects all Γ_j for $j \in \gamma_i$. However, it does not affect sensors not in γ_j and they may be changing their poses in parallel with sensor i using the same method. This property makes the algorithm distributed over neighborhoods γ_i. The sensors update their poses in an arbitrary order.

5.2.3.1 Termination Condition

The termination condition in the protocol is chosen for ease of distributed implementation. In centralized optimizations, a stopping criterion that can determine when to stop the iterations is to check when the change in the estimate of the optima has become insignificant over the past few iterations. However, in the

distributed setting, the global utility metric is not available to any node. Even if the parameters in control of a particular node are not changing from one iteration to the next, the parameters at other nodes may be changing and determining the stopping time would thus require global coordination. The distributed termination condition is that a node will assume its actuation has terminated when the improvement increment in local utility is below a threshold Δ. In our implementation discussed in section 5.4, the value of Δ is set to 0.1% of the previously measured utility over $\mathcal{V}_i$ and may vary from sensor to sensor.

Note that a sensor need not physically carry out the actuation until it reaches the termination condition of the algorithm. It only needs to communicate its updated pose for the coordination mechanism to work.

5.2.3.2 Example

Before analyzing the convergence and other properties of interest, let us visualize the above update procedure for a simple example with two sensors. Consider a rectangular region with a few obstacles and two cameras placed at diagonally opposite corners, as shown in Figure 5.1. Each camera can pan 90°, in its corner. To reduce the dimensionality of the search space to two for easier visualization, let us ignore zoom. The utility function achieved for all combinations of pan angles at each camera is shown in Fig. 5.2. The pose selection algorithm described above proceeds as follows: sensor C1 first selects a pan, $\theta_p(1)$, which maximizes the utility in its region of influence. This change is configuration is seen as line segment A in Figure 5.2. Then, sensor C2 selects a pan pose, $\theta_p(2)$, for this given value of $\theta_p(1)$, and line segment B shows the change in network configuration. In the next iteration, again C1 selects a new pan $\theta_p(1)$ moving along line segment C.

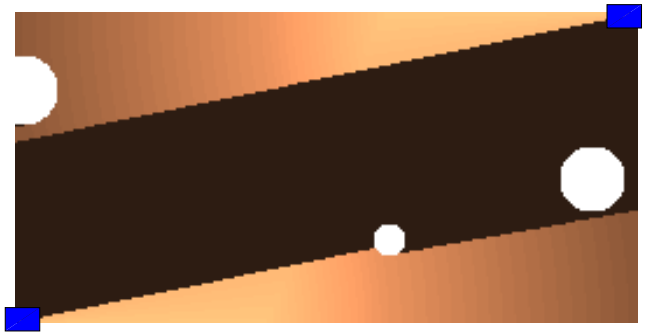

Figure 5.1: Illustrative scenario for motion coordination algorithm. The white cirular regions are obstacles. The darker shade is uncovered region. The lighter shaded regions represent covered areas, where lighter regions represent better detection.

At each step, our algorithm searches along a line in the $2N$-dimensional search space, $\mathcal{S}$, and so we will refer to the above optimization procedure as *incremental line search* (ILS). The procedure is incremental at each node but not at the network level. Multiple nodes may be actuating in parallel. The neighborhoods γ_i may be overlapping implying the reconfiguration process cannot be broken down as occuring in each neighborhood separately but the constraints within each subset γ_i must be satisfied.

Note that in addition to the above method for configuring the network, another motion control algorithm is also required to move the cameras after an event is detected for providing the required high resolution coverage. For this task, we use a simple method that zooms in to the pixel location in the image

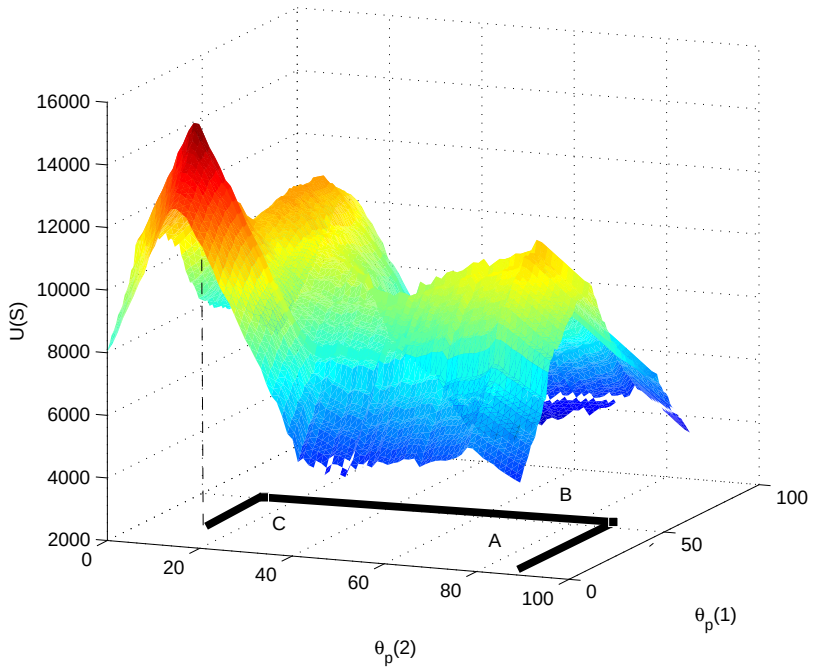

Figure 5.2: Utility function for various possible pan pose combinations. The θ_p values are in degrees, measured counter-clockwise from initial camera pose. The utility function has multiple local maxima, even for this simple scenario.

where an event is detected. One advantage of this approach is that the spatial location of the detected event is not required. More sophisticated methods which may move multiple cameras in response to detected events have been studied in other works [CDB04, CLF01, THM00, STE98].

5.3 Convergence and Other Properties of the Motion Coordination Algorithm

While the proposed algorithm is not guaranteed to find the global optimum, it has several desirable properties that are discussed below, including convergence to a stable state.

An important property of the above optimization procedure is that it does not require a closed form expression for the utility function, but may proceed using only a numerical computation. It does not make any assumptions on the smoothness or differentiability of the objective function. This makes the above procedure amenable to several realistic performance metrics, in the presence of non-linearities in actuation and the effect of obstacles.

Further, the termination condition used is distributed, and hence no global coordination is required for the termination. A side effect of this is that no node in the network may know when the actuation has terminated globally.

Another important property is the convergence of the network configuration to a stable state. Even though the sensors may update their local poses without any global coordination, the network utility function will not oscillate. Further, the utility will reach a local maximum[1], though not necessarily the global one, which is hard to ensure without global coordination. We prove this convergence property below.

Lemma 5.3.1 (Monotonicity of ILS) *Under ILS execution, the global network utility increases monotonically.*

Proof: Assume first that only one sensor i in the entire network updates its pose at a time. Suppose the network configuration after iteration t is denoted $\mathbf{S}_t$. The region $\mathcal{A}$ can be viewed as consisting of two disjoint subregions $\mathcal{V}_i$, the region influenced by sensor i from any of its poses, and $\mathcal{A} - \mathcal{V}_i$. The utility can be expressed as:

$$U(\mathbf{S}_t) = \sum_{p \in \mathcal{V}_i} u(p) + \sum_{p \in \mathcal{A} - \mathcal{V}_i} u(p) \tag{5.11}$$

[1]As seen in Figure 5.2, the maximum found by ILS is not necessarily the local maximum closest to its starting point, unlike gradient descent based methods.

The update at sensor i does not affect the second term and it thus stays constant at this iteration. The first term only depends on the region over which utility is computed by i and since i choses a pose to maximize this term, this term can only increase or stay constant. Thus when only one sensor updates at a given iteration, monotonicity holds:

$$U(\mathbf{S}_{t+1}) \geq U(\mathbf{S}_t) \tag{5.12}$$

Now, suppose multiple sensors update in parallel. However, the coordination over γ_i ensures that no sensor that affects $\mathcal{V}_i$ will update its pose when i is moving. Thus, we can consider the region $\mathcal{A} - \mathcal{V}_i$ independently. For another moving sensor j, we can decompose $\mathcal{A} - \mathcal{V}_i$ into two disjoint sets $\mathcal{A} - \mathcal{V}_i - \mathcal{V}_j$ and $\mathcal{V}_j$. An equation similar to (5.11) can then be written over these two sub-regions. Recursively applying the same argument, all sensors j which update in parallel within the coordination constraint over respective γ_j can only lead to a monotonic increase in the global network utility regardless of update order. □

Theorem 5.3.1 (Convergence of ILS) *The network configuration converges to a stable state using ILS.*

Proof: The proof follows from the fact that a monotonically increasing function can either grow unbounded, or stabilize to a fixed value. Since the definition of $u(p)$ always yields a finite value and a summation over a finite region $\mathcal{A}$ ensures that U cannot grow infinitely and hence the ILS algorithm will cause the network configuration to converge to a stable state. Noting further that the actuation step is lower bounded and can never be infinitesimally small, the convergence must occur in a finite number of steps. □

As long as the decomposition in equation (5.5) holds, ILS can be used for arbitrary performance metrics, other than the one discussed above. Generaliza-

tions include examples where the objective is not classification but tracking the movement of events after detection. Instead of time $\tau(p)$, the metric of interest would be the localization quality which might depend on the angle and distance from the nearest two sensors for any point p.

5.3.1 Graceful Degradation

Note that the monotonicity is valid as long as other environmental parameters such as the obstacles and phenomenon distribution remain stationary. The monotonicity property yields another desirable behavior in the distributed motion coordination protocol: graceful degradation in the presence of rapid environment dynamics. Under such conditions, the network configuration may continue to evolve without ever reaching a globally static configuration, due to frequent medium and phenomenon changes. Between any two instances of an environmental change, the monotonicity property holds. This implies that even when the environmental dynamics are faster than the convergence time of ILS, the network will only try to improve its configuration for the current situation. The improvement in configuration may be smaller than that which the ILS algorithm could have achieved in a static environment, thus degrading the performance gracefully with increasingly faster environment dynamics. The distributed nature of our methods implies that each change will be incorporated into the ILS execution locally rather than having to be transmitted to a central entity.

5.3.2 Relationship to Other Heuristics

Several heuristics have been explored in literature for optimization over combinatorially large search spaces. An important class of such heuristics is that based on stochastic local search methods, such as simulated annealing. While

the optimization problem for network reconfiguration can be solved centrally using simulated annealing, it is not straightforward to extend it to a distributed algorithm. First, a global temperature state may have to be maintained. Second, the monotonicity property discussed above does not hold for the annealing process and convergence proofs are not available for distributed operation. The ILS algorithm always guarantees that any reconfiguration actions it takes will not worsen the utility compared to a static network. Parallelized simulated annealing algorithms, also sometimes referred to as distributed, are significantly different from our approach. They are typically designed for implementation on multiprocessor systems or computer clusters, for reducing the processing time compared to a single processor implementation. The global objective function is still available to each node and each node may anneal the entire set of state variables. The multiple processors are mainly used to search multiple random paths in parallel. The distributed nature of the objective function itself is not considered. Extension of stochastic local search methods to distributed settings, exploiting the decomposition of the optimization objective function over a relevant neighborhood set is an open research problem.

Another potentially useful optimization heuristic is incremental sub-gradient descent. Its similarity to ILS lies in the fact that at each iteration step only a subset of parameters is updated in order to change the global objective function. While the utility function in our system is not differentiable and sub-gradients do not exist, such methods may be applied to our objective function at least centrally, by computing its derivatives using the method of finite differences. However, convergence is an issue when distributed operation is desired. Monotonicity does not hold. Convergence proofs of incremental sub-gradient descent, such as discussed in [Sol95], require the utility function to be continuous and differentiable. Extending such methods to operate with limited neighbor coordinations is still an

open problem.

Some other properties of the ILS algorithm are of interest: the proximity of the converged stable state to the global optimum and the time required for convergence. We will explore these in chapter 7.

5.4 Coordination Protocol Implementation

In this section we develop a motion coordination protocol to implement the distributed optimization algorithm described above. This includes determining a distributed mechanism to ensure coordination among the neighbors, exchanging the information required for calculating the motion steps, and determining the appropriate stopping criterion for the optimization in a distributed manner. This also involves learning the function $q(p)$ from local data without global normalization.

5.4.1 Protocol Specification

The first step is the determination of a mechanism to ensure that for each node i changing its pose, the set of nodes in γ_i stay static, and the number of nodes which can update their pose at any given time is maximized. This can be viewed as a graph coloring problem where for a given node i, all nodes in γ_i are treated to be adjacent to it. Each node must be allotted a color such that no two adjacent nodes have the same color while the number of colors is minimized. With this, nodes of one color can update their poses simultaneously and the number of iterations required to allow each node update once would be equal to the number of colors used. Efficient graph coloring heuristics are known and hence if the entire network graph is known at a central location, any such heuristic may be used.

However, we do not assume that a central view of the network graph is known and propose the following heuristic for achieving a graph coloring in a distributed manner. This procedure is inspired from common RTS-CTS based wireless MAC protocols for avoiding interference, though we do not need the communication channel to be wireless for its execution. The network reconfiguration protocol based on ILS is described below:

Protocol 5.4.1 (Network Reconfiguration Using ILS) *At each node i in the network:*

1. ***Contention:*** *Wait for a random back-off period, and send packet Request To Update (RTU) to each node in γ_i. Wait for $T_{timeout}$. If no CONFLICT message is received, begin updating as per step 2. Each node which receives an RTU packet, refrains from sending an RTU until it receives an Update Finished (UF) packet from each node which had sent it an RTU. If a CONFLICT message is received, wait for UF message from the sender of CONFLICT message, and retry the RTU after random back-off. This ensures that within γ_i, only one node moves at any instant.*

2. ***Update:*** *If an RTU is received anytime during this phase, send a CONFLICT message to the sender of the RTU.*

   (a) ***Medium and Phenomenon Information:*** *Use the medium mapping service to get information about obstacles within $\mathcal{V}_i$. Retrieve the $q(p)$ over the region $\mathcal{V}_i$ as acquired locally in the phenomenon learning phase.*

   (b) ***Neighbor Pose Information:*** *Look up the list of UF packets received up to now. UF packets contain the sender's chosen $\{pan, zoom\}$ pose after an update. Thus the poses of all nodes within γ_i which have*

updated up to now are known. Using these and the medium information, the utility metric over $\mathcal{V}_i$ can be calculated.

(c) ***Pose Selection:*** *Select the pan and zoom settings as per the ILS algorithm. Transmit packet UF=$\{$identity, chosen pose$\}$. Other nodes may now contend to update their poses. After a node receives a UF packet from every node from which it had received an RTU, it goes to Step 1 unless the termination condition (Step 3) is met.*

3. ***Termination:*** *When a node discovers that the pose computed using the ILS algorithm does not change the utility over $\mathcal{V}_i$ by more than a threshold Δ compared to its current pose, it need not update its pose for that iteration. Each node maintains the past two UF packets received from its neighbors. Now, if the poses of all the neighbors have remained constant in the past two UF packets received, the node no longer needs to update its pose. If it has itself transmitted at least two UF packets, it terminates its motion algorithm until such time as another neighbor updates its pose or the information regarding $q(p)$ or the medium changes.*

The protocol requires a random wait before sending a Request to Update (RTU) packet in order to ensure that over a long duration, most nodes will get a chance to update their poses rather than a just few well positioned nodes with a smaller number of neighbors repeatedly winning the contention. No sequential ordering within a neighborhood is imposed, and it is not required that each node get an equal number of chances to update its pose. This is compatible with the distributed termination condition, which may cause certain nodes to stop the update before others and hence this will not cause an undue interruption of updates at other nodes which are still changing their pose.

If a node receives an RTU packet from any neighbor followed by an UF packet which shows a change in pose, it is likely that this node has a further opportunity to optimize its pose and hence it will restart its motion coordination protocol. The node will also restart pose updates if the medium information affecting its covered region is updated or when the phenomenon density learning module indicates a change in $q(p)$ in this node's covered region. Thus a node stops pose updates based on local conditions and may re-enter the update process when required. No node may know when the entire network has reached a stable state. Each node may stop its motion and restart it multiple times before reaching a stable condition. This approach is valid because of the monotonicity property of our algorithm. Due to monotonicity, the stable state is reached even if different parts of the network stop and restart motion at different times. This stopping criterion automatically ensures that updates to node poses due to medium changes lead to relevant pose changes at affected nodes without the need for globally sharing such information.

The protocol requires that each node i knows its set of neighbors γ_i. A conservative list of neighbors may be obtained by computing the radius, r, of the volume V_i which the node may influence assuming there are no obstacles in the medium. Then, all nodes within a distance $2r$ potentially belong to the neighborhood set. More accurate calculations which compute the exact shape of V_i at each node accounting for occlusions due to obstacles may also be used. This process requires a knowledge of node coordinates. Also, this is a one time procedure since node locations do not change; the communication overhead of this step is thus insignificant and we do not dwell on designing a specialized communication strategy for this step.

The protocol assumes a medium information service to learn the obstacles. An example implementation of this service using laser ranging, as shown in chapter 6, is used in our experiments.

5.4.1.1 Phenomenon Learning Phase

The protocol also requires a service to acquire $q(p)$. This is carried out in a distributed manner as follows. Node i maintains locations of all events detected by itself or its neighbors within $\mathcal{V}_i$. Practical methods to detect events are discussed in chapter 6. We assume that when a node detects an event, it informs all its neighbors about it. Since only a sub-region of $\mathcal{V}_i$ is covered by selected poses of the sensor and its neighbors, events which occur in uncovered parts of $\mathcal{V}_i$, are not detected and do not affect the learning process. Since the total number of events in the network is not known to node i, $q(p)$ is not normalized but the count of events at a point p is incremented whenever an event is detected there. Thus, $q(p)$ acquired locally need not be a consistent probability density function in a global sense, but it serves its purpose of providing higher weight in the local utility function, to points where more events occur. To adapt to changing environment dynamics, the $q(p)$ data is periodically aged as follows. After every time duration T_q, the sensor i scales the $q(p)$ at each point in $\mathcal{V}_i$ by 0.5. The aging step is:

$$q(p) \leftarrow 0.5 * q(p) + q'(p) \quad \forall \quad p \in \mathcal{V}_i \tag{5.13}$$

where the temporary variable $q'(p)$ stores the event count since the previous aging step. This aging procedure thus gives higher weight to more recent events as the contribution of older events degrades by 0.5 every T_q. The duration T_q is expected to be a long duration over which sufficient events may be accumulated.

The aging procedure has the beneficial side effect that it prevents the count

variables from overflowing, and this is helpful for a practical implementation.

The phenomenon distribution learning thus continues perennially and every T_q, the update of $q(p)$ may trigger a network reconfiguration to occur.

The specific aging procedure used may be changed based on how rapidly the system is required to adapt to changing environmental dynamics.

More sophisticated models for maintaining the phenomenon distribution which maintain separate states for the system, each corresponding to a different event distribution my also be employed. For instance, a traffic monitoring system may use different probability distributions at different times of the day: one state for morning times when more traffic seems headed for the business district and another state for evening times when more traffic seems headed away from the business district. When a service to learn $q(p)$ is not available, this distribution is assumed to be uniform.

In this chapter, we described a distributed algorithm for motion coordination along with a network protocol to implement it. The protocol assumes certain services such as obstacle mapping and phenomenon distribution information to be available. We discuss these services in the next chapter.

CHAPTER 6

Medium Mapping and Phenomenon Detection

In the previous chapter we showed how the motion coordination algorithm could use information about the medium obstacles to further enhance the network configuration. Also, we had mentioned before (chapter 4) that for the final actuation that is required to provide the high resolution coverage of any location, an event or phenomenon of interest must be detected at that location. This detection procedure must occur at low resolution coverage. The detection of events is also used for learning the phenomenon distribution over space by building a spatial event distribution histogram as more and more events are detected over time, as discussed in section 5.4.1.1. In this chapter, we discuss both these supporting services of medium mapping and event detection.

6.1 Medium Mapping

Much of the work presented in this section was performed in collaboration, and is also described in [KCK05a].

The signal of interest generated in the environment must travel through some medium to reach the sensor transducer. The medium may attenuate it and the extent of attenuation tolerated depends on the transducer noise. Also, obstacles in the medium may block the signal entirely. These obstacles may even create occluded regions that are not sensed by any of the sensors in the network. The

deployment environment and presence of obstacles is usually not under the control of the system designer and hence the system is required to adapt to the given environment.

Our goal is to provide methods for sensor networks to actively measure the sensing medium and determine the presence of obstacles. Acquiring such a medium model has many benefits.

Estimate Uncertainty. The model may be used to determine the occlusions to sensing and provide an estimate of sensing uncertainty. One such method to model the sensing capacity of a sensor network given the occlusions was provided in [RNK04].

Reconfiguration. The network may attempt to overcome the occlusions. For instance, if some of the nodes are mobile, they may be moved in order to minimize occlusions. In our network, we use limited motion to overcome the effect of obstacles.

Determine Choke Points. In certain applications where the sensed targets are mobile, the knowledge about obstacles may help generate the medium model and use it to determine choke points which a target must cross if it has to enter the occluded regions. Data from such choke points may be used to estimate presence of targets in occluded regions.

Data Aggregation. The information on occlusions for each sensor may help guide the aggregation process when data from multiple sensors is combined. For instance, a simple strategy may be to ignore data from nodes which indicate a detection in regions known to be occluded from their view. Further, energy resources being spent on sensing at nodes whose transducers are occluded may be saved, and devoted to communications, aggregation

or other network activity.

Additionally, the medium maps may also act as secondary data inputs for higher layer applications to help determine context. For instance, the presence of several tree-trunk shaped obstacles may indicate to the application that the sensor network is operating in an outdoor region while the presence of wall and ceiling like obstacles may help it infer that the network is operating indoors. Such context information can be used in several ways.

Sensing performance has traditionally been characterized in terms of a sensing range and transducer noise. We believe that explicit medium information will help sensor networks provide better performance guarantees than those based on circular disk models alone.

Environment mapping is commonly studied in robotics for robot navigation and path control. The use of context information has been explored in various other domains such as pervasive computing and location aware services. However, the nature of context information and mapping constraints differ in the case of sensor networks. We will note the commonalities and differences in subsequent sections.

6.1.1 Enabling Self-Awareness

We propose a sensor network architecture in which supplementary sensors are added for medium mapping. Since these sensors may not be required for the sensor network application directly, and we refer to them as *self-awareness sensors*. The other sensors, which in our work are cameras, are referred to as application sensors. Figure 6.1 depicts a block diagram of the proposed architecture. Much of this architecture design is motivated by the system concerns that arose in the

development of our prototype system, and thus, the design is tightly coupled to practical considerations of its use cases.

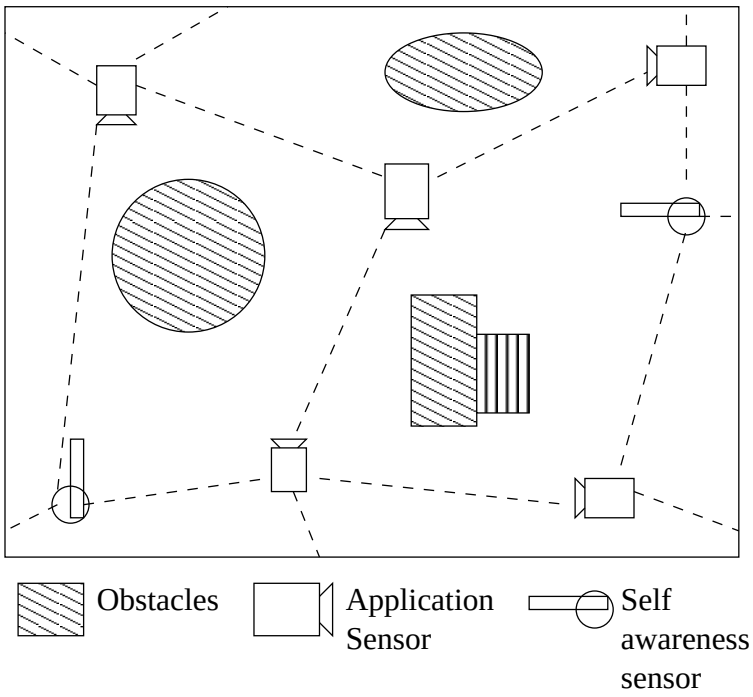

Figure 6.1: System architecture, consisting of self-awareness and application sensors.

The figure reveals one of our key system design choices: that the self-awareness sensors need not be present at the same nodes as the application sensors. There are several reasons for this choice. Firstly, the self-awareness sensors may be required to be deployed at a vastly different density than the application sensors. In our system for instance, the range of the camera depends on the application and was calculated to be 7.3m when a sensing resolution of $100 pixels/m$ was required, while the self-awareness sensor has a range of more than 100m. For a given set of obstacle locations in the medium, the numbers of the two types of sensors required may well be different and thus, adding a self-awareness sensor at every node might be an unnecessary overhead. Secondly, the medium dynamics may

be much slower than the dynamics of the phenomenon sensed by the application sensors. In this case, a few mobile self-awareness sensors could acquire and update the medium map [HH03] while many more application sensors actively track the rapid dynamics of the phenomenon of interest.

It may be noted that supplementary sensors have been used in other ways to reduce sensing uncertainty – such as the use of magnetic sensors to help augment the vehicle tracking performance of a video sensor network. However, the use of self-awareness sensors is not quite the same thing as the use of multiple sensing modalities. In multi-modal sensing, the data fusion process is highly application dependent. If the primary sensor data, the images in the above example, are used for another application which is not interested in magnetically active objects, that supplementary sensor is not of relevance. In our approach, the application processing is independent of the self-awareness sensors; the medium information is used to estimate or improve the quality of application sensor data, and any application which uses the sensor data benefits from this.

The prototype system that we developed for providing a concrete context to explore this problem space is described first.

6.1.1.1 System Hardware

The self-awareness sensor node in our prototype test-bed consists of:

1. a laser range sensor, Leica Disto Pro [Lei],
2. a pan-tilt platform, Directed Perception PTU-D46-17N, [Dpe], to move the direction of the laser beam, and
3. an embedded processing platform, Intel Xscale based Stargate [Sta].

The laser ranger is interfaced to the Stargate using a serial port, over which the control commands are sent to acquire range readings from it. The pan-tilt platform is also interfaced using a serial port, for sending it commands to change its orientation. Since the Stargate has only one directly accessible serial port, we added a PCMCIA to serial port card to the Stargate for creating another serial port. The prototype is shown in Fig. 6.2.

Figure 6.2: Prototype self-awareness node.

6.1.2 System Design Issues

Conceptually, the medium mapping process can be viewed as this: the self-awareness sensors collect data about the medium characteristics and then provide this data to the application sensors. Now, there arise several issues in the process of collecting and distributing such self-awareness data with minimum resource overhead.

First, the range data must be collected as fast as possible, in order to enable faster updates and to minimize the node active time. The naïve method would be to take a range measurement at a sufficiently fine granularity and determine which regions are blocked from view. However, the environment has certain structure to it and it is intuitive to expect that if such structure can be exploited, we can reduce the number of readings to be collected, thereby speeding up the data acquisition process. Implementing this procedure on a practical laser ranger and pan-tilt platform reveals the various issues in doing this. Our aim is to determine useful strategies to minimize data acquisition time, which are expected to work in a wide variety of environments in view of the system limitations.

Second, the medium map has a significant data size. This motivates a study of efficient methods for sharing this data among the application and self-awareness nodes. The storage and communication strategies may attempt to minimize the data size, but the compression techniques should not lead to extensive processing overheads for retrieval and update. The storage strategies for a data set typically depend upon the nature of queries that must be answered using the stored data. Our objective is to determine the relevant strategies to store and share medium map data in a manner that enables answering queries about the medium occlusions for the application sensors.

There are further design steps required to complete the self-awareness process. The medium information may have to be appropriately converted to a form that enables the application sensor to determine which portions of its field of view are occluded. For instance, in our test-bed the spatial coordinates of an obstacle may have to be mapped to the corresponding pixel coordinate in the image taken by a camera. For the case of cameras, this process is known as external calibration and existing methods [HS97] can be used for this step.

Also, since the self-awareness sensors are not necessarily present at the application sensor node and a single self-awareness node will typically not be able to map the entire medium, self-awareness data from multiple nodes has to be combined to develop a coherent medium map. In our test-bed we assume that each node is localized, in a common coordinate system. Such an assumption is valid for sensor networks since most nodes are static and localization is a basic service required for many other sensor network applications. Given the location information, the medium data from different locations can be combined using the appropriate spatial transformations and we do not dwell on it further.

6.1.2.1 Technology Choice

We have selected a laser range sensor to measure the medium characteristics. There are other means to achieve the same functionality. One alternative is to use stereo-vision to derive depth maps. This approach has limitations of accuracy compared to a laser sensor and may miss small obstacles in the environment. Also, stereo-vision algorithms require detecting key features in the environment which can then be identified in the multiple images collected by the cameras in the stereo-system. It may not work in all environments where such key features are hard to detect. Further, the stereo-vision generated depth map is relative and a known dimensional measure is required in the environment to scale the depth measurements correctly.

These issues motivated us to use a range sensor. Among range sensors, there are various options, such as ultrasound ranging and infra-red ranging. Both these alternatives give lower accuracy than the laser, and the distance range of the infra-red sensors is usually lower than that of laser based ones. However, both these are usually available at a lower cost, and may be of interest in scenarios where

the low accuracy is not a deterrent. The map acquisition algorithms discussed in later sections are in fact applicable to these types of range sensors as well. The data sharing methods developed in our prototype are applicable to all the above alternatives.

Advanced three dimensional imaging technologies, such as based on single photon avalanche devices [NRB04] may make three dimensional imaging more feasible in the future. This may yield more alternatives to realize the self-awareness sensing functionality that we propose for sensor networks.

Mapping based on range sensors has also been considered in mobile robot navigation. While our problem is similar, the solution is different and the resultant design issues are distinct. For a robot, medium mapping is a primary task necessary for navigation. Even if the environment map were available a-priori, the range sensor on a robot would be actively used to avoid obstacles in the path. In the case of a sensor network, the demands from the self-awareness sensor are less stringent. First, the self-awareness data is not being used for active navigation of a mobile robot. Each node need not have a self-awareness sensor. The static nature of most sensor nodes also enables carrying out the mapping process at a much slower pace than required for a robot. A direct consequence of this is in the technology choice – the laser range sensor used in our work is significantly cheaper than those typically used on robots and has a slower response time for taking range readings. The pan-tilt actuation used in our prototype is much slower than required for real time navigation, and can be achieved with lower energy expenditure. Second, the assumption on the availability of localization also causes our work to differ significantly from robotic mapping. In the case of a team of multiple robots exploring an unknown environment, the processes of localization and mapping are dependent [DNC01] on each other. Combining the

maps generated at multiple robots is not straightforward and different techniques such as maximum sub-graph isomorphism have been explored for that purpose. On the other hand, for sensor networks, if localization is available as is needed for many sensor network applications, combining the self-awareness data from multiple nodes is simpler. Thus, the medium mapping problem in sensor networks is more tractable than the corresponding robotics problem, and we expect to be able to solve it with a lower resource overhead.

6.1.3 Adaptive Medium Mapping

There are three basic types of maps [Cho]:

1. Grid based: These maps divide the space into discrete elements which are mapped as empty or occupied [ME85, TB96].

2. Feature based: These maps are a collection of landmark features in the environment [SSC90, LDC92].

3. Topology based: These maps represent distinctive places in the environment as nodes in a graph and the interconnections or paths between them as the edges [KW94, RN99].

For the purpose of determining sensing occlusions, the most relevant maps are the grid based ones. These provide a detailed model of the sensing medium, based on which the application sensors may estimate their sensing performance.

The process to generate a grid based medium map proceeds as follows. Range measurements are taken by orienting the laser at varying pan and tilt from a fixed location to form a depth map for the space around the self-awareness node. Such depth maps from multiple self-awareness nodes may then be combined to develop

a medium map for the region of deployment. Figure 6.3-(a) shows a small section of a possible deployment environment with obstacles of various shapes. Figure 6.3-(b) shows one horizontal plane in the depth map generated by scanning the laser placed at one corner of the region, and Figure 6.3-(c) shows a similar scan from a node placed near another corner. The white regions in the scans represent clear field of view while the dark regions represent occluded areas. Note that the second node does not scan the entire quadrant scanned by the first one. Both nodes scan 90 degrees. Combining the two scans for this small section, in the plane represented, yields the medium map shown in Figure 6.3-(d). The occluded regions could either be obstacles or spaces between obstacles which are empty but not accessible from the laser locations.

Suppose the medium map is stored as a three dimensional matrix where each entry represents a voxel (a small volume element) in space. Each entry in the matrix denotes whether the corresponding voxel is empty, occupied or unknown. Such a matrix is referred to as an occupancy grid (OG). The data collection task is to take range readings at different pan and tilt angles and determine which voxels are empty or occupied. Voxels not accessible from a self-awareness sensor node's position remain unknown in the OG generated at that node, and have the same effect as occupied voxels in the calculation of clear field of view. Entries in the OG are filled using the range readings taken by the laser range sensor at different pan and tilt angles. At each orientation, the voxels along the free line of sight of the laser are designated as empty.

Let us now consider the practical considerations which affect the time taken for collecting the laser range data. Our experience with the laser device used in our prototype indicates that it must be stationary when acquiring a range reading, for accuracy of measurement. If the laser beam is continuously moved,

(a) Sample Deployment Environment

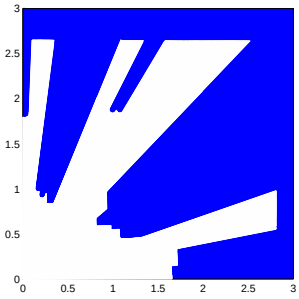

(b) Depth map A

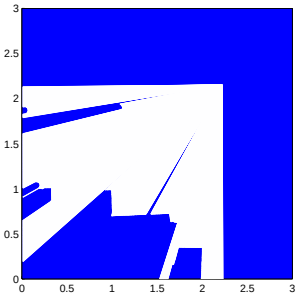

(c) Depth map B

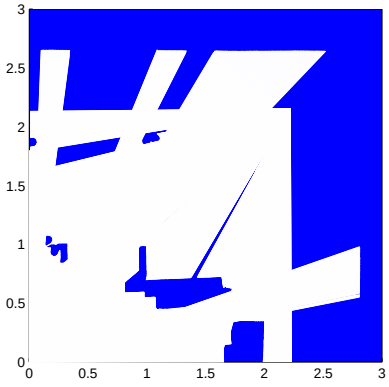

(d) Medium map

Figure 6.3: Map generation process.

the device still returns range measurements. However, the time taken to acquire a range reading increases by an unpredictable amount, which makes it is impossible

to determine the orientation, and hence the relevant voxels in the OG, which corresponds to the returned range reading. Thus, the laser is moved in small steps along the pan and tilt axis and the readings are acquired when the device is stationary. With this, the time taken, T, to acquire a reading at a particular pan and tilt position can be modeled as consisting of three components:

$$T = t_{move} + t_{axdx} + t_{read} \tag{6.1}$$

where t_{move} represents the time taken by the pan-tilt platform to move to the next position at a constant speed using the pan and tilt motors, t_{axdx} represents the additional time taken due to acceleration and deceleration phases in executing the motion step since constant speed cannot maintained throughout the motion, and t_{read} represents the time taken for the laser range sensor to acquire a reading.

The parameters t_{move} and t_{axdx} depend on the capabilities of the pan-tilt platform, and t_{read} depends on the laser unit, and the reflectivity and the angle of incidence of the surface at which the laser beam is pointed. For a constant pan and tilt range scanned by the laser at a given granularity, suppose the total angular distance moved is d_ω and the number of readings taken is N. The total time taken to execute the scan becomes:

$$T_{scan} = d_\omega * t_{move} + N\{t_{axdx} + t_{read}\} \tag{6.2}$$

The time taken thus varies with N. If we reduce N, and thus increase the angular step size at which the laser stops to take a reading, T_{scan} can be reduced. Our objective is to generate the OG in a manner that exploits the structure in the environment in order to reduce the number of readings taken by the laser.

6.1.4 Reducing the Scan Time

For many signals, a frequency spectrum analysis yields that the signal needs to be sampled only at a coarse granularity. Considering the range scan in space as the signal to be sampled (such as shown in Fig 6.3-(b,c)), indicates that the Nyquist sampling interval is quite small due to the presence of sharp discontinuities in the environmental features, and the value of N derived in this manner is very high. Thus, we need to exploit other forms of structure in this signal. We propose two heuristics to exploit such structure. These are described in terms of the pan motion of the laser[1] and the goal is to minimize the number of readings for a constant pan scan range.

6.1.4.1 Adaptive Filter Based Algorithm

The first method is based on the use of an adaptive filter to learn the medium structure from the readings acquired and when the laser readings match those predicted based on the adaptive filter, the scan step size may be increased to reduce the number of points measured. We refer to this method as adaptive filter based (AFB) algorithm and use least-mean-square (LMS) adaptation as our adaptive filter. LMS is a gradient descent based heuristic for the filter adaptation. Suppose the filter at time step i is represented by a length n column vector $\mathbf{h}(i)$, the previous n values of the scan are represented by a column vector $\mathbf{x}(i)$, and $e(i)$ is the error in the prediction, calculated using:

$$e(i) = \mathbf{h}^T(i)\mathbf{x}(i) - x(i+1) \tag{6.3}$$

[1]Similar methods apply to tilt motion.

where $x(i+1)$ is the measurement at time step $(i+1)$. Then the gradient search equation to minimize the square-error becomes:

$$\mathbf{h}(i+1) = \mathbf{h}(i) - \mu \bigtriangledown (|e(i)|^2) \tag{6.4}$$

where the gradient $\bigtriangledown(\cdot)$ is taken with respect to filter coefficients $\mathbf{h}$, and μ is a constant step size for the gradient descent. Simplifying the above expression leads to a computationally efficient filter update equation:

$$\mathbf{h}(i+1) = \mathbf{h}(i) - \mu e(i)\mathbf{x}(i) \tag{6.5}$$

We deviate slightly from the conventional LMS filter in that the step size at which readings are taken varies as we adapt the angular step size using the AFB algorithm. Whenever the prediction error $e(i)$ is below a threshold, we increase the angular step size for the laser pan motion, as described in the next subsection. The step size cannot be increased beyond a certain limit which depends on the size of the smallest feature of interest to be mapped. The problem of adaptive filter design is not addressed as part of this work; several adaptive filters are available, and may be explored depending on the specific needs of the system [Hay01].

6.1.4.2 Adaptive Linear Prediction Algorithm

The second method is more domain specific and exploits the nature of the signal being sampled. Since adaptive filters are not specially designed for depth maps, they require significant learning data. However, observe that when sampling at a fine granularity, many of the surfaces in the medium, especially for indoor built environments, can be approximated as consisting of small planes, or in one plane of pan motion, a curve consisting of small line segments. When scanning this curve, the number of samples taken need only be sufficient to reproduce the line

segments. Thus, when range data indicates that the laser is taking measurements along a line, we may increase the angular step size of the pan motion.

This prediction method proceeds as follows: Determine the coordinates of the points on the sampled curve corresponding to the previous two range readings. Use these to determine the equation of the line joining them. Now predict the coordinates of the next point along this line, which the laser will hit when moved by its current angular step size. At the next laser pan step, calculate the error between the predicted point and the measured point. If the error is below a threshold, increase the angular step size. The exact algorithm to control the step size appears in the next subsection. We will refer to this method as the adaptive linear prediction (ALP) algorithm.

Some further improvements can be applied to both the AFB and ALP algorithms as described below.

First, when the laser range extends beyond the area of interest, such as when the laser is near an edge of the deployment area, we need not scan the exact structure of the medium and may increase the angular step size to the maximum limit dictated by the minimum obstacle size to be detected. The step size would be reduced as soon as a feature of interest is detected within the region of interest.

Second, for a given angular step size, the scan resolution in space varies with distance from the laser. This can be seen in Fig. 6.4: the spatial resolution $\Delta\alpha$ is higher than $\Delta\beta$ for the same angular step $\Delta\theta$. Thus, $\Delta\theta$ may be increased when scanning obstacle A, as the OG is stored at a constant resolution in space.

Third, when the step size has been increased using an adaptive method and a high error is encountered, it is likely that a large change in the scanned depth occurred in the region between the current and the previous readings. Thus, if we back-track, i.e., move the laser back to the previous position and then scan

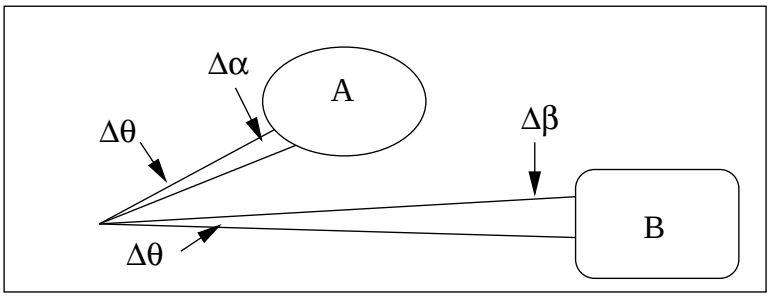

Figure 6.4: Varying spatial resolution with obstacle distance.

the region of large change using a small step size, the quality of reproduction can be improved significantly with a small increase in the number of readings taken.

6.1.5 Algorithm Implementation and Evaluation

The precise ALP and AFB algorithms derived from the above discussion are stated together in Fig. 6.5. The key difference among the two algorithms is in the prediction step. The values of parameters used are summarized in Table 6.1. The parameter $\Delta\theta_0$ represents the minimum angular step size required to achieve a desired spatial resolution, for the maximum laser range in the environment. The step size μ was chosen to be 0.03. Larger step sizes were tried, and while they yield faster convergence and somewhat lower error, they lead to divergence of the LMS filter in some cases. The filter length was kept at $n = 3$. A larger filter length can learn more complex shapes but needs a longer adaptation time and the signal characteristics may change over such time as the laser moves from one obstacle to another with different a shape. Optimizing the LMS filter for various environment categories is part of future work. We now evaluate these algorithms by comparing them to a constant step size approach, both using simulations, which allows testing over several obstacle placements, and using experiments on our prototype hardware.

1. **Initialization:** Set $\Delta\theta = \Delta\theta_0$. Take first M range measurements by panning the laser in steps of $\Delta\theta$. Set $k = 0$, $i = 0$.
   If method is AFB, initialize adaptive filter $\mathbf{h}$ to zeros. $M = \text{length}(\mathbf{h})$.
   If method is ALP, $M = 2$.

2. **Prediction:** Predict the next point, based on previous M readings (using AFB or ALP methods described in previous subsection).

3. **Measurement:** Pan laser by $\Delta\theta$ and take next reading.

4. **Update:** Calculate error $e(i)$ between the predicted point and measured point.
   IF $e(i) < e_{thresh}$:

   (a) Set $k = k + 1$.

   (b) Set $\Delta\theta = \Delta\theta_0 + k\delta$

   (c) **IF** $\Delta\theta > \Delta\theta_{max}$, Set $\Delta\theta = \Delta\theta_{max}$

   (d) For AFB, update $\mathbf{h}$ using equation (6.5).

   ELSE

   (a) Set $k = 0$.

   (b) Set $\Delta\theta = \Delta\theta_0$.

   (c) **Back-track:** Move laser to previous pan position.

5. If scan not completed, set $i = i + 1$, and go to step 2.

Figure 6.5: Adaptive step size control algorithm for medium mapping.

Parameter	Value
e_{thresh}	1 cm
μ	0.03
$length(\mathbf{h})$	3
δ	0.05°
$\Delta\theta_{max}$	$\Delta\theta_0 + 1°$

Table 6.1: Algorith parameter values.

6.1.5.1 Simulations

To test the proposed methods, we generate several random obstacle placements in a square region, place the laser ranger in one corner of the square and simulate the range readings that would be collected when the laser is panned with the step size computed as per the adaptive methods. As a base case, the readings are also generated if the laser were to be panned with a periodic step size kept at $\Delta\theta_0$. The obstacles generated are rectangles and circles, placed randomly and overlapping with each other leading to arbitrary shaped obstacles, such as shown in Fig. 6.6(a). Ten such random obstacle topologies were generated. A simulated laser scan using adaptive step sizes is shown in Fig. 6.6(b), where the varying step size between successive pan positions is apparent, and the back-tracking near obstacle edges may be seen as well. The angular step size increases as the filter learns a curve and falls back again when the curve changes significantly.

Error performance of a scan is calculated as follows. From the application perspective, the OG generated from the range scan data is of interest. A high resolution periodic scan is first carried out and the OG generated from it is used as the ground truth. Then, for each simulated scan, the corresponding OG is generated and the error is measured in terms of the number of voxels

which differ with respect to the ground truth OG. A two dimensional OG is used for the simulations, considering only the pan motion of the laser. The exact same techniques can be applied in the tilt direction as well to generate the three dimensional OG. The number of differing pixels is normalized by the number of total pixels in the OG, and the error is plotted as a percentage.

For each topology, multiple scans are carried out with $\Delta\theta_0$ varying from 0.09° to 0.9°. Increasing $\Delta\theta_0$ implies reducing the resolution of the scan and thus increasing the error. For each scan, we count the number of readings taken when a periodic scan is used and when the adaptive algorithms are used. To compare the savings in time when using the adaptive methods, we plot the number of readings taken for the same error using the periodic and adaptive schemes.

The simulation data needs to be averaged over the random topologies. Since each topology may lead to different error values with varying $\Delta\theta_0$, the number of readings, N, required cannot be directly averaged. We divide the error axis into small intervals and consider the average of number of readings taken for error across multiple topologies divided into these intervals. These averaged plots are shown in Fig. 6.6(c). The error-bars show the standard deviation across multiple topologies.

The figure shows that at low error the adaptive scans require much fewer readings than the periodic scan. Among AFB and ALP, ALP performs better since it is designed specifically for the nature of the sampled signal. As the angle step is increased for the periodic scan, the error increases and the number of readings reduces. However, the advantage due to adaptive methods dwindles as the step size for the periodic scan has also increased. The portions of the scan where the adaptive methods can use an increased step size now form a smaller fraction of the total scan.

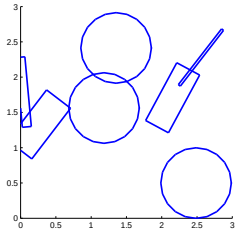

(a) Sample deployment

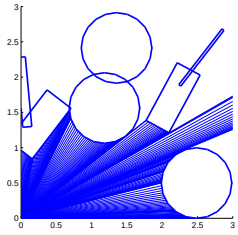

(b) Sample AFB scan

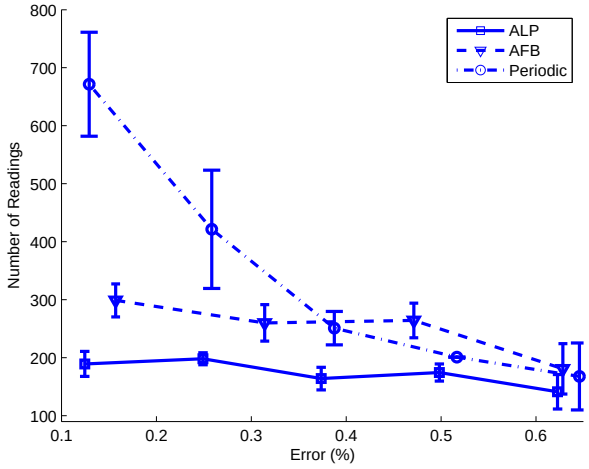

(c) Error performance

Figure 6.6: Comparing the number of readings taken with varying error performance for the three scanning strategies.

6.1.5.2 Experiment

We now experimentally compare the performance of these algorithms using our prototype self-awareness node. Apart from validating the implementation of our proposed methods on an embedded platform, the experiments include additional effects not modeled in the simulations. First is the presence of sensing errors in the laser readings and pan motion. Secondly, while in the simulation, only the number of readings could be plotted, in the experiment we can measure the total

savings in time. These includes the time for motion and the time for taking a laser reading. The time for taking a laser reading varies with the color of the surface scanned and even for the same number of readings, the difference in the positions of those readings on some dark colored spots in the environment may cause an increase in time consumed; such effects were not modeled in the simulation.

The environment used in our experiment was a $2m$ square space with some objects placed as obstacles. The results are shown in Fig. 6.7. Only the better adaptive method, ALP, was used.

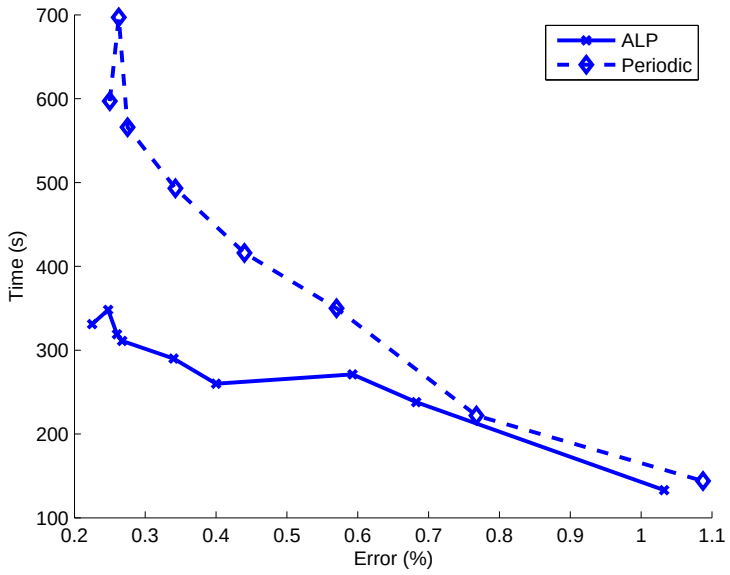

Figure 6.7: Comparing the adaptive and periodic scan strategies using the prototype self-awareness node.

These results are similar to those seen in simulations. The evaluation clearly shows that significant savings in time can be achieved using the adaptive methods.

Apart from the savings in time, another side effect of the adaptive methods is a saving in storage and communication overhead as discussed next.

6.1.6 Sharing the Self-awareness Data

After each laser sensor has collected the range scan, using either a periodic scan or the adaptive methods, the data at each self-awareness node must be used to determine the medium occlusions at each application node. There are several design choices in doing this, differing in how the data is stored and how the depth maps from multiple laser sensors are combined.

Data-sharing schemes depend on the nature of queries that need to be answered based on the stored data. In our system, the application sensors are only interested in determining the occluded regions from their point of view. The individual occupancy grid (OG) generated by a laser scan (such as seen in Fig. 6.3(b)) may be stored at each laser node. To generate the medium map all laser nodes with overlapping fields of view must transmit their OG's to a common location where the medium map is then computed. The individual OG's are first translated along the spatial axes in a global reference frame, depending on the laser coordinates and then an 'OR' of their overlapping voxels is computed. The OR operation assumes that the occluded voxels (obstacle surfaces or unknown) are stored as zeros and the clear regions as ones. This generates a combined OG, referred to as the medium map (as was seen in Fig. 6.3(d)). Relevant portions of such a medium map once generated can be distributed to each application sensor.

6.1.6.1 Computing the Field of View at Application Sensors

We can improve the above process if we observe that the medium map need not be calculated centrally for the application sensors to be able to calculate their occlusions. Each self-awareness node need not compute its OG, but may just store the raw coordinates of the points scanned by the laser ranger. Let us refer to these points as range coordinates. The range coordinates which were used

to compute the OG's seen in Figures 6.3(b) and 6.3(c) are shown in Figures 6.8(a) and 6.8(b). We present a distributed method using which the raw range

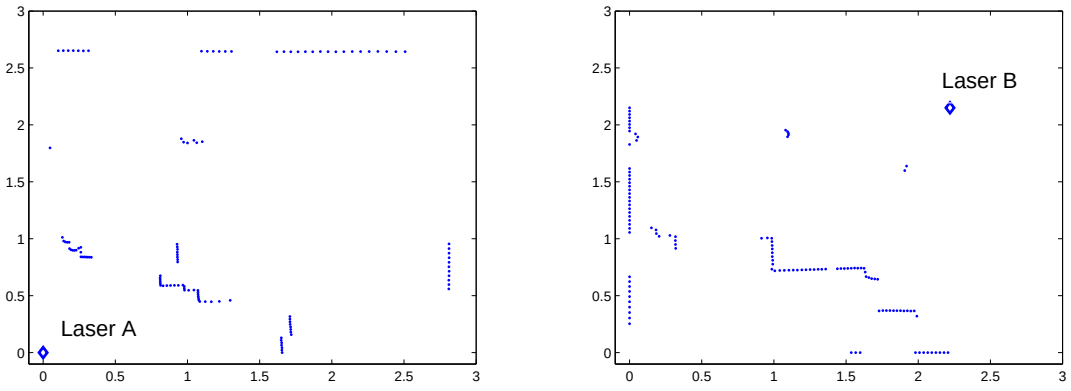

(a) Range coordinates A

(b) Range coordinates B

Figure 6.8: Range coordinates used to compute occupancy grids (OG's)

coordinates at the individual laser nodes are directly used by the application sensors to determine their occlusions.

Suppose the nominal range of the laser is known to be R_l, and that of the application sensor is R_s; the actual ranges may be much shorter due to presence of obstacles. An application sensor now accesses those laser nodes which are within R_l distance, and queries the range coordinates stored by the laser, as well as the coordinates of the laser itself. The application sensors now computes their own OG's, to represent which voxels in their field of view are unoccupied, as follows: connect the laser node coordinates to each of the range coordinates, and all voxels through which the connecting lines pass are deemed to be unoccupied. The application sensor only generates the OG for a circular area of radius R_s around it and not the entire R_l.

As an illustration, consider the $3m \times 3m$ area seen in Fig. 6.3 and the corresponding range coordinates in Fig. 6.8. Laser A was placed at $(x, y) = (0, 0)$ and

laser B was placed at $(2.22, 2.15)$. Suppose an application sensor, say, a camera with full 360° pan range, is placed at $(0.5, 1)$, and has $R_s = 1$. It first accesses the range coordinates from laser A and computes its local OG by checking which pixels are unoccupied, as shown in Fig. 6.9(a). The OG is computed at a resolution of $1cm$, which means that each grid point in the OG is separated by $1cm$. Next, it accesses the range coordinates from laser B. Again, it connects the range

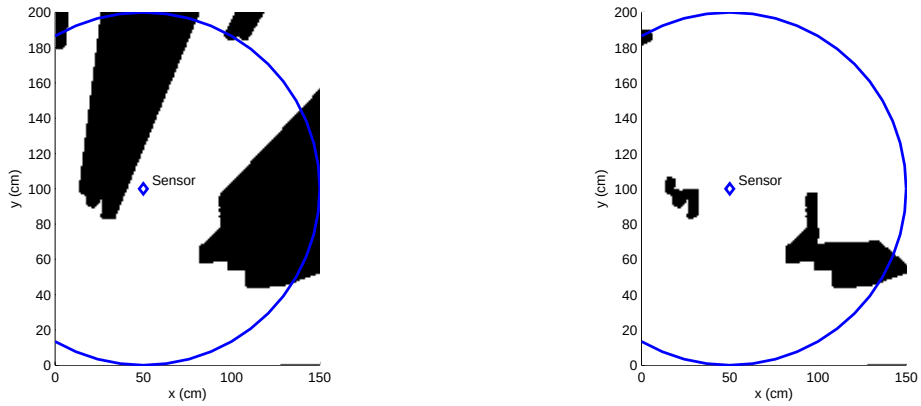

(a) OG, using laser A

(b) OG, using lasers A and B

Figure 6.9: Example: Generating a combined OG directly at the application sensor.

coordinates with the laser coordinates and computes the unoccupied pixels, thus discovering further pixels in its OG which are unoccupied. This OG is seen in Fig. 6.9(b).

6.1.6.2 Evaluation

In our proposed approach, no global medium map is generated. This approach has several advantages compared to the laser nodes first generating their OG's, exchanging them, generating the medium map and then distributing it to the application sensors.

Memory Requirements: The application sensors calculate the OG only within their sensing range, R_s. The size of the OG is proportional to the cube of R_s (or the square of R_s when only the horizontal plane is considered). If $R_s < R_l$, which is the case in our system, this means that each application sensor has to compute a much smaller OG than at a laser node. This is significant, since embedded nodes have limited memory, and increasing the memory size in increases their power consumption and cost.

Communication and Storage Overhead: The communication overhead in our approach is only the data-size of the range coordinates. This is significantly lower than the OG at a laser, and the combined OG's (medium maps) generated using the data from multiple lasers. For instance, at a resolution of $1cm$, the size of the OG matrix in two dimensions is 10^4 binary values per square meter, while the range coordinates only store a few points corresponding to obstacles in the same area. The number of points stored can further be reduced using the adaptive methods discussed in the previous sections.

It may be noted that the OG need not be communicated in its raw form but could be compressed using a data compression or image compression method. Our approach of storing range coordinates can be viewed as a domain specific compression scheme which is expected to perform better than the general compression techniques. Fig. 6.10 shows the storage space required for our proposed approach with Periodic, AFB, and ALP methods, as well as that required for storing the OG when using a data compression technique: TIF-packbits compression, which is a lossless compression method exploiting the repetition of bits, and an image compression technique: JPEG, which uses a transform to derive an efficient data representation. The sizes are for the same data sets as generated in the previous section.

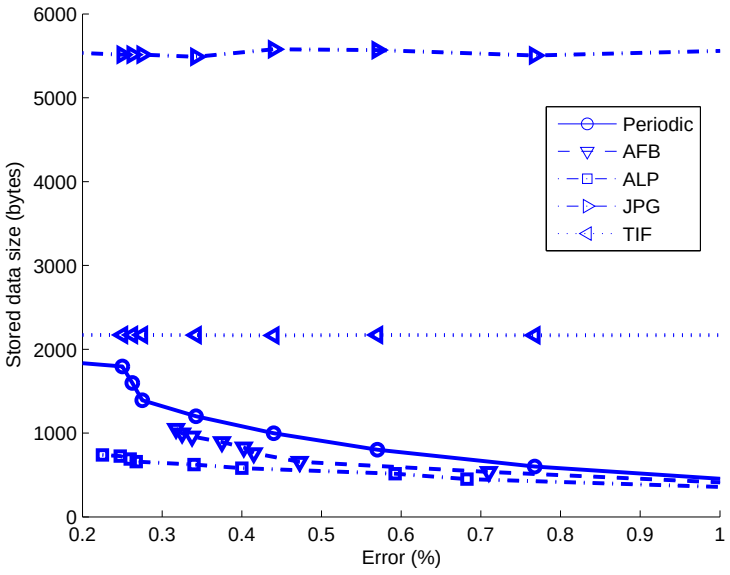

Figure 6.10: Comparison of data size for multiple storage strategies, with varying scan error.

Our storage approach clearly has lower data size. Also, the general compression methods operating on the OG as a whole are unable to achieve any significant reduction in size as the tolerable reproduction error is increased by reducing the number of range coordinates. Reduced data size saves communication energy, bandwidth, and the energy required to write to flash memory.

A trade-off in this approach is that for an application sensor, the time to compute the OG from the range coordinates is larger than the time to decompress a medium map image if sufficient memory is available to hold the entire medium map. However, the computation of the OG from range coordinates is carried out over only the application sensor's range, a much smaller region than the medium map generated by the laser nodes. Thus, computation time is not significant, and when memory is limited, it may in fact be lower than the image decompression time. Further, computation costs are typically lower in sensor nodes than the

costs of flash memory writes and communications, and hence this approach is still preferred.

Resolution Flexibility: The application sensor is free to compute its field of view at a much lower resolution than the data generated at the laser. Without application information, the laser node may have to compute the medium map at the highest resolution possible with the collected data, and generate a much larger OG matrix than required.

Reduced Remote State Dependence: The proposed method is completely distributed, and dependence on the state of remote nodes is minimal. Firstly, no data exchange is required among the self-awareness nodes. Since R_l may be large, such communication may have required data to be sent over large distances. Reducing this overhead saves significant bandwidth. Secondly, the application sensors are not required to know the state of progress of the self-awareness nodes coordination and determine if the combined medium map has been generated. They may access each self-awareness node's data asynchronously. Such reduced state dependence not only simplifies design in distributed systems but also helps improve system robustness because in case of a node's failure, its effect on other nodes is reduced. The modular and decoupled operation yields a significant advantage when the sensor network is executing multiple applications and services.

Efficient Updates: The medium may change over time and our data sharing method allows for efficient updates. First, transmitting only the range coordinates to the application sensors reduces the size of data communicated. This approach has at least as much advantage in communication overhead as seen in Figure 6.10 with respect to the size of the update data to be exchanged. Second, the asynchronous data access mode, rather than having to wait for the

self-awareness nodes to generate a coherent map, allows for update information to be incrementally incorporated with minimal delay as and when the medium changes.

The updates may be exchanged using either a push or a pull approach. In the push approach, the laser nodes send an update to the application sensor whenever a change is detected and in the pull approach, the application sensor queries the laser nodes for updates. Depending upon the nature of the deployment, one of these methods would be preferred. For instance, if the medium changes infrequently, then the self-awareness nodes may push the updates. This saves the overhead of the application nodes periodically polling for updates when not many updates are expected. However, if medium changes are frequent, the push approach will lead to a high overhead. In this case, the application sensors should query for updates at the frequency they require. The pull approach is also useful for power management as it allows application sensors to enter low power modes without worrying about medium changes when they are not even sensing. In our system we have selected the pull approach to keep the update process at each application sensor decoupled from the self-awareness node's operation. The laser periodically collects data and publishes it at a known location. In our prototype, we use the common HTTP protocol for data exchange. The range coordinate data is stored in a web accessible folder on the self-awareness node. The application sensors access this data as required.

There are other enhancements possible to the update process if the overhead of maintaining remote nodes' state is acceptable. For instance, each self-awareness node may maintain the locations of the application sensors which access it. Then, it could compute which portions of its range coordinate data affect each application sensor. In case of updates to the range coordinates data, the laser would

compute which application sensors are affected and publish a flag indicating such change. Now, when an application sensor accesses a self-awareness node, it first looks at the update flag corresponding to itself. If the flag indicates that the data has changed, it downloads the new data, else the unnecessary communication cost of the redundant update is eliminated.

6.1.7 Related Work

While the use of medium characterization methods specifically for sensor networks is little explored, several related aspects of the problem have been researched. The most closely related problem is that of mapping in robotics, such as discussed in [TB96, ME85, DNC01] among many other works. Our problem differs as we do not need to support simultaneous mapping and localization. Also, since localization may be decoupled from mapping in sensor networks, the problems of combining the medium maps from different sensor nodes differs significantly from robotics. Further, the sensor nodes are only interested in computing the occluded regions, rather than generating a global map for navigation. This allows us to use lower resource overheads and use simpler methods than required for robots.

Learning world models for enhancing computation performance has also been considered for context awareness and location aware computing [CK00, BC04]. These are orthogonal to the medium characterization problem for sensor networks since the nature of queries about the world are very different. Those world models are designed to help the system determine where the user is, what activity the user is engaged in and the state of the objects in the user's environment. In sensor networks on the other hand, the query of interest is the location of occlusions for the sensor. The use of medium mapping was also considered in [HH03]. However, adaptive methods to optimize the scanning process were not considered. Also,

their system involved only one mobile mapping node and distributed mapping and data sharing methods were not relevant.

Another related body of work is the design of adaptive filters for predicting a signal from its previous values [Hay01]. We use these methods in our specific context of adapting the sampling step size. We also propose a different prediction method specific to the problem domain using linear extrapolation. The use of varying sampling step size was also considered in [BRY04] to reduce the number of samples taken but their techniques were not designed for mapping obstacles.

While our work forms an important first step toward realizing the autonomous operation of sensor networks with performance control, several new issues were revealed during our development process, which are yet to be explored in greater depth. One of these is the intelligent separation of mobile events from obstacles, so that depth maps are not generated based on transient occlusions such as due to human motion within the network. Further, the application specific trade-offs in the push vs. pull methods for updates may be studied in more detail.

6.2 Phenomenon Detection

We now discuss the methods used in our system for detection of phenomenon. As mentioned before, the detection is a crucial step in the method that we use for actuation, since the high resolution sensing is provided only at locations where a phenomenon of interest is detected. It is thus important for the detection to take place at low resolution. Several methods for detection may be applicable depending on the phenomenon being sensed. As part of our work, we implemented three example methods for a couple of different applications. These are discussed below.

6.2.1 Ellipse Detection

One of the example applications for a network of cameras such as our system is to detect objects of interest in a user's environment for various ubiquitous computing applications. One approach for detecting objects using cameras is to place a visual tag on each object of interest. Methods have already been proposed to design tags and recognize a tag given a high resolution image of the tag[IL01]. Our system can thus provide the sensing infrastructure required to obtain the high resolution images.

An example tag used in the tag recognition system developed in [IL01] is shown in Figure 6.11.

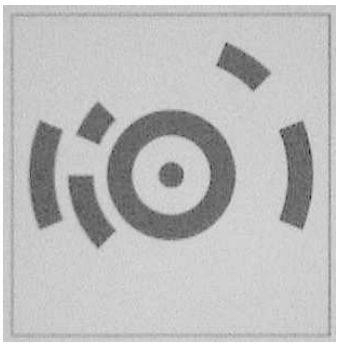

Figure 6.11: Example visual tag used for object detection.

The circular pattern seen in the tag is a visual code for an identification number. The exact pattern of the tag depends on the identification number which is to be represented. The tag design is such that it has two concentric circles in the middle of the pattern. These concentric circles are common for any tag number and are used to detect the tag in the field of view of the camera.

The circles may appear as ellipses depending on the angle which the plane of

the tag makes with the camera's image plane. The interesting thing to note is that ellipses can be detected at a much lower resolution than that required for recognizing the tags. Several methods are available for detecting ellipses, such as based on Hough transform [Ver91] as discussed in [AMN95, CL04] or other methods including genetic algorithms [XJ02, YKG04, EAB92].

In our system implementation we used the same method as in [IL01] and the prototype was demonstrated at [KCH05].

6.2.2 Color Detection

Consider again the tag recognition application mentioned above. Apart from using ellipse detection to detect a tag in the field of view, another method that may be used if the tags can be restricted to be of a unique color is to use color detection. The color should be chosen so as not to be present on other objects as far as possible so as to avoid false positives in the detection phase. Color detection can also be achieved at much lower resolution than that required for recognition of the tags.

There are several methods for color detection. A simple method involves checking the values of the red, green, and blue components to find out which one dominates. For instance, if the green value is higher by a threshold factor than the other two components, we declare the pixel to be predominantly green. Suppose the threshold factor is f, and the red, green, and blue components of a pixel are rpresented by R, G, B, then, the pseudo-code for this method is:

if $(G/R) > f$ **and** $(G/B) > f$

then Pixel is GREEN

The value of the threshold factor f may be chosen depending on allowed tolerance in color matching.

A second method is based on a computation of the Euclidean distance between the color of the test pixel and the reference color. Suppose the reference color to be detected is represented by a vector $[R_f, G_f, B_f]$. Suppose the test pixel has a value $[R, G, B]$. Then, the Euclidean distance, D, is:

$$D = \sqrt{(R - R_f)^2 + (G - G_f)^2 + (B - B_f)^2} \tag{6.6}$$

The reference color may be picked to match the tag color, say green, represented by $[R_f, G_f, B_f] = [0, 255, 0]$. The detection procedure compares the distance, D, with an allowed tolerable error threshold and if D is smaller than the threshold, the color is declared to match.

More advanced methods are available based on transformations of the pixel vectors. For instance, pixel values in the red, green, and blue (RGB) format may be converted to the hue, saturation, and value (HSV) vector space, where the hue specifies the color and the saturation value may be used to allow for tolerances in the purity of the color. Several color detection techniques are surveyed in [VSA03].

In our system we used threshold based color detection, with $f = 1.5$, and implemented it for two different colors: green and red. The implemented system was demonstrated at [KCK05b].

6.2.3 Motion Detection

As another application consider logging high resolution images of all vehicles entering a particular campus area, as shown in Figure 1.1 in chapter 1. One method to detect vehicles using low resolution coverage is to use motion detection. We implemented motion detection methods specifically to detect vehicles as part of our work.

The processing carried out to detect moving vehicles in the image data is described below.

1. A background image is first captured to be used as prior knowledge of the scene being photographed. This background image is updated using an autoregressive filter as described in [SDB00]. The update step for each pixel $I(i, j)$ in the image matrix is:

$$I(i, j) = a * I_{captured}(i, j) + (1 - a) * I(i, j) \tag{6.7}$$

   where $I_{captured}$ denotes the most recently captured image while I is the maintained background image. The parameter a satisfies $0 \leq a \leq 1$ and is typically close to zero. A larger value will lead to a faster update but will also cause some of the motion events to be incorporated into the background. We use $a = 0.05$. The objective of the update is to to adapt the background image to gradual changes such as due to light variations or addition of background objects in the outdoor scene (Fig. 6.12(a)).

2. Each frame captured by a camera is subtracted from the background image and the pixel values above a minimum threshold in the difference image are denoted as motion pixels. A sample frame is shown in Fig. 6.12(b) and the difference image in Fig. 6.13(a). The shade in Fig. 6.13(a) corresponds to the magnitude of the difference value. Pixels with small magnitude difference may arise due to sensor noise even when there is no change in the background and hence differences below a noise threshold are ignored. The sensor noise depends on the camera hardware used and may vary with light levels of the scene. We chose a noise threshld suitable for our hardware in an outdoor setting.

(a) Background (b) Frame

Figure 6.12: Detecting regions of interest using motion detection.

3. Adjacent motion pixels in the difference image are clustered into groups, referred to as *blobs*. Each blob is shown in a different shade in Fig. 6.13(b). Based on the geometry of the scene, the maximum distance being viewed by the camera and theminimum known size for a vehicle of interest one may calculate the minimum area of the image that a vehicle occupies in terms of number of pixels. Blobs with pixel counts lower than that are likely to have arisen due to uninteresting motion events. Thus, blobs with pixel count below a minimum threshold are discarded. In the figure these blobs are also shown but a new shade is not used for such blobs. Several uninteresting motion events, such as tiny blobs corresponding to the edges of the foliage moving in the wind, may be seen in the figure. These are rejected as far as the phenomenon detection method is concerned.

4. Thresholding the blobs by pixel count serves as a first filter for rejecting uninteresting events. However blobs with pixel count greater than the threshold used may arise due to motion events corresponding to pedestrians at certain locations who may appear larger than vehicles by being closer to the

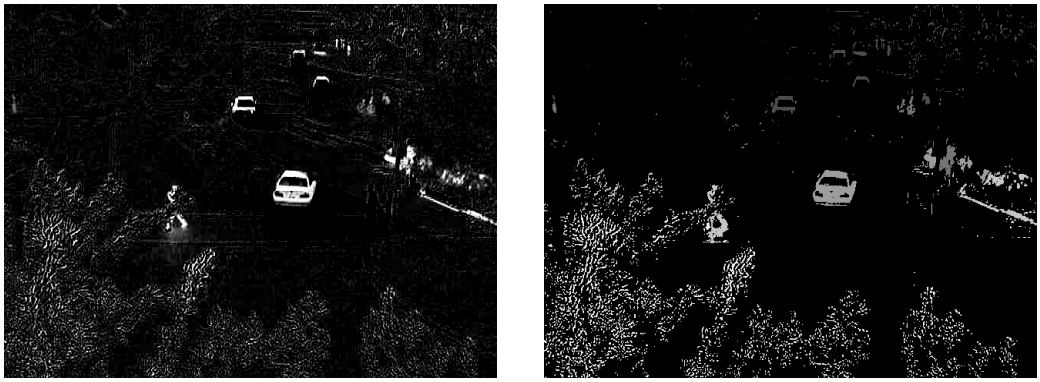

(a) Motion Pixels (b) Blobs

Figure 6.13: Differencing to detect pixels which change.

camera. To filter out such uninteresting motion events due to pedestrians, we exploit the difference in the expected shape of a vehicle and pedestrian. A rectangle surrounding each blob with pixel count above the minimum threshold is calculated (Fig. 6.14(a)). The aspect ratio of each rectangle, i.e., the ratio of its height to the width is calculated. Blobs with aspect ratio, r, such that $0.2 \leq r \leq 1$ are assumed to be arising from vehicles. Blobs with an aspect ratio greater than 1 may arise due to pedestrians moving in the scene (height is greater than width) and blobs with an aspect ratio lower than 0.2 may arise due to noise blobs corresponding to edges that occur in the difference image due to small unavoidable camera shake.

5. For each blob which passes the two filters above, the centroid blobs is calculated. This centroid represents the average location of all the pixels that constitute that blob. We assume the centroid to be the location of the motion event corresponding to that blob. The calculated centroids for the filtered blobs are shown superimposed on the captured frame in Fig. 6.14(b). These locations represent the phenomenon of interest where high

resolution coverage is desired.

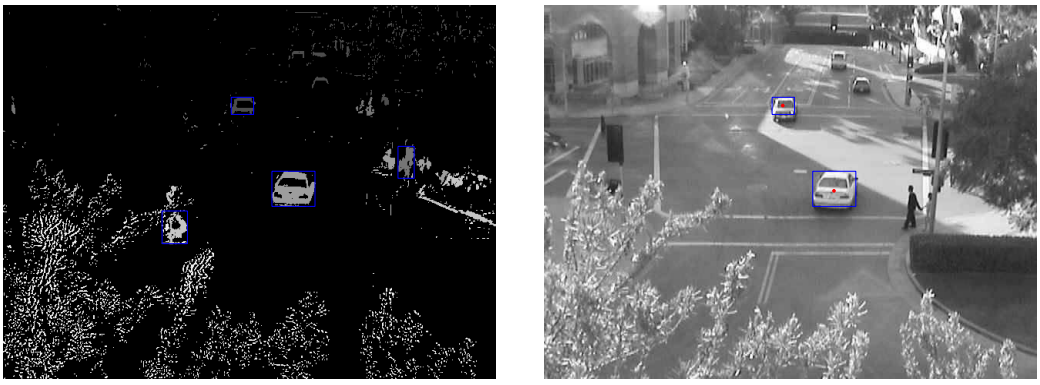

(a) Aspect Ratio (b) Filtered Events

Figure 6.14: Filtering motion events of interest for phenomenon detection.

The above procedures yields the location of the events in the image pixel coordinates. This is sufficient for controlling the actuation when only a camera which detects a phenomenon in its field of view must actuate to it since then, the camera can direct its actuation based on its its own pixel coordinates. However, if a camera other than the one used for detection must be used for the actuation step, more detailed information about the event coordinates in the three dimensional space may be required.

For our scenario for the latter application of imaging vehicles, where the plane of the road is known, the image coordinate may be projected to the road surface using geometric calculations. This may not be feasible in some applications and the true coordinates of the events in 3-space may be needed. More sophisticated detection methods, such as triangulation of the detected phenomenon's location by having it imaged via two or more cameras, may be studied for that objective.

In this chapter we have described the supporting services relevant for our motion coordination algorithm. Next, we consider the simulations and experiments

performed to evaluate our proposed methods and demonstrate their operation on a real system.

CHAPTER 7

Simulations, Prototype, and Experiments

In this chapter, we evaluate the motion coordination methods in simulation and study some interesting properties of the ILS algorithm beyond convergence to a stable state. Further, we demonstrate the implementation of our proposed methods on a prototype system consisting of pan-tilt-zoom cameras and actuated lasers. We also experiment with our proposed methods on real world data using a practical application as a concrete use case for our proposed methods.

7.1 Simulations

Three properties are of primary interest for a distributed optimization algorithm such as the incremental line search proposed in chapter 5. The first is whether the algorithm converges to a stable state. The second property of interest is the proximity of the converged state to a true optimum. The third property of interest is the speed of convergence.

We have already proved convergence to a stable state, in section 5.3. Since we used a realistic sensing performance model, our assumptions are valid under practical implementation constraints and hence the algorithm will converge to a stable state. As an illustration, let us visualize the operation of the algorithm for an example scenario and a randomly generated event distribution, for various choices of design parameters. Figure 7.1(a) shows a random initial deployment

of 10 sensors with a few obstacles. The shade at a point represents the utility at that point due to the best-suited sensor for it, darker shades corresponding to higher utility. The white regions are uncovered and the black circles represent obstacles. Suppose the event distribution has not been acquired as yet. Also, we first set $\alpha = 0$ in the metric calculation of equation (5.3): ILS will try to maximize network utility – which may depend on a few points with high utility, rather than due to more covered points.

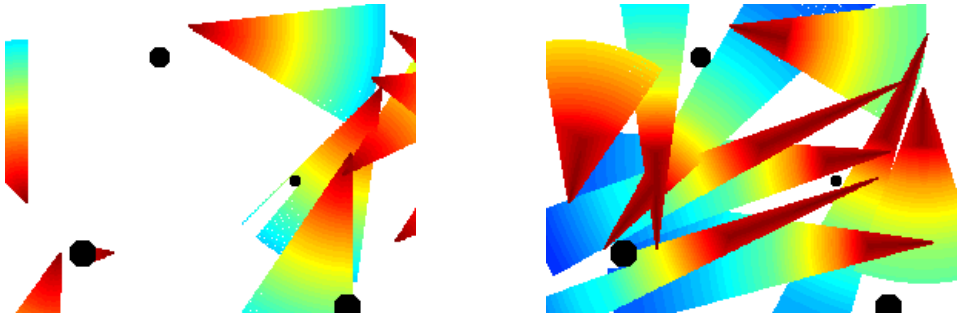

(a) Random initial configuraion. (b) Optimized Config. 1

Figure 7.1: Illustration of ILS convergence (a) random initial network configuration (b) optimized configuration with $w = 0.1$, showing significantly improved coverage than (a).

The final configurations found by executing ILS with $w = 0.1$, corresponding to low weight for the detection performance and a higher weight for time to actuate is shown in Figure 7.1(b). The coverage may now be seen to be much better.

As an alternative, one may set the weight $w = 0.9$ and the resultant configuration is shown in 7.2. The shades within covered regions here are different since in this case the utility is dominated by the resolution of coverage rather than the

time to actuate. The exact choice of the weight parameter depends on desired behavior, which is application specific and we do not dwell on it further here.

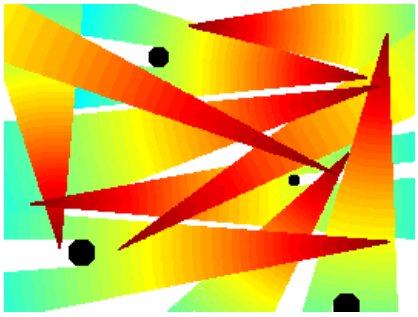

Figure 7.2: Illustration of ILS: optimized coverage using $w = 0.9$, showing a different stable state.

Suppose next that the event distribution shown in Figure 7.3(a) is acquired. The figure axes represent the spatial extent and the shade at each location corresponds to the event density at that location. In the simulation this event distribution is generated as a sum of two Gaussian distributions. The ILS algorithm can use this distribution in the calculation of its utility metric. The optimized configuration is shown in Figure 7.3(b) with $w = 0.1$ - the prominence of higher zoom (narrower field of view) in the diagonal region with higher event density is apparent. Suppose however that the area covered is also to be kept high and thus α is set to 0.8. This yields the configuration in Figure 7.3(c).

The above illustration shows how the ILS algorithm can be tuned for different behaviors as desired by the user application.

We now discuss the other two properties of interest in simulations.

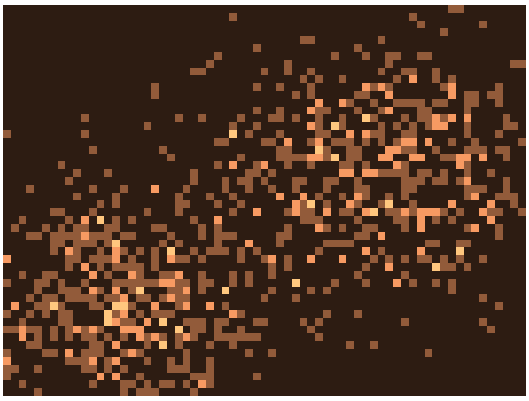

(a) Sample Event Distribution

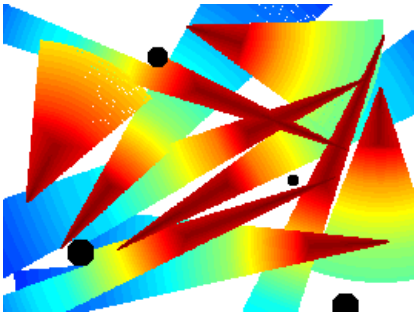

(b) Optimized Config. 3

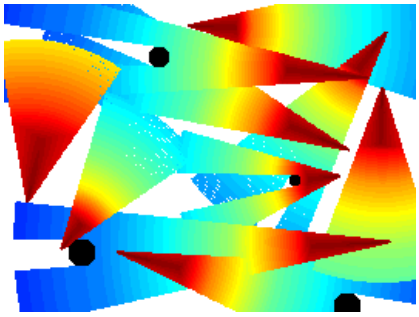

(c) Optimized Config. 4

Figure 7.3: Illustration of ILS (a) a sample event distribution, where brighter areas show higher event density (b) optimized configuration after learning the event distribution, and (c) optimized configuration with α set to a high value.

7.1.1 Accuracy of Converged State

As was proved in section 5.2.1, the optimization problem being solved is NP-hard and our proposed algorithm is a computationally tractable heuristic to solve it, with certain desirable characteristics such as its distributed nature. It may

however not converge to the true optimum. Hence, we wish to evaluate:

1. Is the configuration found by ILS better than the configuration achieved without using ILS but by allowing each node to take its individual decision, and

2. Is the configuration found by ILS close to the true global optimum.

Few analytical proofs are available for convergence to a global optimum for distributed operation. Comparison of the converged state to the true optimum is not feasible since the computation of the true optimum for a representative setting becomes NP-hard. Hence, we simulate the behavior of ILS for certain random scenarios and study how good the converged state is. Different orders in which the sensors update their poses, due to differences in the contention success pattern achieved due to the random waits at the sensors, lead to different search paths in the search space. Also, in the contention phase of the network protocol, certain sensors may win the contention more often than others, and update their pose more often. We simulate the operation of ILS for ten random contention success patterns, and plot the network utility in Figure 7.4.

Note that the network utility is not available to any individual node, and is made available in the simulations by considering the poses of all nodes centrally for the purpose of evaluation. The solid curves show the evolution of utility with iteration for different contention success patterns. The dotted line shows the utility achieved by a naïve method: updating the pose of each sensor locally without any coordination with its neighbors.

The graph shows that:

1. while the convergence time varies among multiple contention success orders, the final utility with ILS is always better than a naïve local method.

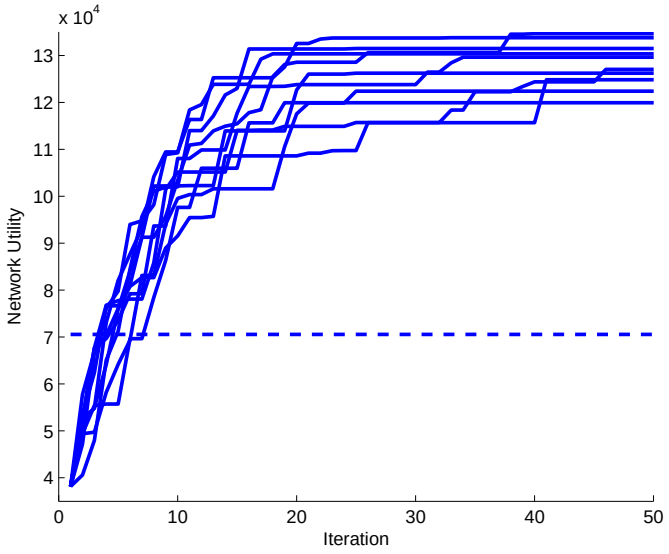

Figure 7.4: Optimization accuracy: convergence with ten random search paths. Each curve shows a different random contention success pattern. The various converged states have a utility within 10.9% of the best case.

2. the final utilities, which are local minima, found in multiple random runs are within 10.9% of the best case. This suggests, though does not prove, that ILS behaves well for several random instances. This is also expeted due to the relationship of ILS to incremental subgradient methods. It has been known that incremental methods are less likely to get stuck in poor local optima or stationary points, compared to gradient descent methods since they do not suffer from the gradient descent effect of finding the local maxima closest to the starting point [Sol95].

Based on such arguments and our simulation results, we conjecture that ILS discovers a good quality stable configuration with high probability. The monotonicity property always guarantees that ILS will never worsen a configuration, and the graph shows that using ILS has a significant advantage compared

to a naïve approach.

7.1.2 Convergence Speed

We now address the third important consideration: time to converge. Again, this is studied through simulations. The simulation scenario consists of a network of $N = 25$ sensors spread across 100×50 meters, and maximum camera range $R_{max} = 8m$ at widest zoom. Several random topologies are simulated. The convergence performance for each random topology is plotted in Figure 7.5.

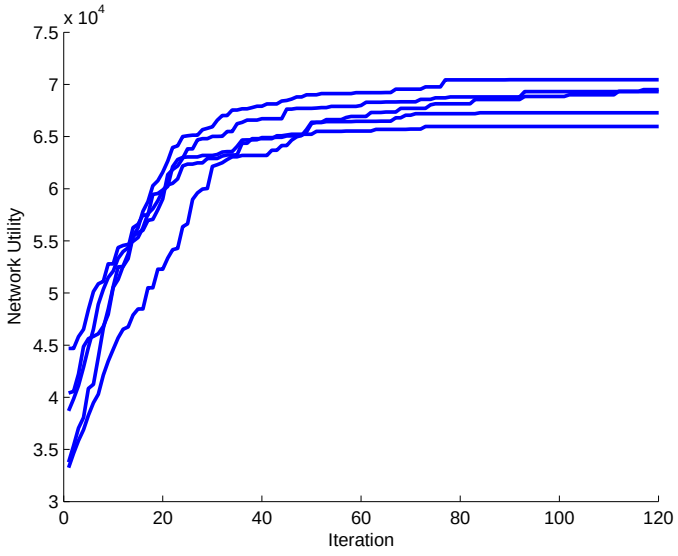

Figure 7.5: Convergence: evolution of utility with increasing number of iterations. Each curve corresponds to a random location topology and random initial poses of the sensors.

To consider the worst case execution time, we consider each sensor's update as a separate iteration, even though several of these occur in parallel. The time taken for each iteration is considered next. Each iteration consists of the contention phase wait of $T_{timeout}$. This setting depends on the communication layer used.

For instance, for 802.11 MAC, the per hop delay is expected to be less than 10ms [TS04, GK04] and, if γ_i spans 10 hops as a worst case estimate, the total round trip delay would be limited to $200ms$. At least one sensor wins the contention and computes its optimal pose. This has the delay of pan motion and zoom motion. The longest pan step may be 340° degrees which takes 2 seconds. The longest zoom step (see Figure 3.14-(b)) allowing a maximum zoom setting of 5 in detection mode (leaving the remaining zoom range of 20 available for providing high resolution coverage for recognition), is $1.3s$. A single update time is thus $2 + 1.3 + 0.2 = 3.5s$.

The number of iterations required to achieve the final utility is about 80 as seen in the graph for each random topology, and even in the worst case this requires 4 minutes 40 seconds. The number of iterations is about 3 times the number of sensors, implying that on an average each sensor updates three times. Even with increasing network size, due to parallelism in updates, the convergence time will stay at the same order. Thus the stable state is discovered in only a few minutes for the hardware capabilities in our system. Since the phenomenon learning phase (which must wait for several events to occur in order to estimate or update the $q(p)$) and medium dynamics are expected to be much slower, convergence time is not an important consideration for our system, and ILS can repeatedly be used to update the network configuration whenever new environmental information becomes available.

Time to converge may be an important concern in other applications of ILS where the system must deal with rapid dynamics. The graceful degradation behavior of ILS discussed in section 5.3.1 then helps ensure that ILS does not worsen the situation.

7.2 Prototype System

Let us now consider the execution of ILS on the test-bed shown in Figure 1.2. The test-bed has four pan-tilt-zoom cameras [Son04]. The motion capabilities of this camera have already been tabulated (Table 3.2). It also has two self-awareness nodes described in section 6.1.1.1. Some objects of various shapes are placed to emulate obstacles in the covered space. Any available networking technology that has sufficient bandwidth to support video data, may be used and we used Ethernet. The cameras also allow for a WiFi card to be added in its PCMCIA slot and that may be used if a wireless connection is preferred. Since we did not have access to change the firmware on the camera, we developed our software on an external processing platform but the methods could well be implemented on the camera processor itself in actual production.

Rather than beginning with a random configuration, we arrange the cameras along the edges to form a regular tessellation covering the entire rectangular region of interest. However, the obstacles in the rectangular region, render the regular tessellation ineffective.

The first requirement is the information about medium obstacles. We collect this using laser ranging. Range scans from the bottom left corner and the top right are shown in Figures 7.6(a) and 7.6(b) repectively. Note that these scans exploit the adaptive scanning enhancements discussed in section 6.1 and hence the scan step size is seen to be greater when scanning a structured environmental feature, such as a straight line, since it matches the adaptive algorithm's predicted structure. A backtracking procedure allows the algorithm to reduce the scan step size and re-scan the missed portion in case a large deviation from the predicted structure is observed. Combining the two scans yields the obstacle map shown in Figure 7.6(c) by the dark patches. Figure 7.6(c) also shows the initial network

configuration.

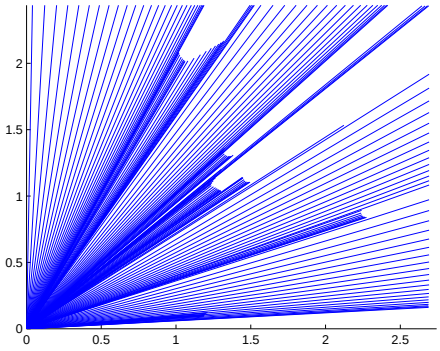

(a) Range scan 1

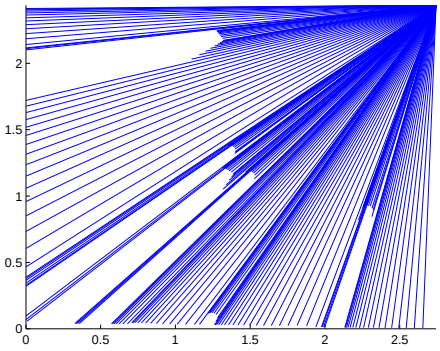

(b) Range scan 2

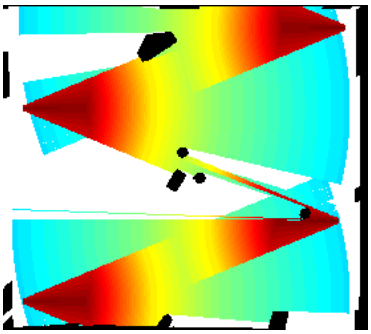

(c) Obstacles and Initial Configuration

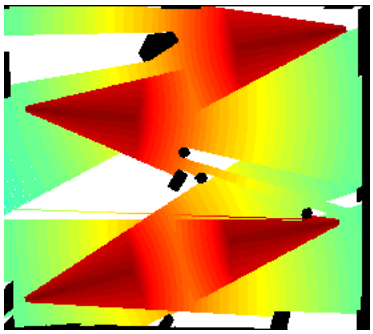

(d) Final configuration

Figure 7.6: Gathering medium information for ILS operation (a) range scan from laser in bottom left corner (b) range scan from laser in top right corner, (c) map of obstacles in the medium and the initial network configuration, (d) optimized configuration found by ILS - it changes both the pan and zoom settings of the cameras to increase sensing performance characterized by time required for recognition.

In this configuration, each sensor node has all other nodes as its neighbors. The test-bed can thus be viewed as one neighborhood set in a larger network.

The final network configuration found by the ILS algorithm is shown in Figure 7.6(d). The experiment used $w = 0.1$, thus giving more weight to the time required for actuation and the parameter α was set high to maximize covered area. These results not only verified that the ILS algorithm behaves as designed but also helped us ensure that all the algorithms and methods proposed can be implemented in a real system.

The testbed software also includes certain supporting components to enable visualization of the experiment's progress. The images captured by the network cameras are compressed JPEG files for ease of transfer over the network. Our camera controller software decompresses each image. It also calculates the occluded pixels based on the laser ranger readings. The occluded pixels are plotted superimposed on the raw image for visualizing the camera's field of view as it evolves under ILS. A snapshot of the visualization of four separate processes, each controlling one of the network cameras is shown in Figure 7.7.

A central experiment monitoring program was also developed in Matlab for controlling the cameras centrally for various experiments. The graphical user interface to this program alows setting various parameters in the experiment, and is shown in Figure 7.8.

Further, a manual control interface was developed which exposed the camera's actuation capabilities to a human user through an HTML interface. This manual control interface allows a user to manually over-ride the settings found by ILS if so desired. The complete system software in operation, including the manual over-ride may be seen in Figure 7.9.

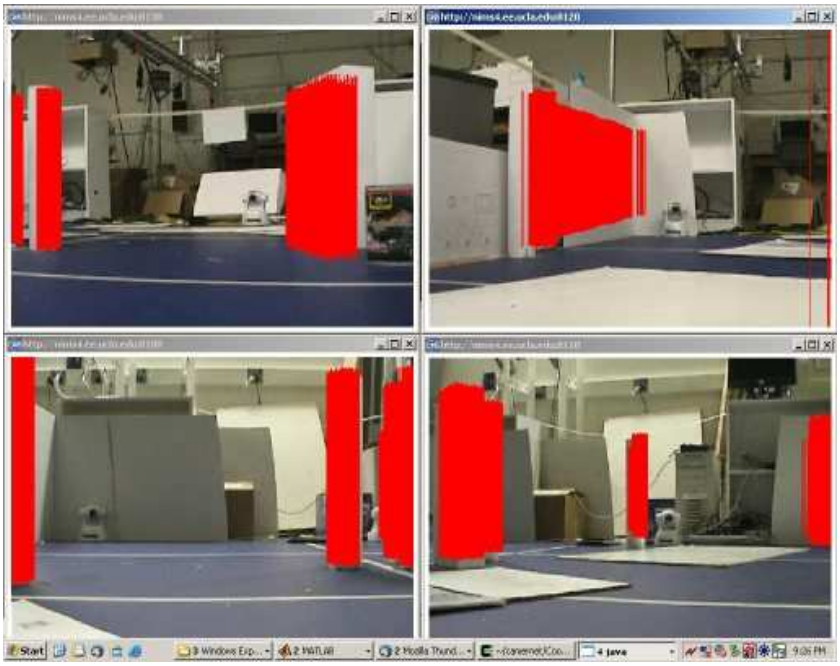

Figure 7.7: GUI snapshots of the four processes controlling the network cameras in the testbed.

7.3 Experimental Evaluation

We also evaluate the proactive motion coordination methods on an experimental system using real world event data. One key parameter of interest in comparing an actuated system against a system of static cameras is the actuation delay required for actuating after an event is detected. Since the reactive methods required to carry out the actuation step in response to a detected event are not developed as part of our work, we assume a simple method where each camera will zoom in to an event detected in its field of view. Issues in the reactive phase, such as scheduling the camera for multiple simultaneous events [CDB04]

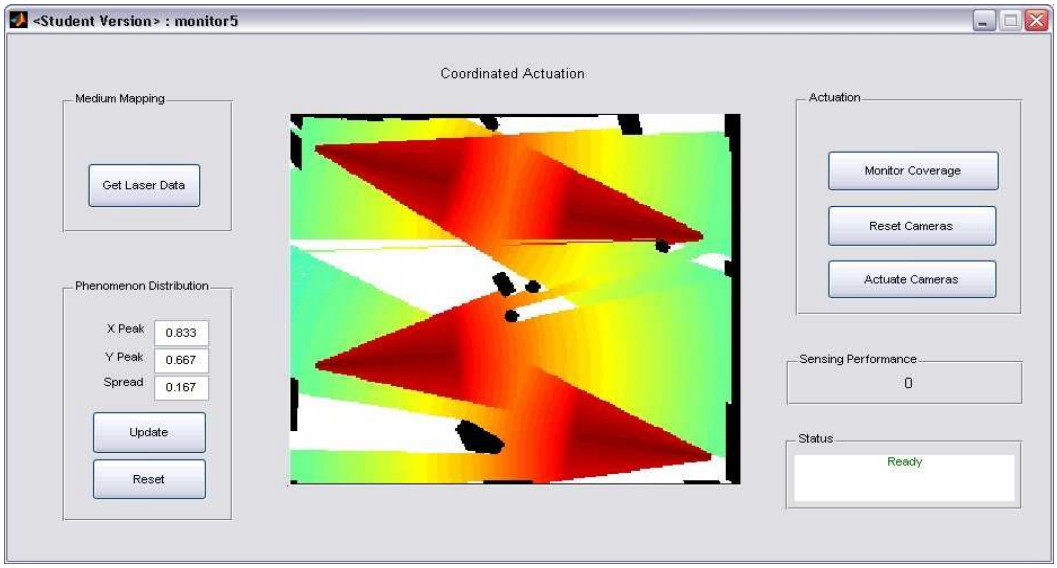

Figure 7.8: Experiment monitoring software.

or tracking an event as it moves through the covered area [CRZ04, CLF01] are not being studied here.

While most of our design choices apply generically to any camera network where resolution is to be increased, some of the analysis is performed in the context of the example application mentioned briefly in section 1, and specified concretely here. Consider the access road to a building shown in Fig. 1.1(a). This image is captured from a camera mounted on a 2nd floor patio of the building itself. Suppose the entire sealed road area in this scene is to be photographed at a resolution good enough to visually recognize a vehicle, say $200 pixels/m$. The vehicle license plate, if captured in the image, will be legible at this resolution. However, cameras may be installed only within the building premises and not on

Figure 7.9: System software in operation alongside the testbed.

the roads themselves since the building owners may not have jurisdiction over the road infrastructure or the sidewalks. Given that the application is interested in photographing vehicles, assuming that the minimum vehicle width is $1.5m$, and also assuming that motion detection can work reliably if the one of the moving object dimensions is at least 15 pixels, we see that $R_{det} = 10 pixels/m$. For the required $R_{sense} = 200 pixels/m$, this yields $z = 20X$. The camera we use in our system [Son04] has a zoom range, z_{hw}, greater than this. The range of pan and tilt required, for the reactive actuation when an event is detected, is equal to the angle of field of view at the zoom setting used for detection. For instance, the angle of field of view is 45° at the widest zoom setting, $z = 1$, and the pan range of the camera is greater than this. The available actuation capabilities of the

camera are compared to those required in Table 7.1.

Capability	**Required**	**Available**
Zoom	z=20X	$z_{hw} = 25$X
Pan	$\theta_{fov} = 45°$	$\theta_{pan} = 370°$
Tilt	30°	115°

Table 7.1: Required actuation ranges and hardware capabilities.

We will compare the network configurations achieved by our method and other methods by measuring the actuation delay per event averaged over a large number of events.

To obtain a realistic trace of event locations in the covered area of interest, we used motion detection, as described in section 6.2.3, on a live stream of images coming from a camera mounted to view the scene shown in Fig. 1.1(a). Note that we are not addressing the problem of detection method design in this thesis and assume that the detection performance achieved by the available method, such as motion detection in our example, is sufficient for system operation.

A total of 5000 events were detected using the above procedure in a live video stream. A histogram of these events over the scene coordinates is shown in Fig.7.10. Lighter shades correspond to regions with more events. The complete image stream, and the event coordinates obtained via motion detection are available through our CVS repository [Kan].

The proactive motion coordination methods are evaluated using this event trace for a set up of four cameras looking at the scene for which this event trace is collected. The actuation delay performance of a particular network configuration is calculated as follows: for each event in the trace, the time required by the camera to zoom in to provide the high resolution coverage is computed. The

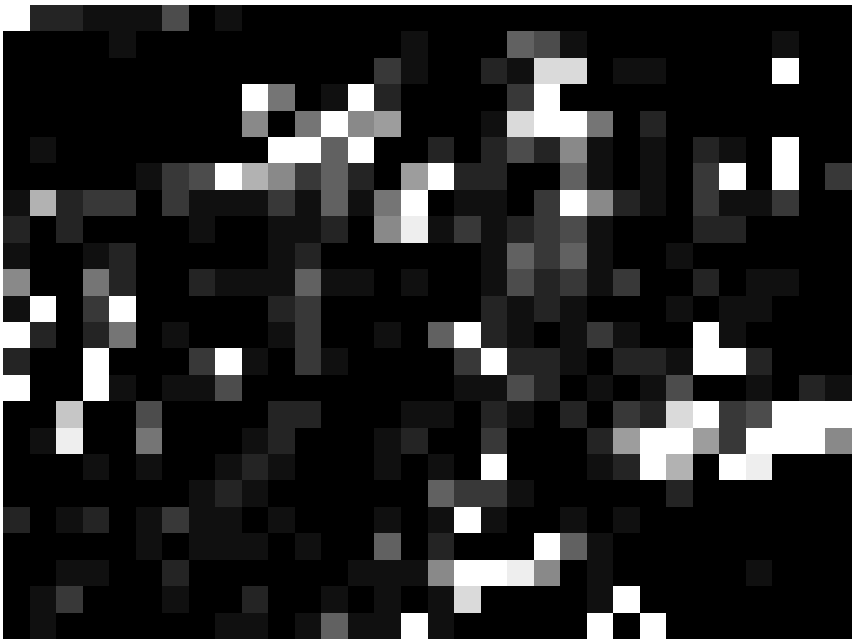

Figure 7.10: Event trace

time is computed for that camera which has detection coverage (low resolution coverage) over the event location. This time varies with the extent of zoom, pan, and tilt motion required to reach that event, and can be computed using the documented pan and tilt speeds for the camera along with the measured zoom change speed of the camera (Figure 3.14(b)). An average of the computed time for each event is taken over all events, for each configuration as the delay performance of that configuration.

We compare four alternatives, labeled in the following graphs using the acronyms below:

1. TESS, a regular tessellation: The four cameras are arranged regularly with their zoom set to widest and each camera looking straight ahead.

2. ILS(UNIF): The ILS algorithm is used to optimize the configuration. Only

5X of the zoom is used since the remaining 20X is required for the reactive phase. Similarly, the excess pan range not required for the reactive phase is used. The tilt is ignored, but can be used in the same manner as pan.

3. ILS: The ILS algorithm is used with a knowledge of the true event distribution. The histogram generated from the event trace is used as the event distribution, and since this comes from the trace itself, it is a true event distribution. If the observed event distribution varies from the distribution learned by the system, the delay performance may suffer somewhat; the exact deviation depends on the error in the learned distribution itself.

4. RAND: The cameras are configured randomly. Ten random configurations are tried and the average and standard deviation of the quantities being evaluated are plotted.

In the utility metric used for ILS, the tuning parameter w allows biasing the algorithm toward actuation delay or detection quality. Suppose we bias it to actuation delay, by using a higher weight $w = 0.9$ for the delay term and $(1-w) = 0.1$ for the detection term. The delay performance for the four alternatives is plotted in Fig. 7.11(a). The corresponding detection performance, measured in terms of the fraction of the events detected is plotted in Figure 7.11(b). The lighter shade bar segment on top of the bar for RAND is the standard deviation across the multiple random runs. Clearly ILS yields the best delay performance. The detection performance is comparable, though not exactly the same, for all alternatives except RAND. It is above 90%, showing that when ILS optimizes for delay, the penalty on detection is not significant. For applications where the detection performance is at a premium, delay may have to be sacrificed by chosing the configuration with the highest detection performance.

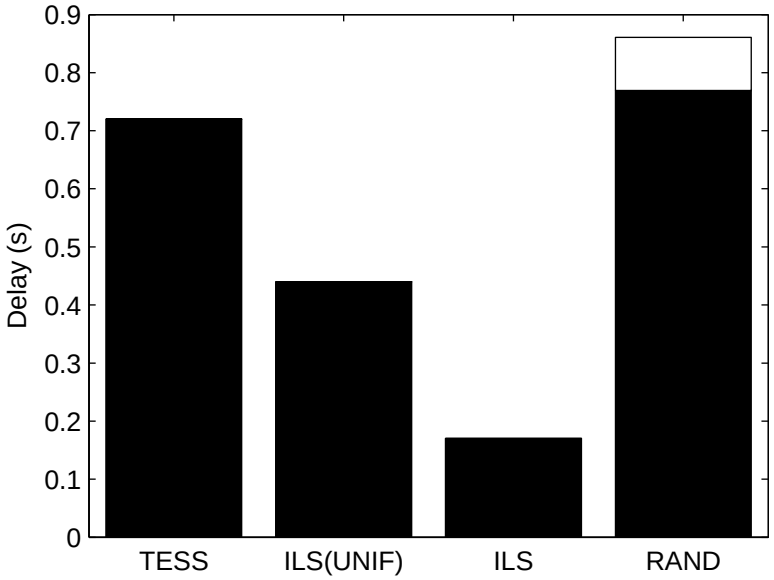

(a) Actuation delay

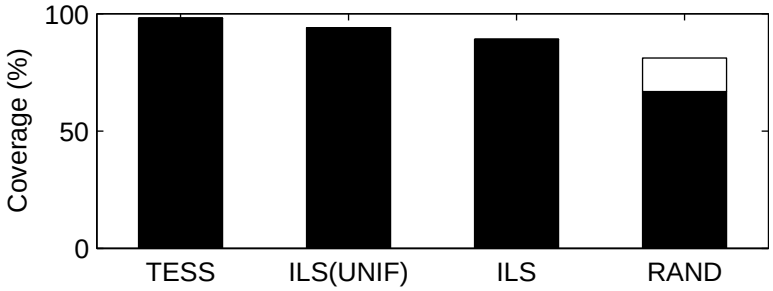

(b) Detection coverage

Figure 7.11: Performance of different network configurations, when optimization is weighted for actuation delay.

Note that internally, the ILS algorithm is not using delay but the utility metric defined in section 5.1.3 for optimizing the configuration. This utility metric for the four alternatives is plotted in Fig. 7.12, to see how this internal measure relates to the observed application level performance metrics. The configurations obtained using ILS have higher utility. This is expected as the ILS algorithm changes the starting configuration to increase the utility metric. Among these, the utility is higher when the true event distribution is used.

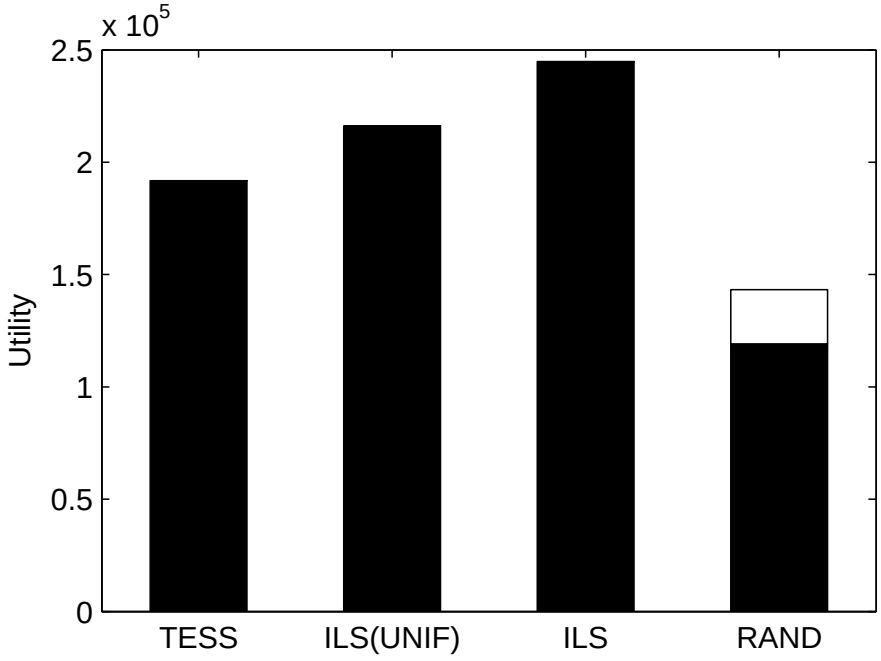

Figure 7.12: Utility metric evaluated for various configurations.

On the other hand, we could bias the utility metric for detection performance, using the tuning parameter w provided by our algorithm. The results for this choice, i.e., the weight for delay term set to $w = 0.1$, and that for detection term set to $(1 - w) = 0.9$, are shown in Figs. 7.13 and 7.14. As may be seen in Fig. 7.13(b), the detection performance has improved. Since the detection performance was already high, the improvement relative to Fig. 7.11(b) is small.

The above evaluations show the delay required using our prototype hardware to increase the resolution of sensing by over an order of magnitude. Clearly, when such delay is acceptable, our methods can be used to improve the sensing performance significantly, or conversely, to provide significant savings in sensing resources for a given sensing performance. Further, the graphs above indicate the flexibility of our algorithm provided through the tuning parameters for biasing

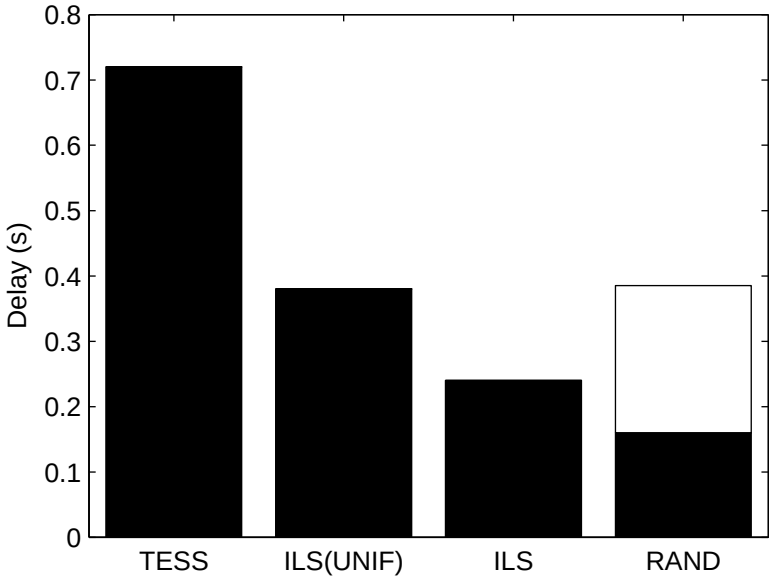

(a) Actuation delay

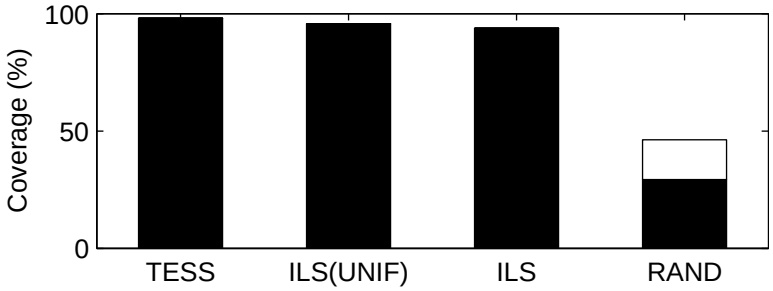

(b) Detection coverage

Figure 7.13: Performance of different network configurations, when configuration optimization is weighted for detection performance.

its operation for the metric of user interest.

The delay can be further reduced by increasing the number of cameras. For instance, if each camera in our system is replaced with 4 similar cameras, then each camera is responsible for only a quarter of the original volume covered for detection and a lower actuation time is sufficient to cover the reduced volume. In our prototype, we use four cameras based on equipment availability. In actual

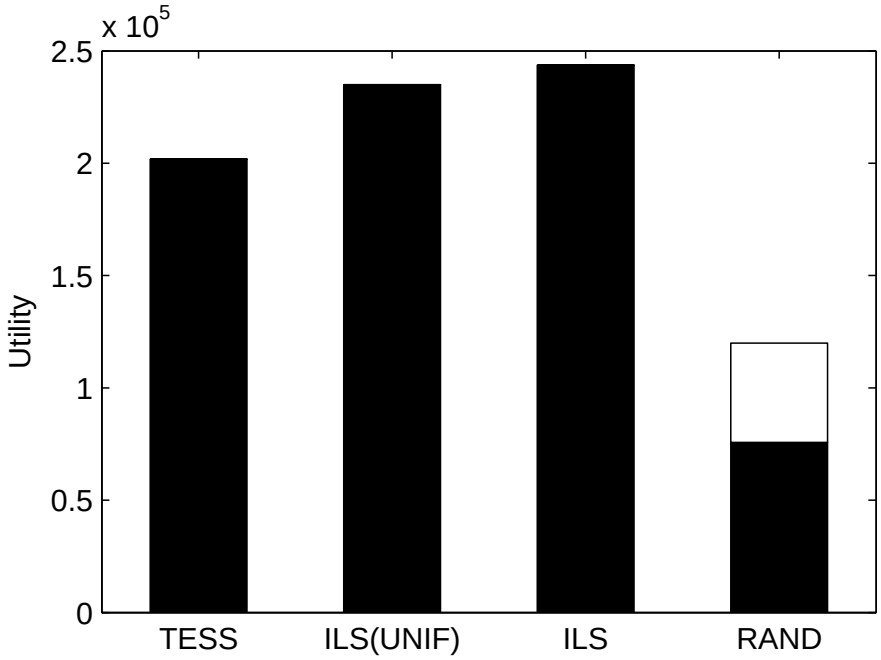

Figure 7.14: Utility metric for various configurations, when detection performance is weighted higher.

production, the number of cameras may be determined based on the desired delay tolerance and the expected number of simultaneous events in the scene.

CHAPTER 8

Conclusions and Future Work

In this dissertation we discussed why using small motion is a potentially useful alternative to improve the sensing performance of embedded sensor networks and provided a framework of distributed methods to effectively exploit the small motion.

While it has been known before that motion and even small motion has a sensing advantage, a quantitative understanding of the potential benefits and an in-depth analysis of the related trade-offs was lacking. Our work has evaluated the exact extent of sensing advantage that may be achieved using small motion and also compared it to other alternatives such as using a high density of static sensors or a low density of unconstrained mobile nodes. We showed that small motion can lead to several orders of magnitude advantage in sensing resolution depending on certain trade-offs and in our particular prototype, we demonstrated four orders of magnitude advantage. We also discussed several reasons which make the use of small or constrained motion more practical than other alternatives for a variety of scenarios.

Further, while motion has been used before for increasing the range of coverage or for tracking mobile phenomenon before, the precise delay trade-off in the use of motion had not been discussed. We quantified the delay trade-off in using small motion for providing high resolution coverage for a specific methodology of using motion: using a low resolution view for detecting the phenomenon of interest and

then using motion to provide high resolution sensing at required locations.

We also presented a framework for optimizing the configuration of a mobile sensor network with limited motion capabilities. Prior work has considered the use of motion for optimizing the deployment in terms of area covered, increasing the extent of coverage by having a sensor patrol a set of sensing points, or even the use of motion to track a mobile phenomenon. However, the use of motion to increase the resolution of coverage by using a low resolution view for detection has not been studied in depth before. Using motion for configuring the network in order to minimize motion delay had not been considered in prior work. We provided methods that allow minimizing the motion delay required for providing high resolution coverage. We showed that solving this problem optimally was NP-hard and provided computationally tractable heuristics to address the situation.

The motion coordination methods we developed for the above objective were distributed in nature. This leads to extreme scalability of the proposed methods in terms of the number of nodes in the network since the motion coordination algorithm required communication only in a well defined neighborhood, the size of which depends only on the network density and does not grow with the number of nodes. The distributed motion coordination algorithm developed as part of this work was shown to have several desirable properties, including provable convergence, graceful degradation and the ability to operate with realistic sensor models.

In addition to the motion coordination method, we also presented practical methods to learn the environmental parameters which affect the network configuration. Specifically, our methods could exploit information about the obstacles in the medium and the expected distribution of events in the space covered. Practical methods for acquiring this information about the environment were also

developed and demonstrated with prototype hardware implementations.

Finally, we implemented all our proposed methods on a prototype system to not only verify their realizability but also study their behavior with respect to certain performance considerations. We also conducted experiments to evaluate our methods on real world data collected using our prototype in the context of practical application examples.

8.1 Future Directions

Most of the methods developed as part of our work are the first in the domain of minimizing actuation delay in using motion for high resolution sensing. Thus, significant future research is feasible to improve the proposals of our work.

An interesting problem for future research is the integration of the proactive methods for network reconfiguration presented in our work with the reactive methods used to perform the final actuation in response to detected events. The network configuration provided by our proactive methods can be exploited by the reactive methods to achieve the best delay performance in the face of multiple events detected by multiple sensors. The scheduling of actuation steps and the allocation of appropriate sensing resources to the detected events presents interesting research challenges. For instance, methods may be developed to prioritize the detected events based on their dwell time in the field of view of the network, and then use the allocating the cameras in the derived priority order to those events.

Future work also includes fundamental considerations that relate the number of actuated cameras required for given event dynamics in terms of the number of events in the environment and their dwell times and mobility characteristics.

The appropriate strategy to use all available sensors for detection and actuation for high resolution sensing on demand, or allocating a fixed number of sensors for constant detection while others are used for actuation may be studied as part of this problem as well.

The ILS algorithm may further be extended to exploit the temporal dimension and determine sequences of configurations to be visited over a given time period rather than finding a single optimal configuration. Further, our methods may be extended to include the case of tracking mobile events rather than just providing high resolution coverage once for each event.

References

[AB03] MD Naish A Bakhtari, M Eskandari and B Benhabib. "A Multi-Sensor Surveillance System for Active-Vision Based Object Localization." In *IEEE International Conference on Systems, Man and Cybernetics*, volume 1, p. 10131018, Washington, D.C., October 2003.

[AKS03] A Antoniades, HJ Kim, and S Sastry. "Pursuit-evasion strategies for teams of multiple agents with incomplete information." In *42nd IEEE Conference on Decision and Control*, Maui, Hawaii, USA, December 2003.

[AMB05] S Aranda, S Martinez, and F Bullo. "On optimal sensor placement and motion coordination for target tracking." In *IEEE Int. Conf. on Robotics and Automation*, Barcelona, Spain, April 2005.

[AMN95] AS Aguado, ME Montiel, and MS Nixon. "Ellipse Detection via gradient direction in the Hough transform." In *Proc. IEE International Conference on Image Processing and its Applications*, pp. 375–378, July 1995.

[APP02] T Arai, E Pagello, and LE Parker. "Editorial: advances in Multi-Robot Systems." *IEEE Transactions on Robotics and automation*, **18**(5):655–661, October 2002.

[AXI] AXIS. "Axis 2100 Network Camera." Product Datasheet, Axis Communications, http://www.axis.com/documentation/datasheet/2100/2100_ds.pdf.

[BC04] G Biegel and V Cahill. "A Framework for Developing Mobile, Context-aware Applications." In *IEEE Percom*, Orlando, FL, March 2004.

[BMK02] J Burke, E Mendelowitz, J Kim, and R Lorenzo. "Networking with knobs and knats: Towards ubiquitous computing for artists." In *Ubiquitous Computing, Concepts and Models Workshop*, Gothenburg, Sweden, 2002.

[BP98] I Benyahia and JY Potvin. "Decision Support for Vehicle Dispatching Using Genetic Programming." *IEEE Transations on Systems, Man, and CyberneticsPart A: Systems and Humans*, **28**(3), May 1998.

[BR03] Z Butler and D Rus. "Event-Based Motion Control for Mobile-Sensor Networks." *IEEE Pervasive Computing*, **2**(4):34–42, October-December 2003.

[BRD05] NP Bichot, AF Rossi, and R Desimone. "Parallel and Serial Neural Mechanisms for Visual Search in Macaque Area V4." *Science*, **308**(5721):529–534, April 2005.

[BRY04] M Batalin, M Rahimi, Yan Yu, Duo Liu, A Kansal, G Sukhatme, WJ Kaiser, M Hansen, GJ Pottie, and D Estrin. "Call and Response: Experiments in Sampling the Environment." In *ACM SenSys*, November 2004.

[BSP04] B Batagelj, F Solina, and P Peer. "15 seconds of fame - an interactive, computer-vision based art installation." In *Proceedings of the 12th ACM International Conference on Multimedia*, pp. 764–765, New York, NY, USA, October 2004.

[CD00] X Chen and J Davis. "Camera Placement Considering Occlusions for Robust Motion Capture." Technical Report CS-TR-2000-07, Computer Science, Stanford University, 2000.

[CDB04] C Costello, C Diehl, A Banerjee, and H Fisher. "Scheduling an Active Camera to Observe People." In *ACM 2nd International Workshop on Video Surveillance and Sensor Networks*, New York City, NY, USA, October 2004.

[CEE01] A Cerpa, J Elson, D Estrin, L Girod, M Hamilton, and J Zhao. "Habitat monitoring: Application driver for wireless communications technology." In *ACM SIGCOMM Workshop on Data Communications in Latin America and the Caribbean*, 2001.

[Cho] Howie Choset. "The Wide World of Mapping." WTEC Workshop: Review of US Research in Robotics.

[Chv75] V Chvatal. "A Combinatorial theorem in plane geometry." *Journal of Combinatorial Theory Series*, **18**:39–41, 1975.

[CK00] G Chen and D Kotz. "A Survey of Context-Aware Mobile Computing Research." Technical Report TR2000-381, Dept. of Computer Science, Dartmouth College, November 2000.

[CL04] Z Cheng and Y Liu. "Efficient Technique for Ellipse Detection Using Restricted Randomized Hough Transform." In *International Conference on Information Technology: Coding and Computing (ITCC'04)*, volume 2, p. 714, 2004.

[CLF01] R Collins, A Lipton, H Fujiyoshi, and T Kanade. "Algorithms for cooperative multisensor surveillance." *Proceedings of the IEEE*, **89**(10):1456 – 1477, October 2001.

[CMB04] J Cortes, S Martinez, and F Bullo. "Spatially-distributed coverage optimization and control with limited range interactions." *ESAIM, Control, Optimization and Calculus of Variations*, January 2004.

[CMB05] J Cortes, S Martinez, and F Bullo. "Analysis and design tools for distributed motion coordination." In *American Control Conference*, Portland, OR, June 2005.

[CN88] W P Chin and S Ntafos. "Optimum watchman routes." *Information Processing Letters*, **28**:3944, 1988.

[CNN93] S Carlsson, BJ Nilsson, and SC Ntafos. "Optimum Guard Covers and m-Watchmen Routes for Restricted Polygons." *International Journal of Computational Geometry Applications*, **3**(1):85–105, 1993.

[CRZ04] M Chu, J Reich, and F Zhao. "Distributed Attention for Large Video Sensor Networks." In *Intelligent Distributed Surveillance Systems 2004 seminar*, London, UK, February 2004.

[DNC01] MWM Gamini Dissanayake, P Newman, S Clark, HF Durrant-Whyte, and M Csorba. "A Solution to the Simultaneous Localization and Mapping (SLAM) Problem." *IEEE Transactions on Robotics and Automation*, **17**(3):229–241, June 2001.

[Dpe] "Directed Perception." http://www.dperception.com.

[DR04] D Devarajan and R Radke. "Distributed metric calibration for largescale camera networks." In *First Workshop on Broadband Advanced Sensor Networks (BASENETS), in conjunction with BroadNets*, San Jose, October 2004.

[EAB92] T Ellis, A Abbood, and B Brillault. "Ellipse Detection and Matching with Uncertainty." *Image and Vision Computing*, **10**(5):271–276, June 1992.

[EGH00a] A Efrat, LJ Guibas, S Har-Peled, DC Lin, JSB Mitchell, and TM Murali. "Sweeping simple polygons with a chain of guards." In *SODA '00: Proceedings of the eleventh annual ACM-SIAM symposium on Discrete algorithms*, pp. 927–936, San Francisco, California, United States, 2000.

[EGH00b] D Estrin, R Govindan, and J Heidemann. "Embedding the Internet: introduction." *Communications of the ACM*, **43**(5):38–41, 2000.

[ES04] UM Erdem and S Sclaroff. "Optimal Placement of Cameras in Floorplans to Satisfy Task Requirements and Cost Constraints." In *Omnivis2004, The fifth Workshop on Omnidirectional Vision, Camera Networks and Non-classical cameras*, Prague, May 2004.

[Far01] CR Farrar. *Lecture notes on Structural Health Monitoring using Statistical Pattern Recognition*, chapter Historical overview of structural health monitoring. Los Alamos Dynamics, Los Alamos, NM, 2001.

[FGP06] S Funiak, C Guestrin, M Paskin, and R Sukthankar. "Distributed Localization of Networked Cameras." In *Inormation Processing in Sensor Networks*, Nashville, TN, USA, April 2006.

[Fis78] S Fisk. "A short proof of Chvatal's watchmen theorem." *Journal of Combinatorial Theory Series*, **24**:374, 1978.

[FLS02] JT Feddema, C Lewis, and DA Schoenwald. "Decentralized Control of Cooperative Robotic Vehicles: Theory and Application." *IEEE Transactions on Robotics and Automation*, **18**(5), October 2002.

[GA81] H. El Gindy and D Avis. "A linear algorithm for computing the visibility polygon from a point." *Journal of Algorithms*, **2**:186–197, 1981.

[GJ96] D Geman and B Jedynak. "An Active Testing Model for Tracking Roads in Satellite Images." *IEEE Trans. Pattern Anal. Mach. Intell.*, **18**(1):1–14, 1996.

[GK04] N Gupta and PR Kumar. "A Performance Analysis of the 802.11 Wireless LAN Medium Access Control." http://www.ece.rice.edu/čamp/MAC/MAC_Analysis.pdf, 2004. Submitted to Communications in Information and Systems , Jan'04, revised June'04.

[GKS04] S Ganeriwal, A Kansal, and MB Srivastava. "Self-aware Actuation for Fault Repair in Sensor Networks." In *IEEE International Conference on Robotics and Automation (ICRA)*, April 2004.

[GLL99] LJ Guibas, JC Latombe, SM LaValle, D Lin, and R Motwani. "A visibility-based pursuit-evasion problem." *International Journal of Computational Geometry and Applications*, **9**(4/5):471–, 1999.

[GMK03] B Grocholsky, A Makarenko, T Kaupp, and HF Durrant-Whyte. "Scalable Control of Decentralised Sensor Platforms." In *Information Processing in Sensor Networks: 2nd Int Workshop, IPSN03*, pp. 96–112, 2003.

[GP04] V Gazi and KM Passino. "Stability Analysis of Social Foraging Swarms." *IEEE Transactions on Systems, Man, and CyberneticsPart B: Cybernetics*, **34**(1), February 2004.

[Gro02] B Grochoslsky. *Information Theoretic Control of Multiple Sensor Platforms*. PhD thesis, Australian Center for Field Robotics, Department of Aerospace, Mechatronic and Mechanical Engineering, University of Sydney, March 2002.

[HAG06] TC Harmon, RF Ambrose, RM Gilbert, JC Fisher, M Stealey, and WJ Kaiser. "High Resolution River Hydraulic and Water Quality Characterization Using Rapidly Deployable Networked Infomechanical Systems (NIMS RD)." Technical Report 60, Center for Embedded Networked Sensing, University of California Los Angeles, February 30 2006.

[Hay01] S Haykin. *Adaptive Filter Theory*. Prentice Hall, 4th edition, 2001.

[HH03] RK Harle and A Hopper. "Building World Models by Ray Tracing within Ceiling Mounted Positioning Systems." In *UbiComp 2003*, pp. 1–17, Seattle, WA, USA, October 2003.

[HMS02a] A Howard, MJ Mataric, and GS Sukhatme. "An Incremental Self-Deployment Algorithm for Mobile Sensor Networks." *Autonomous Robots Journal (Special Issue on Intelligent Embedded Systems)*, **13**(2):113–126, 2002.

[HMS02b] A Howard, MJ Mataric, and GS Sukhatme. "An Incremental Self-Deployment Algorithm for Mobile Sensor Networks." *Autonomous Robots Journal (Special Issue on Intelligent Embedded Systems)*, **13**(2):113–126, 2002.

[HS97] J Heikkila and O Silven. "A Four Step Camera Callibration Procedure with Implicit Image Correction." In *IEEE Computer Vision and Pattern Recognition*, pp. 1106–1112, 1997.

[IL01] D Lpez de Ipia and SL Lo. "Video-Based Sensing for Wide Deployment of Sentient Spaces ¨" In *2nd PACT Workshop on Ubiquitous Computing and Communications*, Barcelona, Catalonia, Spain, September 2001.

[JLM03] A Jadbabaie, J Lin, and AS Morse. "Coordination of Groups of Mobile Autonomous Agents Using Nearest Neighbor Rules." *IEEE Transactions on Automatic Control*, **48**(6):988–1001, June 2003.

[Kan] A Kansal. "Coordinated Actuation project, NESL CVS repository." http://cvs.nesl.ucla.edu/cvs/viewcvs.cgi/CoordinatedActuation/.

[KCH05] A Kansal, JM Carwana, A Hallajpour, WJ Kaiser, and MB Srivastava. "Coordinated Actuation for Sensing Uncertainty Reduction." In *ACM/IEEE IPSN 2005 Demonstration Abstracts*, Los Angeles, CA, USA, April 2005.

[KCK05a] A Kansal, J Carwana, WJ Kaiser, and MB Srivastava. "Acquiring Medium Models for Sensing Performance Estimation." In *IEEE SECON*, September 2005.

[KCK05b] A Kansal, JM Carwana, WJ Kaiser, and MB Srivastava. "Coordinating Camera Motion for Sensing Uncertainty Reduction." In *ACM Sensys*, p. 307, San Diego, CA, USA, November 2005.

[KCL98] T Kanade, RT Collins, AJ Lipton, P Burt, and L Wixon. "Advances in Cooperative Multi-Sensor Video Surveillance." In *Proc. DARPA Image Understanding Workshop*, pp. 3–24, 1998.

[KFL01] FR Kschischang, B Ferry, and HA Loelinger. "Factor graphs and the sum-product algorithm." *IEEE Transactions on Information Theory*, **47**(2):498–519, 2001.

[KKP04] A Kansal, WJ Kaiser, GJ Pottie, and MB Srivastava. "Actuation Techniques for Sensing Uncertainty Reduction." Technical Report 51, Center for Embedded Networked Sensing (CENS), University of California, Los Angeles, 2004.

[KPS03] WJ Kaiser, GJ Pottie, MB Srivastava, GS Sukhatme, J Villasenor, and D Estrin. "Networked Infomechanical Systems (NIMS) for Ambient Intelligence." Technical Report 31, UCLA-NSF Center for Embedded Networked Sensing, December 2003.

[KW94] D Kortenkamp and T Weymouth. "Topological mapping for mobile robots using a combination of sonar and vision sensing." In *Twelfth National Conference on Artificial Intelligence*, pp. 979–984, Menlo Park, July 1994. AAAI Press/MIT Press.

[KYK04] A Kansal, E Yuen, WJ Kaiser, GJ Pottie, and MB Srivastava. "Sensing uncertainty reduction using low complexity actuation." In *ACM Symposium on Information Processing in Sensor Networks*, pp. 388–395. ACM Press, 2004.

[LDC92] JJ Leonard, HF Durrant-Whyte, and IJ Cox. "Dynamic Map Building for an Autonomous Mobile Robot." *International Journal of Robotics Research*, **11**(4):286–298, 1992.

[Lei] "Leica Laser Distancemeter." http://www.leica-geosystems.com.

[LLG97] Steven M LaValle, D Lin, LJ Guibas, JC Latombe, and R Motwani. "Finding an Unpredictable target in a Workspace with Obstacles." In *IEEE International Conference on Robotics and Automation*, pp. 737–742, Albuquerque, NM, April 1997.

[LWF03] XY Li, PJ Wan, and O Frieder. "Coverage in Wireless Ad Hoc Sensor Networks." *IEEE Transactions on Computers*, **52**(6), June 2003.

[MC96] E Marchand and F Chaumette. "Controlled camera motions for scene reconstruction and exploration." In *IEEE Computer Vision and Pattern Recognition*, pp. 169–176, San Francisco, CA, USA, June 1996.

[MC00] E Marchand and N Courty. "Image Based Virtual Camera Motion Strategies." In *Graphics Interface Conference*, Montreal, Qc, Canada, May 2000.

[MCB04] WE Mantzel, H. Choi, and RG Baraniuk. "Distributed camera network localization." In *38th Asilomar Conference on Signals, Systems and Computers*, November 2004.

[ME85] H Moravec and A Elfes. "High Resolution Maps from Wide Angle Sonar." In *IEEE International Conference on Robotics and Automation*, pp. 116–121, St. Louis, MO, 1985.

[MGE02] W Merrill, L Girod, J Elson, K Sohrabi, F Newberg, and WJ Kaiser. "Autonomous Position Location in Distributed, Embedded, Wireless Systems." In *IEEE CAS Workshop on Wireless Communications and Networking*, Pasadena, CA, September 2002.

[MHT00] I Mikic, K Huang, and M Trivedi. "Activity monitoring and summarization for an intelligent meeting room." In *IEEE Workshop on Human Motion*, Austin, Texas, December 2000.

[MKP01] S Meguerdichian, F Koushanfar, M Potkonjak, and MB Srivastava. "Coverage Problems in Wireless Ad-hoc Sensor Networks." In *Twentieth Annual Joint Conference of the IEEE Computer and Communications Societies (INFOCOM)*, volume 3, pp. 1380–1387, April 2001.

[MLR04] D Moore, J Leonard, D Rus, and S Teller. "Robust distributed network localization with noisy range measurements." In *Proceedings of the Second ACM Conference on Embedded Networked Sensor Systems (SenSys)*, p. 5061, Baltimore, MD, November 2004.

[MPS02] A Mainwaring, J Polastre, R Szewczyk, D Culler, and J Anderson. "Wireless Sensor Networks for Habitat Monitoring." In *First ACM Workshop on Wireless Sensor Networks and Applications*, Atlanta, GA, USA, September 2002.

[MSL04] M Maroti, G Simon, A Ledeczi, and J Sztipanovits. "Shooter Localization in Urban Terrain." *IEEE Computer Magazine*, August 2004.

[MU02] T Matsuyama and N Ukita. "Real-Time Multitarget Tracking by a Cooperative Distributed Vision System." *Proceedings of the IEEE*, **90**(7):1136–1150, July 2002.

[Nil94] BJ Nilsson. *Guarding Art Galleries, Methods for Mobile Guards.* PhD thesis, Department of Computer Science, Lund University, 1994.

[NRB04] C Niclass, A Rochas, PA Besse, and E Charbon. "A CMOS Single Photon Avalanche Diode Array for 3D Imaging." In *IEEE International Solid-State Circuits Conference*, pp. 120–121, February 2004.

[OM02] G Olague and R Mohr. "Optimal camera placement for accurate reconstruction." *Pattern Recognition*, **35**:927–944, 2002.

[OM04] R Olfati-Saber and RM Murray. "Consensus Problems in Networks of Agents With Switching Topology and Time-Delays." *IEEE Transactions on Automatic Control*, **49**(9):1520–1533, September 2004.

[OR87] J O'Rourke. *Art Gallery Theorems and Algorithms*. Oxford University Press, New York, 1987.

[Pac04] "Packbot, The Next Step in Unmanned Tactical Mobile Robots." http://www.packbot.com, 2004.

[PG02] JS Perry and WS Geisler. "Gaze-contingent real-time simulation of arbitrary visual fields." In *Human Vision and Electronic Imaging, SPIE Proceedings*, San Jose, CA, 2002.

[PK00] GJ Pottie and WJ Kaiser. "Wireless integrated network sensors." *Communications of the ACM*, **43**(5):51–58, 2000.

[PKP04] A Pandya, A Kansal, GJ Pottie, and MB Srivastava. "Fidelity and Resource Sensitive Data Gathering." In *42nd Allerton Conference on Communication, Control, and Computing*, June 2004.

[PMT01] I Pavlidis, V Morellas, P Tsiamyrtzis, and Steve Harp. "Urban Surveillance Systems: From the Laboratory to the Commercial World." *Proceedings of the IEEE*, **89**(10):1478–1497, October 2001.

[PS04] S Poduri and GS Sukhatme. "Constrained Coverage for Mobile Sensor Networks." In *IEEE International Conference on Robotics and Automation*, pp. 165–172, New Orleans, LA, May 2004.

[PT02] LE Parker and C Touzet. *Distributed autonomous Robotic Systems 4*, chapter Multi-robot Learning in a Cooperative Observation Task, pp. 391–401. Springer, 2002.

[RAS00] J Rabaey, J Ammer, JL da Silva Jr., and D Patel. "PicoRadio: Ad-hoc wireless networking of ubiquitous low-energy sensor/monitor nodes." In *IEEE Computer Society Workshop on VLSI*, pp. 9–12, Orlando, Fl, USA, April 2000.

[RBI05] MH Rahimi, R Baer, OI Iroezi, JC García, J Warrior, D Estrin, and MB Srivastava. "Cyclops: in situ image sensing and interpretation in wireless sensor networks." In *SenSys*, pp. 192–204, 2005.

[RN99] D Radhakrishnan and I Nourbakhsh. "Topological Localization by Training a Vision-based Transition Detector." In *Proceedings of IROS 1999*, volume 1, pp. 468 – 473, October 1999.

[RNK04] Y Rachlin, R Negi, and P Khosla. "Sensing Capacity for Target Detection." In *IEEE Information Theory workshop*, San Antonio, USA, October 2004.

[SCI05] E Shechtman, Y Caspi, and M Irani. "Space-Time Super-Resolution." *IEEE Transactions on Pattern Analysis and Machine Intelligence*, **27**(4):531–545, April 2005.

[SDB00] M Saptharishi, C Diehl, K Bhat, J Dolan, and P Khosla. "CyberScout: Distributed Agents for Autonomous Reconnaissance and Surveillance." In *Mechatronics and Machine Vision 2000*, pp. 93–100, September 2000.

[SHS01] A Savvides, CC Han, and MB Srivastava. "Dynamic Fine Grained Localization in Ad-Hoc Sensor Networks." In *Proceedings of the Fifth International Conference on Mobile Computing and Networking (Mobicom)*, pp. 166–179, Rome, Italy, July 2001.

[SKJ06] AA Somasundara, A Kansal, DC Jea, D Estrin, and MB Srivastava. "Controllably Mobile Infrastructure for Low Energy Embedded Networks." *IEEE Transactions on Mobile Computing (TMC)*, **5**(8), August 2006.

[SMP01a] M Srivastava, R Muntz, and M Potkonjak. "Smart kindergarten: sensor-based wireless networks for smart developmental problem-solving enviroments." In *Proceedings of the Seventh ACM Annual International Conference on Mobile Computing and Networking (MobiCom)*, pp. 132 – 138, July 2001.

[SMP01b] M Srivastava, R Muntz, and M Potkonjak. "Smart kindergarten: sensor-based wireless networks for smart developmental problem-solving enviroments." In *Proc. ACM MobiCom*, pp. 132 – 138, July 2001.

[SNC04] "Sony SNCCS3N." http://bssc.sel.sony.com/Professional/, 2004. CS Mount Fixed Network Color Camera.

[Sol95] MV Solodov. *Nonmonotone and Perturbed Optimization*. PhD thesis, University of Wisconsin, Madison, 1995.

[Son04] "Sony SNC-RZ30N Data Sheet." http://bssc.sel.sony.com/, 2004.

[SS02] A Savvides and MB Srivastava. "A distributed computation platform for wireless embedded sensing." In *IEEE nternational Conference on Computer Design: VLSI in Computers and Processors*, pp. 220 –225, September 2002.

[SS03] P Steurer and MB Srivastava. "System design of smart table." In *Proceedings of the First IEEE International Conference on Pervasive Computing and Communications (PerCom 2003)*, pp. 473 –480, March 2003.

[SSC90] R Smith, M Self, and P Cheeseman. "Estimating uncertain spatial relationships in robotics." *Autonomous Robot Vehicles*, **1**:167–193, 1990.

[Sta] "Stargate Xscale processor platform." http://www.xbow.com/.

[STE98] S Stillman, R Tanawongsuwan, and I Essa. "A System for tracking multiple people with multiple cameras." Technical Report GIT-GVU-98-25, Georgia Institute of Technology, Graphics, Visualization, and Usability center, 1998.

[Suj02] VA Sujan. "Task Directed Imaging In Unstructured Environments By Cooperating Robots." In *The Third Indian Conference on Computer Vision, Graphivs and Image Processing*, Ahmedabad, India, December 2002.

[TB96] S Thrun and A Bücken. "Integrating Grid-Based and Topological Maps for Mobile Robot Navigation." In *Proceedings of the AAAI Thirteenth National Conference on Artificial Intelligence*, Portland, Oregon, 1996.

[TH] K Toyama and GD Hager. "Incremental Focus of Attention for Robus Visual Tracking." Department of Computer Science, Yale University.

[THM00] M Trivedi, K Huang, and I Mikic. "Intelligent environments and Active Camera Networks." In *Proc IEEE Intl' Conf. systems, man, and Cybernetics*, volume 2, pp. 804–809, 2000.

[TS04] O Tickoo and B Sikdar. "Queueing Analysis and Delay Mitigation in IEEE 802.11 Random Access MAC based Wireless Networks." In *IEEE Infocom 2004*, Hong Kong, March 2004.

[Ver91] D Vernon. *Machine Vision*, chapter 6. Prentice-Hall, 1991.

[VSA03] V Vezhnevets, V Sazonov, and A Andreeva. "A Survey on Pixel-Based Skin Color Detection Techniques." In *Proc. Graphicon*, pp. 85–92, Moscow, Russia, September 2003.

[WEG03] H Wang, J Elson, L Girod, D Estrin, and K Yao. "Target classification and localization in a habitat monitoring application." In *Proceedings of the IEEE ICASSP 2003*, Hong Kong, April 2003.

[Win03] "Wind River Canopy Crane Research Facility." http://depts.washington.edu/wrccrf/12haplot/, 2003. 12-ha Permanent Plot Tree Data.

[WR05] KC Wang and P Ramananthan. "Collaborative sensing using sensors of uncoordinated mobility." In *Proceedings of International Conference on Distributed Computing in Sensor Systems (DCOSS)*, pp. 293–306, June 2005.

[WXZ03a] X Wang, G Xing, Y Zhang, C Lu, R Pless, and C Gill. "Integrated Coverage and Connectivity Configuration in Wireless Sensor Networks." In *ACM SenSys*, Los Angeles, CA, November 2003.

[WXZ03b] X Wang, G Xing, Y Zhang, C Lu, R Pless, and C Gill. "Integrated Coverage and Connectivity Configuration in Wireless Sensor Networks." In *ACM SenSys 2003*, Los Angeles, USA, November 2003.

[XJ02] Y Xie and Q Ji. "A New Efficient Ellipse Detection Method." In *16th International Conference on Pattern Recognition (ICPR'02)*, volume 2, p. 20957, 2002.

[YKG04] J Yao, N Kharma, and P Grogono. "Fast Robust GA-Based Ellipse Detection." In *17th International Conference on Pattern Recognition (ICPR'04)*, volume 2, pp. 859–862, 2004.

[ZSR02] F Zhao, J Shin, and J Reich. "Information-driven dynamic sensor collaboration for tracking applications." *IEEE Signal Processing Magazine*, **19**(2):61–72, 2002.